

Finite Element Seismic Analysis of Guyed Masts

by

Matthew Grey



**A thesis submitted for the degree of
Master of Science by Research
at the University of Oxford**

St Cross College

Hilary Term 2006

Abstract

Finite Element Seismic Analysis of Guyed Masts

A thesis submitted for the degree of Master of Science by Research

Matthew Grey
St Cross College
Hilary Term 2006

Guyed masts are a specialized type of structure commonly used in the broadcasting industry to support equipment at substantial heights. The dynamic analysis of these structures under seismic loading is a much understudied field that requires investigation. The complex nature of their analysis arises from the nonlinear force–deflection relationship of the cable supports as well as P- Δ effects in the mast. These lead to the structure exhibiting significant nonlinear characteristics even under working load conditions. Full nonlinear analysis of guyed masts is rarely performed as it is complex and time consuming. Masts are usually designed by equivalent static methods for wind and ice loading only, with the seismic load case often assumed to be less onerous. The validity of this assumption is investigated as part of this research.

In this project four existing guyed masts in the UK with heights ranging from 99m to 312m are accurately analysed under various seismic loading conditions using SAP2000 structural analysis software. The research aims to gain an understanding into the distribution and magnitudes of forces developed during typical seismic and design wind events, establish indicators and trends that may aid in guyed mast design, and identify the circumstances in which seismic loading may be the governing load case. Investigations into the ‘travelling wave’ effect, the significance of vertical motion, and the suitability of a response spectrum analysis are also undertaken. Applicable sections of Eurocode 8 are followed wherever possible.

It is shown that when subjected to substantial seismic events with peak ground accelerations in the region of 4m/s^2 , significant forces can develop in masts that are comparable to those produced during a wind assessment using the Patch Load method. The distribution of forces can be appreciably different from a wind loading analysis and any regions with irregular or inconsistent distribution of wind response forces can be vulnerable to seismic loading, particularly when mean hourly design wind speeds are less than 22m/s. It is also shown that enough common or predictable seismic behaviour exists between masts to suggest that the development of a simplified seismic analysis method for guyed masts is feasible.

Acknowledgments

I would like to thank my supervisors, Dr Martin Williams and Dr Tony Blakeborough for their guidance and support during my studies here at Oxford. Working with such respected and inspirational individuals has been a privilege and has confirmed my interest in advanced structural design.

Thanks must go to David McKenzie and Simon de Neumann at Flint and Neill Partnership for supplying all of the data that characterized the masts used in this research and for their ongoing support throughout the project.

Thanks to Campbell Reith consulting engineers for their financial support that has helped make my studies at Oxford possible.

To my family and the Collier family, thanks for your love and support throughout my Oxford experience, and finally my thanks to my wife and best friend, Lisa.



Photograph: 152m guyed mast near Beckley, Oxford¹

¹ Photograph by the author

Table of Contents

ABSTRACT	i
ACKNOWLEDGEMENTS	ii
LIST OF FIGURES	viii
LIST OF TABLES	xi
LIST OF SYMBOLS AND NOTATION	xii
1 INTRODUCTION	1
1.1 CURRENT DESIGN METHODS	3
1.1.1 <i>Design for Wind</i>	3
1.1.2 <i>Earthquake Response and Design</i>	4
1.2 RESEARCH INVOLVING GUYED MASTS.....	5
1.3 OBJECTIVES OF RESEARCH	8
2 REVIEW OF APPLICABLE THEORY AND DESIGN CODES	10
2.1 INTRODUCTION TO VIBRATION THEORY	10
2.1.1 <i>The Single Degree of Freedom Oscillator</i>	11
2.1.2 <i>Multiple Degree of Freedom Systems</i>	14
2.1.3 <i>Dynamic Analysis by Numerical Integration</i>	18
2.2 CABLE THEORY	20
2.2.1 <i>Static Analysis</i>	20
2.2.2 <i>Dynamic Analysis</i>	24
2.3 EARTHQUAKE GROUND MOTION AND SPATIAL VARIATION OF MOTION	26
2.4 OVERVIEW OF RELEVANT SECTIONS OF EUROCODE 8: PART 1 AND PART 6	28
2.4.1 <i>Response Spectrum</i>	29
2.4.2 <i>Modal Response Spectrum Analysis</i>	30
2.4.3 <i>Time History Representation</i>	31
2.4.4 <i>Tension Limits</i>	32
2.5 GUYED MAST DESIGN USING BS8100-4:1995	32
2.5.1 <i>Overall Wind Resistance</i>	32
2.5.2 <i>Mean Load Effects</i>	34

2.5.3	<i>Dynamic Loading</i>	34
2.5.4	<i>Total Design Load Effect</i>	36
3	MODELLING METHODS AND ASSUMPTIONS	37
3.1	MAST ASSUMPTIONS.....	37
3.1.1	<i>Static Load case Comparison of Beam Model</i>	37
3.1.2	<i>Modal Comparison of Beam Model</i>	39
3.2	CABLE MODELLING METHODS AND ASSUMPTIONS	40
3.2.1	<i>Pretension</i>	43
3.3	GENERAL ASSUMPTIONS.....	43
4	MASTS USED FOR ANALYSIS	45
4.1	MAST GEOMETRY	45
4.2	MASS BREAKDOWN OF MASTS	48
4.3	STAY PRETENSION	51
4.4	RELATIVE HORIZONTAL STIFFNESS OF STAYS	52
5	MODAL ANALYSIS	54
5.1	INTRODUCTION AND METHODOLOGY	54
5.2	RESULTS AND DISCUSSION	55
5.2.1	<i>Lateral Modes</i>	55
5.2.2	<i>Mode Shapes</i>	57
5.2.3	<i>Vertical Modes</i>	59
6	WIND ANALYSIS	61
6.1	INTRODUCTION AND METHODOLOGY	61
6.2	WIND SPEEDS AND LOADING PROFILES	62
6.3	RESULTS AND DISCUSSION	64
7	SEISMIC ANALYSIS	69
7.1	DETAILS OF ANALYSES.....	69
7.1.1	<i>Stage 1 – Uniform Ground Motion</i>	69
7.1.2	<i>Stage 2 – The Travelling Wave Effect</i>	69
7.1.3	<i>Stage 3 – Uniform Ground Motion without Vertical Motion</i>	71

7.2	MODELLING METHODS AND ASSUMPTIONS FOR SEISMIC ANALYSES	71
7.2.1	<i>Time Integration Method</i>	71
7.2.2	<i>Damping</i>	72
7.3	ACCELEROGRAMS AND TIME HISTORIES.....	72
7.3.1	<i>Scaling and Comparison of Time Histories</i>	74
7.3.2	<i>Input for SAP2000</i>	76
8	STAGE 1: UNIFORM GROUND MOTION – RESULTS AND DISCUSSION	78
8.1	MAST BENDING MOMENTS	78
8.2	MAST SHEAR	86
8.3	MAST DEFLECTIONS	98
8.4	MAST AXIAL FORCES	103
8.5	CABLE TENSIONS AND CABLE BEHAVIOUR	108
8.5.1	<i>Peak Tensions</i>	108
8.5.2	<i>Other Cable Behaviour</i>	113
8.6	ACCELERATION PROFILES.....	114
9	STAGE 2: TRAVELLING WAVE EFFECT – RESULTS AND DISCUSSION.....	117
9.1	MAST FORCES.....	117
9.2	CABLE TENSIONS	120
10	STAGE 3: UNIFORM GROUND MOTION WITHOUT VERTICAL MOTION – RESULTS AND DISCUSSION	123
10.1	MAST FORCES.....	123
10.2	CABLE TENSIONS	127
11	RESPONSE SPECTRUM ANALYSIS.....	128
11.1	INTRODUCTION	128
11.2	DETAILS OF ANALYSES.....	128
11.2.1	<i>Response Spectra</i>	128
11.2.2	<i>Directional and Modal Combination Rules</i>	129
11.3	RESULTS AND DISCUSSION	130
11.3.1	<i>Mast Forces</i>	130
11.3.2	<i>Cable Tensions</i>	134

12	SUMMARY AND CONCLUSIONS	136
12.1	RESPONSE TO SIMULTANEOUS GROUND MOTION	136
12.1.1	<i>Bending Moments</i>	137
12.1.2	<i>Shear Forces</i>	137
12.1.3	<i>Axial Forces</i>	138
12.1.4	<i>Cable Tensions</i>	139
12.2	COMPARISON OF SEISMIC RESPONSE TO DESIGN WIND RESPONSE	139
12.3	RESPONSE TO TRAVELLING WAVE EFFECT	142
12.4	EFFECT OF VERTICAL MOTION	143
12.5	RESPONSE SPECTRUM ANALYSIS	143
12.6	SUMMARY AND NEED FOR FURTHER RESEARCH.....	144
13	REFERENCES	146
14	APPENDICES.....	149
	APPENDIX 1: ACCELEROGRAMS USED IN SEISMIC ANALYSES	149
	APPENDIX 2: EXTREME CABLE FORCES PRODUCED IN SEISMIC ANALYSES.....	151

List of Figures

Figure 2-1 The single degree of freedom oscillator	11
Figure 2-2 Dynamic magnification curves for a SDOF structure subject to forced harmonic loading	13
Figure 2-8 Displacements in the i th mode of vibration.....	16
Figure 2-3 Typical plot of equation 2.21 for Rayleigh damping.....	17
Figure 2-4 Simply supported cable with uniformly distributed load.....	20
Figure 2-5 First two symmetric cable mode shapes.....	25
Figure 2-6 First two antisymmetric cable mode shapes.....	25
Figure 2-7 Type 1 elastic response spectrum for soil type C, design acceleration of $3m/s^2$ and 5% damping ...	29
Figure 3-1 Percentage difference between the lattice and beam models.....	38
Figure 3-2 Lattice and beam cantilever mode shapes.....	39
Figure 3-3 Simple inclined cable	41
Figure 3-4 Plot of force–deflection relationship for an inclined cable using various models.....	41
Figure 4-1 Mast A – geometry	46
Figure 4-2 Mast B – geometry	46
Figure 4-3 Mast C – geometry.....	47
Figure 4-4 Mast D – geometry.....	47
Figure 4-5 Mast A – mass distribution	50
Figure 4-6 Mast B – mass distribution	50
Figure 4-7 Mast C – mass distribution	50
Figure 4-8 Mast D – mass distribution.....	50
Figure 4-9 Mast A Stay level force–deflection.....	52
Figure 4-10 Masts B Stay level force–deflection.....	53
Figure 4-11 Mast C Stay level force–deflection.....	52
Figure 4-12 Mast D Stay level force–deflection	53
Figure 5-1 Plot of the most significant flexural periods against mast height	56
Figure 5-2 Mast A – mode shapes.....	57
Figure 5-3 Mast B – mode shapes.....	58
Figure 5-4 Mast C – mode shapes	58
Figure 5-5 Mast D – mode shapes	58
Figure 6-1 Mast A – mean wind load profile	62
Figure 6-2 Mast B – mean wind load profile	62
Figure 6-3 Mast C – mean wind load profile.....	63
Figure 6-4 Mast D – mean wind load profile.....	63
Figure 6-5 Mast A – design wind moments.....	65
Figure 6-6 Mast B – design wind moments.....	65
Figure 6-7 Mast C – design wind moments.....	65
Figure 6-8 Mast D – design wind moments	65
Figure 6-9 Mast A – design wind shear	66
Figure 6-10 Mast B – design wind shear	66
Figure 6-11 Mast C – design wind shear.....	66
Figure 6-12 Mast D – design wind shear.....	66
Figure 6-13 Mast A – design wind axial forces	67
Figure 6-14 Mast B – design wind axial forces	67
Figure 6-15 Mast C – design wind axial forces	67
Figure 6-16 Mast D – design wind axial forces.....	67
Figure 7-1 El Centro accelerogram in dominant (X) direction for $3m/s^2$ scaling.....	73
Figure 7-2 Parkfield accelerogram in dominant (X) direction for $3m/s^2$ scaling	73
Figure 7-3 EC8 accelerogram in dominant (X) direction for $3m/s^2$ scaling	73
Figure 7-4 Response spectra (5% damping) for accelerograms in dominant direction at $3m/s^2$ scaling	75
Figure 7-5 Horizontal displacement time histories ($3m/s^2$ scaling).....	77
Figure 8-1 Mast A – bending moment envelopes (about Y axis) for $4m/s^2$ scaling.....	78
Figure 8-2 Mast A – bending moment envelopes (about X axis) for $4m/s^2$ scaling.....	78
Figure 8-3 Mast B – bending moment envelopes (about Y axis) for $4m/s^2$ scaling.....	79
Figure 8-4 Mast B – bending moment envelopes (about X axis) for $4m/s^2$ scaling.....	79

Figure 8-5 Mast C – bending moment envelopes (about Y axis) for $4m/s^2$ scaling.....	79
Figure 8-6 Mast C – bending moment envelopes (about X axis) for $4m/s^2$ scaling.....	79
Figure 8-7 Mast D – bending moment envelopes (about Y axis) for $4m/s^2$ scaling.....	80
Figure 8-8 Mast D – bending moment envelopes (about X axis) for $4m/s^2$ scaling.....	80
Figure 8-9 Mast A – absolute bending moments for EC8 time histories.....	82
Figure 8-10 Mast A – absolute bending moments for El Centro time histories.....	82
Figure 8-11 Mast B – absolute bending moments for EC8 time histories.....	82
Figure 8-12 Mast B – absolute bending moments for El Centro time histories.....	82
Figure 8-13 Mast C – absolute bending moments for EC8 time histories.....	83
Figure 8-14 Mast C – absolute bending moments for El Centro time histories.....	83
Figure 8-15 Mast D – absolute bending moments for EC8 time histories.....	83
Figure 8-16 Mast D – absolute bending moments for El Centro time histories.....	83
Figure 8-17 Average NMR vs mast height and average span.....	86
Figure 8-18 Mast A – shear force envelopes (X direction) for $4m/s^2$ scaling.....	87
Figure 8-19 Mast A – shear force envelopes (Y direction) for $4m/s^2$ scaling.....	87
Figure 8-20 Mast B – shear force envelopes (X direction) for $4m/s^2$ scaling.....	87
Figure 8-21 Mast B – shear force envelopes (Y direction) for $4m/s^2$ scaling.....	87
Figure 8-22 Mast C – shear force envelopes (X direction) for $4m/s^2$ scaling.....	88
Figure 8-23 Mast C – shear force envelopes (Y direction) for $4m/s^2$ scaling.....	88
Figure 8-24 Mast D – shear force envelopes (X direction) for $4m/s^2$ scaling.....	88
Figure 8-25 Mast D – shear force envelopes (Y direction) for $4m/s^2$ scaling.....	88
Figure 8-26 Mast A – absolute shear force envelopes for EC8 time histories.....	90
Figure 8-27 Mast A – absolute shear force envelopes for El Centro time histories.....	90
Figure 8-28 Mast B – absolute shear force envelopes for EC8 time histories.....	90
Figure 8-29 Mast B – absolute shear force envelopes for El Centro time histories.....	90
Figure 8-30 Mast C – absolute shear force envelopes for EC8 time histories.....	91
Figure 8-31 Mast C – absolute shear force envelopes for El Centro time histories.....	91
Figure 8-32 Mast D – absolute shear force envelopes for EC8 time histories.....	91
Figure 8-33 Mast D – absolute shear force envelopes for El Centro time histories.....	91
Figure 8-34 Average normalized shear ratio versus mast height and average span.....	93
Figure 8-35 Mast A – peak mast base shear and total base shear vs PGA scale factor.....	94
Figure 8-36 Mast B – peak mast base shear and total base shear vs PGA scale factor.....	94
Figure 8-37 Mast C – peak mast base shear and total base shear vs PGA scale factor.....	95
Figure 8-38 Mast D – peak mast base shear and total base shear vs PGA scale factor.....	95
Figure 8-39 Mast C – total base shear magnitude for EC8 analyses (time 10s-20s).....	96
Figure 8-40 Peak total base shear/mast weight vs mast height for EC8 and El Centro analyses.....	97
Figure 8-41 Mast A – peak deflection for EC8 time histories.....	98
Figure 8-42 Mast B – peak deflection for EC8 time histories.....	98
Figure 8-43 Mast C – peak deflection for EC8 time histories.....	99
Figure 8-44 Mast D – peak deflection for EC8 time histories.....	99
Figure 8-45 Mast A – EC8-4 stay level deflection, X-direction (time history).....	100
Figure 8-46 Mast B – EC8-4 stay level deflection, X-direction (time history).....	100
Figure 8-47 Mast C – EC8-4 stay level deflection, X-direction (time history).....	100
Figure 8-48 Mast D – EC8-4 stay level deflection, X-direction (time history).....	100
Figure 8-49 Mast A – EC8 and El Centro time history deflection comparison (levels A and C).....	101
Figure 8-50 Mast A – EC8 and El Centro time history deflection comparison (levels C and E).....	101
Figure 8-51 Mast C – EC8 and El Centro time history deflection comparison (levels B and D).....	102
Figure 8-52 Mast D – EC8 and El Centro time history deflection comparison (levels C and E).....	102
Figure 8-53 Mast A – peak axial force for $4m/s^2$ scaling.....	103
Figure 8-54 Mast B – peak axial force for $4m/s^2$ scaling.....	103
Figure 8-55 Mast C – peak axial force for $4m/s^2$ scaling.....	104
Figure 8-56 Mast D – peak axial force for $4m/s^2$ scaling.....	104
Figure 8-57 Mast A – peak base axial forces.....	104
Figure 8-58 Mast B – peak base axial forces.....	105
Figure 8-59 Mast C – peak base axial forces.....	104
Figure 8-60 Mast D – peak base axial forces.....	105
Figure 8-61 Increase in base axial Force for EC8 and El Centro Analyses.....	106
Figure 8-62 Dynamic axial force distribution for EC8 and El Centro analyses ($4m/s^2$ scaling).....	107

Figure 8-63 Mast A – level A1 cable tensions.....	107
Figure 8-64 Mast A – level B1 cable tensions.....	108
Figure 8-65 Mast A – level C1 cable tensions.....	108
Figure 8-66 Mast B – level A1 cable tensions.....	108
Figure 8-67 Mast B – level B1 cable tensions.....	109
Figure 8-68 Mast B – level C1 cable tensions.....	108
Figure 8-69 Mast B – level D1 cable tensions.....	109
Figure 8-70 Mast B – level E1 cable tensions.....	110
Figure 8-71 Mast C – level A1 cable tensions.....	109
Figure 8-72 Mast C – level B1 cable tensions.....	110
Figure 8-73 Mast C – level C1 cable tensions.....	110
Figure 8-74 Mast C – level D1 cable tensions.....	111
Figure 8-75 Mast D – level A1 cable tensions.....	110
Figure 8-76 Mast D – level B1 cable tensions.....	111
Figure 8-77 Mast D – level C1 cable tensions.....	111
Figure 8-78 Mast D – level D1 cable tensions.....	112
Figure 8-79 Mast D – level E1 cable tensions.....	112
Figure 8-80 Mast B – level A1 cable tension response (EC8, 3m/s ² scaling).....	113
Figure 8-81 Mast A – EC8 acceleration profiles in X direction.....	114
Figure 8-82 Mast B – EC8 acceleration profiles in X direction.....	114
Figure 8-83 Mast C – EC8 acceleration profiles in X direction.....	115
Figure 8-84 Mast D – EC8 acceleration profiles in X direction.....	115
Figure 9-1 Mast A – stage 2 bending moment envelopes (about Y axis).....	117
Figure 9-2 Mast B – stage 2 bending moment envelopes (about Y axis).....	118
Figure 9-3 Mast C – stage 2 bending moment envelopes (about Y axis).....	119
Figure 9-4 Mast D – stage 2 bending moment envelopes (about Y axis).....	120
Figure 10-1 Mast A – stage 3 axial force distribution.....	124
Figure 10-2 Mast A – stage 3 bending moment distribution (about Y axis).....	124
Figure 10-3 Mast A – stage 3 shear force distribution (X direction).....	125
Figure 10-4 Mast D – stage 3 axial force distribution.....	125
Figure 10-5 Mast D – stage 3 bending moment distribution (about Y axis).....	125
Figure 10-6 Mast D – stage 3 shear force distribution (X direction).....	126
Figure 11-1 El Centro response spectra used (3m/s ² scaling).....	129
Figure 11-2 EC8 response spectra used (3m/s ² scaling).....	129
Figure 11-3 Mast A – EC8 response spectrum bending moment envelopes.....	131
Figure 11-4 Mast A – EC8 response spectrum shear force envelopes.....	131
Figure 11-5 Mast B – El Centro response spectrum bending moment envelopes.....	132
Figure 11-6 Mast B – El Centro response spectrum shear force envelopes.....	132
Figure 11-7 Mast C – EC8 response spectrum bending moment envelopes.....	132
Figure 11-8 Mast C – EC8 response spectrum shear force envelopes.....	133
Figure 11-9 Mast D – El Centro response spectrum bending moment envelopes.....	133
Figure 11-10 Mast D – El Centro response spectrum shear force envelopes.....	133
Figure 12-1 European wind map [35].....	141
Figure 14-1 El Centro accelerogram in Y direction for 3m/s ² scaling.....	149
Figure 14-2 El Centro accelerogram in vertical direction for 3m/s ² scaling.....	149
Figure 14-3 Parkfield accelerogram in Y direction for 3m/s ² scaling.....	149
Figure 14-4 Parkfield accelerogram in vertical direction for 3m/s ² scaling.....	150
Figure 14-5 EC8 accelerogram in Y direction for 3m/s ² scaling.....	150
Figure 14-6 El Centro accelerogram in vertical direction for 3m/s ² scaling.....	150

List of Tables

<i>Table 2-1 Extract from Eurocode 8 Ground types (Table 3.1-Eurocode 8:1)</i>	28
<i>Table 3-1 Results of static bending comparison for lattice and beam models</i>	38
<i>Table 3-2 Results of modal comparison for lattice and beam models</i>	39
<i>Table 4-1 Geometry of masts analysed</i>	45
<i>Table 4-2 Mass breakdown of masts</i>	48
<i>Table 4-3 Nominal cable diameters (mm)</i>	51
<i>Table 4-4 Initial pretension force and UTL of stays</i>	51
<i>Table 4-5 Cable horizontal stiffnesses</i>	52
<i>Table 5-1 Mast modes with greater than 5% mass participation</i>	55
<i>Table 5-2 Mast vertical natural frequencies</i>	60
<i>Table 6-1 Mast design wind speeds</i>	62
<i>Table 6-2 Mast average wind loading</i>	63
<i>Table 6-3 Cable tensions from wind analysis</i>	64
<i>Table 7-1 Delay times for each support during travelling wave analyses</i>	70
<i>Table 7-2 Significant frequency ranges of masts</i>	75
<i>Table 7-3 Scaled accelerogram properties</i>	76
<i>Table 8-1 Normalized Moment Ratio for peak bending moments</i>	85
<i>Table 8-2 Normalized Shear Ratio for peak shear forces</i>	93
<i>Table 9-1 Mast A – stage 2 key response forces (kN)</i>	117
<i>Table 9-2 Mast B – stage 2 key response forces (kN)</i>	118
<i>Table 9-3 Mast C – stage 2 key response forces (kN)</i>	119
<i>Table 9-4 Mast D – stage 2 key response forces (kN)</i>	120
<i>Table 9-5 Mast A – stage 2 peak cable tensions (kN)</i>	121
<i>Table 9-6 Mast B – stage 2 peak cable tensions (kN)</i>	121
<i>Table 9-7 Mast C – stage 2 peak cable tensions (kN)</i>	121
<i>Table 9-8 Mast D – stage 2 peak cable tensions (kN)</i>	122
<i>Table 9-9 Breakdown of stage 2 cable tension results</i>	122
<i>Table 10-1 Peak base force summary for stage 3 analyses (kN)</i>	123
<i>Table 10-2 Dynamic base axial force variation for stage 3 analyses (kN)</i>	123
<i>Table 10-3 Maximum cable tensions for stage 3 analysis (kN)</i>	127
<i>Table 11-1 Key forces from response spectrum analysis (kN)</i>	130
<i>Table 11-2 Cable tensions from response spectrum analysis (kN)</i>	135
<i>Table 14-1 Mast A cable tensions (kN)</i>	151
<i>Table 14-2 Mast B cable tensions (kN)</i>	151
<i>Table 14-3 Mast C cable tensions (kN)</i>	152
<i>Table 14-4 Mast D cable tensions (kN)</i>	152

List of Symbols and Notation

A	cable cross sectional area (L^2)
AI	Arias intensity (L/T)
BA	base axial force (F)
BS	base shear force as a percentage of mast weight
c	damping coefficient (FT/L)
d	cable sag from chord line (L)
E	elastic modulus of cable (F/L^2)
F_{M+}	design wind response (upper envelope)
F_{M-}	design wind response (lower envelope)
H	total mast height (L)
h	elevation (L)
H_p	horizontal cable reaction force (F)
i_0	turbulence intensity
k	stiffness (F/L)
k_t	horizontal stiffness of a taut wire (zero sag) (F/L)
L_c	length of the chord line joining cable ends (L)
L_i	modal participation factor (ML)
M_i	modal mass (ML^2)
m	mass (M)
NMR	normalized moment ratio
NSR	normalized shear ratio
PGA	peak ground acceleration (L/T^2)
P_{dyn}	dynamic component of axial force (F)
\bar{P}_{MW}	mean wind load on mast (F/L)
\bar{P}_{GW}	mean wind load on guys (F/L)
P_{MW}	patch load on mast (F/L)
P_G	patch load on guys (F/L)
q	uniformly distributed horizontal cable load (F/L)
R_{AW}	wind resistance of the ancillaries (L^2)

R_G	wind resistance of guys (L^2)
R_M	wind resistance of the bare mast section (L^2)
$r(x,y,z)$	modal mass participation ratio
S	cable arc length (L)
T	natural period (T)
t	time (T)
Q	cable tension (F)
u	general displacement term (L)
UTL	ultimate tensile load (F)
UTS	ultimate tensile stress (F/L^2)
V_z	mean hourly wind speed at height z (L/T)
w	weight of the cable per unit length (F/L)
X	horizontal span of cable (L)
y	displacement along y axis (L)
y_g	displacement of ground along y axis (L)
y_r	relative displacement, $y-y_g$ (L)
y_0	initial displacement (L)
Z	vertical span of cable (L)
α	Rayleigh mass damping constant
β	Rayleigh stiffness damping constant
θ	angle of inclination of chord line (degrees)
λ^2	Irvine's geometric cable parameter
ν	specific weight of cable per unit volume (F/L^3)
ξ	damping ratio
ρ_a	density of air at reference temperature and pressure (M/L^3)
ρ_{nm}	cross modal coefficient
σ	tensile stress in cable (F/L^2)
ϕ	mode shape eigen vector
ψ	phase angle (T)
ω_n	circular natural frequency (Hertz)
Ω	loading frequency (Hertz)

1 Introduction

Guyed masts are specialized structures that are most often used to support telecommunications equipment for broadcasting. Although similar to other freestanding towers, their behaviour is very different. The presence of pre-stressed cables supporting a number of spans of the structure allows the lattice frame of a guyed mast to be significantly smaller in both geometry and member size. The reduction in overall weight of the frame makes the guyed mast a popular design option for towers of considerable height. The material cost saving typically becomes important when comparing freestanding versus guyed tower options in the 100m to 150m range. Above this range the material cost saving far outweighs the added design and manufacturing complexities, and a guyed mast is usually preferable. The geometry of a typical 240m guyed mast is shown in Figure 1-1.

The analysis of these structures is complex, although some design codes have simplified their design significantly. They are usually designed as a triangular or square lattice frame with a pinned base. Pre-stressed cables support the frame at near equal spans and extend to supports on the ground at angles typically between 30 and 50 degrees. The projection of the cables means that these structures can occupy extensive areas on the ground and a typical mast of 450m in height could have a distance of 600m between extreme supports.

The slenderness of the mast (beam-column effects), together with the sag of the cables means that the structure exhibits significant nonlinear characteristics even under working conditions. The stiffness of the guy cable changes with the sag of the cable, leading to a nonlinear force-displacement relationship in the structure. The relatively large deflections exhibited by typical mast behaviour, coupled with the high pre-compression effect of the cable supports, means that significant $P-\Delta$ forces can develop. Variations in the axial load in the mast during extreme loading further complicate the analysis of this effect.

Guyed masts are subjected to a wide range of dynamic loadings that typically arise from wind, earthquakes, sudden rupture of guys, galloping of guys, sudden shedding of ice from guys, etc. Since 1959, there have been approximately 100 documented collapses of towers

(both guyed and freestanding) in the United States alone [13]. The majority of these collapses have been attributed to wind and ice loading during major storms; however a number of permanent deflections and collapses caused by earthquakes have also been reported [17]. This is a clear indicator that the behaviour of this family of structures is not fully understood and needs to be investigated further.

In freestanding towers the dynamic behaviour is characterized by the first few fundamental natural frequencies, which allows for a more simplified approach to the assessment of dynamic loading. Guyed masts however, exhibit high modal participation across many modes, and determining the important modes can be extremely complicated.

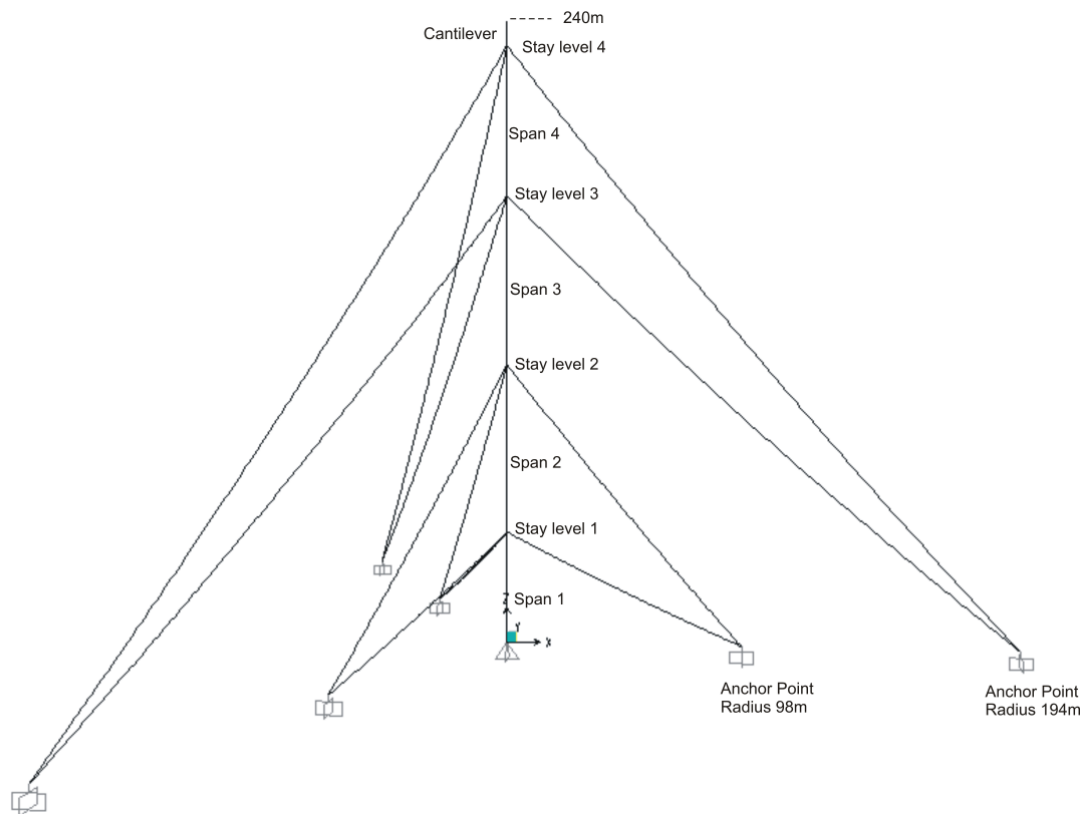


Figure 1-1 Geometry of a typical mast

1.1 Current Design Methods

Although a large number of masts are built each year, information assisting in their analysis, and particularly their dynamic analysis, is sparse and scattered over a number of sources. This, coupled with a competitive marketplace, tight scheduling and lack of resources, means that an advanced nonlinear (or even linear) dynamic analysis is only undertaken in special circumstances. Recently Madugula [29] provided a much needed summary of the dynamic analysis and design of guyed masts. His publication pulls together much of the available information and describes many of the procedures used in the modelling and design of guyed masts. It also covers much of the relevant research produced in recent years and was a good source of information for this research.

1.1.1 Design for Wind

Current codes and guidelines relate predominately to the design of guyed masts under wind loading conditions, with allowances made for the dynamic response of the structure under wind loads, using a number of static methods. The Patch Load method of dynamic wind analysis (equivalent static method) has been developed by a number of researchers [3; 5; 9]. Similar versions of this method of analysis have been adopted by the British Standard BS8100-4, the European Standard EC3 part 3, and the Canadian Standard CSA S37-94. The use of the Patch Load method according to BS8100-4 is described in section 2.5. The requirement for multiple load and analysis cases needed for the Patch Load method has hindered its widespread acceptance for routine design. The British Standard suggests a simplified procedure for the design of masts below 150m in height that specifies the dynamic response of each span of the mast directly from its mean hourly static response using a gust factor that is dependent on the span length and site terrain. The method is based on British wind conditions. A similar procedure is currently being developed in the United States [29].

The American design standard for antenna supporting structures, TIA/EIA-222-F (TIA/EIA 1996) uses a gust factor method that applies a height dependent gust force to the tower based on the fastest mile mean wind speed. The gust factor is dependent on the overall height of

the tower and is applied uniformly to the static winds at all elevations. This assumption that the gust factor is constant over the height of the tower implies that the ratio between the peak dynamic response and the mean response is constant over the tower's height. For freestanding towers with a single dominant vibration mode, this assumption is reasonable and the gust factor method has been shown to be suitable for this type of tower [29]. For guyed towers however, where the dynamic/mean response ratio is not constant, the suitability of the method has been questioned [19; 20]. A revision to this standard (ANSI/EIA/TIA-222-G) was published in August 2005. This revision outlines a new static method based on a 3 second wind speed. The method uses modification factors applied to each static response of the structure at different positions, i.e. mast bending moments:

1.3 to 1.4 for positive moments

1.2 to 1.3 for negative moments

The method seeks to redistribute the response from a static load so that it closely resembles that of a dynamic wind analysis.

1.1.2 Earthquake Response and Design

Research into the seismic response of buildings has been investigated extensively over many years, and consequently most building codes and standards have reasonably sophisticated and proven design methods. Telecommunication towers (both guyed and freestanding) however have received far less research and guidelines available for designers for a simplified analysis are far less plentiful. As a result the rules set out for buildings are often extrapolated for use on towers, which can be misleading; or a seismic assessment is omitted from the design procedure. No approximate static method has been widely adopted for the seismic analysis of tall guyed masts. Unlike other more linear structures, the wide range of significant natural frequencies and nonlinear response makes the defining of realistic acceleration/load profiles extremely complicated.

Eurocode 8 part 6: *Towers, Masts and Chimneys* suggests a simplified static analysis for short towers (less than 60m) or towers of less importance, and a modal response spectrum analysis method (static analysis using SRSS or CQC modal combination rule) for other

linear towers. Draft versions of this standard implied that a nonlinear time history analysis was required for guyed towers with nonlinear behaviour [29], but later drafts (No. 6, July 2004) and the recently published standard imply that the modal response spectrum analysis method is adequate. A time history representation is defined as a suitable definition of seismic action, however minimal guidance is given as to the modelling of masts during this type of analysis.

ANSI/EIA/TIA-222-G, the American design standard for antenna supporting structures has recently introduced seismic requirements for towers that are in high seismic zones but only if they have structural irregularities [21]. The use of a simple equivalent lateral force method is required for short masts. A time history seismic analysis is only required for guyed masts when the distance from the base of the tower to any guy support point is greater than 300m.

1.2 Research Involving Guyed Masts

Some studies have been conducted into the dynamic performance of guyed masts, however most of them relate to determining the fundamental natural frequencies of the mast for application to all dynamic loadings, and many are more applicable to dynamic wind loading. The author was only able to find a similar study by Amiri [1] that modelled the seismic performance of a number of existing masts, and a study by Hensley [8] that modelled the seismic performance of a generic mast.

Most studies address the point of whether the mast can be modelled as a simplified beam or if a full three-dimensional model of the truss lattice is needed. A study by Madugula *et al* [14] modelled two scaled down versions of typical masts as both beam and truss models using the ABAQUS finite element package. The two masts were also modelled physically to verify the finite element models. The study showed good agreement between the natural frequencies of both the beam and truss models as well as with the experimental model, and concluded that the beam model could account accurately for the inherent complexities involved in guyed masts and resulted in appreciable savings in solution time. A similar study by Wahba *et al* [22] looked at six different full scale masts ranging from 46m to 122m. The

masts were modelled both as a full truss model, and as a simplified beam-column, under static wind loading conditions to the Canadian Standard for Antenna Towers. Good agreement was found between the models for all six masts and the same conclusions were drawn.

The equivalent beam properties of a lattice mast are derived using the unit load method for determining displacements under axial, shear, bending and torsional loads and equating them to a beam model under the same loadings. Kahla [12] presents a method for determining these equivalent properties for several triangular mast bracing patterns. The method acknowledges coupling between different degrees of freedom, caused by the non-symmetric shape of various bracing patterns, by the use of a geometric coupling matrix.

Amiri [1] undertook a similar numerical study to the author's present research. Eight existing masts (heights ranging from 150m to 607m) in the United States and Canada were modelled using the nonlinear finite element software ADINA. Each guy cable was modelled as a linkage of ten prestressed truss elements and allowance was made for full geometric nonlinearity. Time history analyses were conducted on the masts, using three 'classic' earthquake accelerograms (1940 El Centro, 1966 Parkfield and 1952 Taft), two of which are used in the author's current research. The input was scaled to match the seismic risk level of 0.34g, the risk level of the Victoria region in Canada. It should be noted that all analyses were conducted without any ancillary loadings present. In this research the ancillary loads are included.

A summary of Amiri's conclusions is as follows:

- *Fundamental natural period of the mast:* The following equation was proposed to estimate this for masts in the 150m to 350m range:

$$T = 0.0083H - 0.74 \quad (1.1)$$

where H is the total height of the mast in metres. A simple check was suggested with an earthquake design spectrum to estimate whether lateral effects are important. Values corresponding to the 0.5-3Hz range were considered sensitive.

- *Base shear:* Significant base shear developed in towers in the 150m to 350m range of the order of 40% to 80% of tower weight. The following equation was proposed to characterize this:

$$BS = 28300H^{-1.17} \text{ (% of W)} \quad (1.2)$$

For taller towers, behaviour was unpredictable and a detailed dynamic analysis was recommended.

- *Axial forces in the mast:* When seismic vertical effects are considered, guyed towers with slacker cables (i.e. below 5% of UTS) were susceptible to unpredictable behaviour and a detailed nonlinear dynamic analysis was recommended. For towers with initial cable tension closer to the recommended 10% of UTS, the maximum dynamic component of axial force at the base of the mast was approximately 80% of total weight of the mast and a detailed study of the mast axial forces was not considered necessary.

The following equation was proposed to characterize the variation in maximum axial force anywhere in the mast:

$$P_{dyn} / BA = 100 - 95(h / H)^2 \text{ (%)} \quad (1.3)$$

where P_{dyn}/BA is the percentage ratio of the maximum dynamic component of axial force in the mast at a section at elevation h (in metres) to the maximum dynamic component of the axial force at the base of the mast.

- *Cable tensions:* The dynamic component of cable tensions varied from 30% to 300% of the initial tension, with typical values for towers ranging in height from 150 to 350m of between 50% and 200%.

Many comparisons will be drawn between Amiri's [1] research and the research reported in this thesis.

A study by Hensley [8] investigated the response of a 120m tall mast using the commercial program ABAQUS to ground motion records from the El Centro and Northridge earthquakes. The study was part of a multi-stage project aimed at analysing the potential for snapping-cable energy dissipaters (SCED) to minimize structural response and investigated the effect of cable pretension, mast properties and the direction of input on mast response. The study yielded several strong trends although some random instances of peak values could not be accounted for. Horizontal displacements generally remained constant or decreased with increased cable pretension, whilst peak vertical displacements were almost linear as a function of guy tension. Maximum bending moments showed a slight decrease with increase in cable pretension, although this trend was more consistent at the middle guy level. Maximum observed cable tensions were generally 200% to 300% of initial tensions, and base shear trends were virtually negligible in both directions. When mast mass and stiffness were varied, the response of the mast was governed by a change in mass rather than stiffness, as the increased stiffness was not sufficient to resist the larger inertial forces produced by the relative mass increase. The study also showed that variation in the direction of seismic motion has very little effect on mast response.

1.3 Objectives of Research

The lack of published research on the seismic behaviour of realistic or existing guyed masts means that a broad range of areas are in need of investigation. The following objectives were set out for this research:

1. Gain an understanding into the magnitude and distribution of forces generated in guyed masts during typical seismic and design wind events.
2. Compare the results of the various analyses and identify the parts of the structure where an indicative wind analysis does not provide enough strength to sustain an earthquake load. Identify the scale of earthquake needed to surpass design forces

produced in a wind loading analysis using the Patch Load method. All the masts analysed in this research were designed or checked to BS8100-4. As EC3 part 3: towers, masts and chimneys, is not yet available in the UK, BS8100-4 was deemed a suitable method for comparison.

3. Assess the effect and significance of the travelling earthquake shear wave on mast response for different earthquake and ground types.
4. Assess the effect of vertical motion on mast response for different types of earthquake.
5. Identify indicators and trends that help in the understanding of the seismic behaviour of these structures and aid designers in estimating seismic response. Compare these indicators with those developed by Amiri [1].
6. Compare the forces produced from a set of linear response spectrum analyses with those produced from a set of nonlinear time history analyses. Identify possible shortcomings with the use of the response spectrum method for guyed masts.

2 Review of Applicable Theory and Design Codes

The analysis and design of guyed masts is complex and draws on many areas of structural theory. Although a large part of this research is concerned with the modelling of guyed masts using SAP2000, it was necessary to review the theory that relates to these structures so that an accurate model could be created, and useful comparisons drawn. This section provides a review of the following:

1. Dynamic theory for both single and multiple degree of freedom structures
2. Static and dynamic behaviour of cables
3. Earthquake groundmotion and its characteristics
4. Design of guyed masts to BS8100-4
5. Relevant sections of EC8 and the use of the response spectrum method

2.1 Introduction to Vibration Theory

In order to understand and interpret any form of seismic analysis it is necessary to have an understanding of the response of structures to dynamic loading. A guyed mast is a complicated multiple degree of freedom structure with nonlinear behaviour and is usually analysed using advanced finite element software. However, the concepts developed for more simple models must be understood before more advanced analyses are attempted. This chapter presents an introduction to the theory that will provide a background for a better understanding of the computer aided analysis.

The oscillatory behaviour of a structure, following an exciting force or initial displacement, is governed by the interaction of its mass m , and its stiffness k . An initial displacement generates a restoring force (stiffness \times displacement) which accelerates the structure back to its equilibrium position. The acceleration causes the mass to gain momentum (mass \times velocity) and overshoot its initial position causing the process to repeat itself (with a change in sign). This process would repeat indefinitely if it were not for various energy dissipating mechanisms present in all structures. The process of energy dissipation is known as damping, and for the purpose of analysis here, it is assumed that all damping takes the form

of linear viscous damping. The damping coefficient c , is the constant of proportionality between force and velocity.

2.1.1 The Single Degree of Freedom Oscillator

The simplest dynamic model is the Single Degree of Freedom (SDOF) oscillator shown in Figure 2-1. It is a model for a simple single story frame with slender columns and an inflexible girder (where it is assumed all the mass resides), or any other model that can be defined (or approximated) by a single mass and displacement. Figure 2-1 shows the parameters used to analyse a typical SDOF structure under a) forced vibration and b) ground motion.

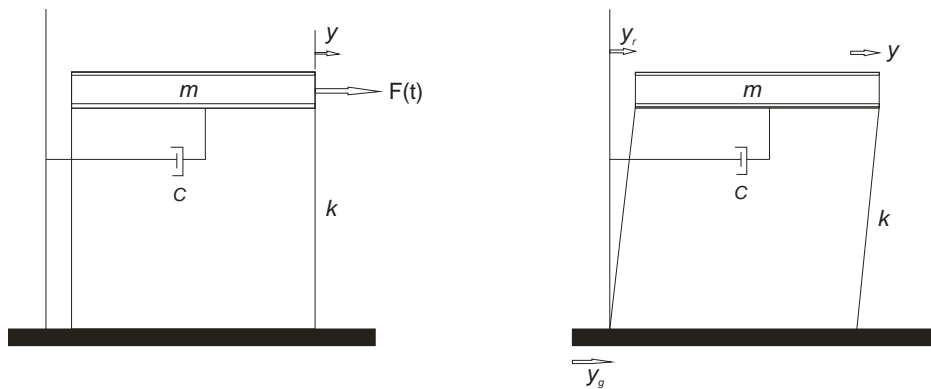


Figure 2-1 The single degree of freedom oscillator

The equation of motion for a linear SDOF oscillator is:

$$m\ddot{y} + c\dot{y} + ky = F(t) \quad (2.1)$$

This shows that the applied force is balanced by the inertia, damping and stiffness forces.

During an earthquake there is no direct force applied to the structure and the above equation becomes:

$$m\ddot{y} + c(\dot{y} - \dot{y}_g) + k(y - y_g) = 0 \quad (2.2)$$

where y_g is the displacement of the ground.

This can be rearranged to take the standard form:

$$m\ddot{y}_r + c\dot{y}_r + ky_r = -m\ddot{y}_g \quad (2.3)$$

where y_r is the relative displacement of the structure given by $y - y_g$.

2.1.1.1 Free Vibrations

The equation of dynamic equilibrium for a SDOF structure with no damping or external force is :

$$m\ddot{y} + ky = 0 \quad (2.4)$$

This mass will undergo free vibration if given an initial displacement y_0 , the solution of which is:

$$y(t) = y_0 \cos \omega_n t \quad (2.5)$$

where $\omega_n = \sqrt{k/m}$, and is known as the circular natural frequency (rad/s).

If damping is included, the equation of motion is:

$$m\ddot{y} + c\dot{y} + ky = 0 \quad (2.6)$$

If $c = 2\sqrt{km}$, the system is said to be critically damped and the structure will return to its initial position without any oscillation. This value for critical damping leads to the damping ratio:

$$\xi = \frac{c}{2\sqrt{km}} = \frac{c}{c_{cr}} \quad (2.7)$$

If $\xi < 1$, the system is underdamped.

For an underdamped system:

$$y(t) = y_0 e^{-\xi\omega_n t} \cos \sqrt{1 - \xi^2} \omega_n t \quad (2.8)$$

This solution is a decaying oscillation. The natural frequency, ω , has been multiplied by $\sqrt{1 - \xi^2}$. For typical damping of less than 5%, this factor is close to 1 and is neglected.

2.1.1.2 Harmonic Vibrations and Resonance

Considering the solution of equation 2.1 in which the dynamic system is excited by a time varying applied harmonic force of the form:

$$F(t) = F_1 \sin \Omega t \quad (2.9)$$

If the frequency of the load, $\Omega \approx \omega_n$, resonance will occur which leads to very large forces being generated.

The equation of motion in this case is:

$$m\ddot{y} + c\dot{y} + ky = F_1 \sin \Omega t \quad (2.10)$$

Damping ensures that the transient vibration is damped out quickly and the solution takes the form of:

$$y(t) = \frac{(F_1/k) \sin(\Omega t + \psi)}{\left[(1 - (\Omega/\omega_n)^2)^2 + 4(\beta\Omega/\omega_n^2)^2 \right]^{1/2}} \quad (2.11)$$

where $\beta = c/2m$ and ψ is the phase angle.

Figure 2-2 shows a plot of the Dynamic Magnification Factor (DMF) for a SDOF structure versus forcing frequency, as a function of the natural frequency. DMF is defined as the ratio of the peak dynamic displacement caused by the harmonic load $F(t)$ to the displacement produced by the static application of the load F_1 . In the case of harmonic ground motion, DMF is defined as ratio of the peak absolute displacement of the structure to the peak displacement of the ground.

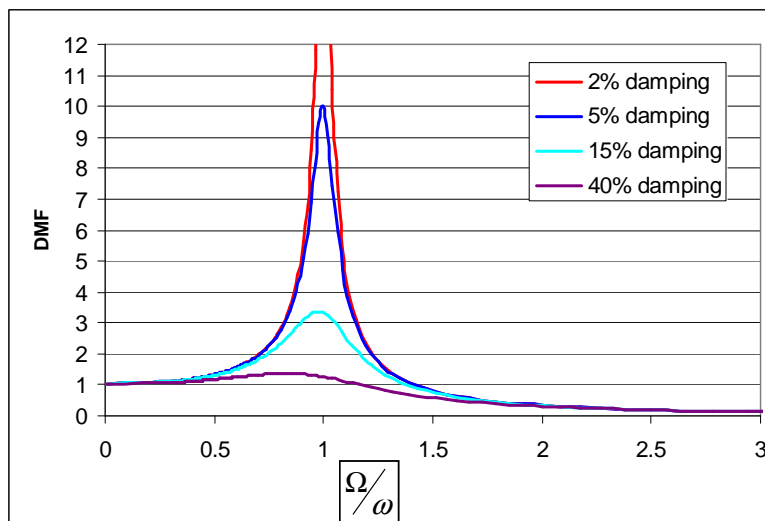


Figure 2-2 Dynamic magnification curves for a SDOF structure subject to forced harmonic loading

The response can be categorized into of three main frequency ranges:

- $\Omega \ll \omega_n$ Rate of forced vibration is lower than the structure's natural frequency

The structure moves with the force as a rigid body.

- $\Omega \approx \omega_n$ *Rate of forced vibration is similar to the structure's natural frequency*
Resonance occurs and there is a large dynamic amplification of the motion of the structure. The main resistance to motion at this stage is damping. For the theoretical case of zero damping the peak displacement is infinite.
- $\Omega \gg \omega_n$ *Rate of forced vibration is higher than the structure's natural frequency*
The mass undergoes less vibration than the force, with the spring and damper acting as absorbers.

2.1.2 Multiple Degree of Freedom Systems

A Multiple Degree of Freedom (MDOF) system is one which requires a second order, ordinary differential equation to describe the motion of each independent degree of freedom. This model is usually needed to describe most structures as the use of a SDOF model is not realistic. For a system with N degrees of freedom, equation 2.3 can be written as a set of equations in matrix form as follows:

$$\mathbf{M}\ddot{\mathbf{y}}_r + \mathbf{C}\dot{\mathbf{y}}_r + \mathbf{K}\mathbf{y}_r = \mathbf{M}\mathbf{p}\ddot{y}_g \quad (2.12)$$

where \mathbf{M} , \mathbf{C} , and \mathbf{K} are the mass, damping and stiffness matrices ($N \times N$), \mathbf{y}_r is the relative displacement vector, \ddot{y}_g is the ground acceleration and \mathbf{p} is a vector with ones in the 'y' directional degrees of freedom, and zero in all remaining positions. The equation can be integrated directly for many degrees of freedom using advanced computer packages such as SAP2000.

2.1.2.1 Natural Frequencies and Mode Shapes

The free vibration case for a MDOF system with no damping gives an important insight into the behaviour of a structure. The equation of motion is written as follows:

$$\mathbf{M}\ddot{\mathbf{y}} + \mathbf{K}\mathbf{y} = 0 \quad (2.13)$$

The solution to this equation has the form:

$$\mathbf{y} = \boldsymbol{\phi} \cos \omega t \quad (2.14)$$

where $\boldsymbol{\phi}$ is an eigenvector, commonly termed the mode shape, and describes the relative displacement of points within a structure.

Differentiating and substituting into equation 2.13 leads to the following equation:

$$(\mathbf{K} - \omega_n^2 \mathbf{M})\boldsymbol{\phi} = 0 \quad (2.15)$$

which can be solved to give N natural frequencies (square roots of eigenvalues), each of which correspond to a different eigenvector, $\boldsymbol{\phi}_n$.

The mode shapes describe the particular deformed shape of the oscillation at a specific natural frequency and are usually mass normalized i.e. scaled with respect to the mass matrix such that:

$$\boldsymbol{\phi}_n^T \mathbf{M} \boldsymbol{\phi}_n = 1 \quad (2.16)$$

The natural frequencies and mode shapes are system properties and are independent of external loading. This type of analysis is useful to a designer in determining the range of loading frequencies that will cause a structure to oscillate, and aids in identifying which parts of a structure will be susceptible to vibration at a particular frequency.

2.1.2.2 Participating Factors and Mass Participation

Identifying the natural frequencies of a structure does not identify the relative importance of each mode in determining its response to acceleration loading. Identifying these important modes becomes increasingly difficult as the number of degrees of freedom of a model increases and this task is made more complicated in a guyed mast model as large numbers of vibration modes develop in the cables that can essentially act independently of the mast. The process of determining the relative importance of each mode is done using participating factors and mass participation ratios.

Modal participating factors represent the extent to which a response is excited in a particular mode. The modal participation factor L_i , and the modal mass M_i are defined as follows:

$$L_i = \sum_j m_j \phi_{ij} \quad (2.17)$$

$$M_i = \sum_j m_j \phi_{ij}^2 \quad (2.18)$$

where

m_j are the lumped masses

ϕ_{ij} the displacement of mass j in mode shape i

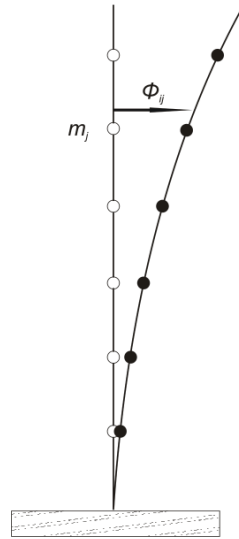


Figure 2-3 Displacements in the i th mode of vibration

The ratio L_i^2/M_i has units of mass and can be thought of as the amount of mass taking part in a particular modal response. The mass participation ratio for a given mode can be found by the following expression:

$$r_i = \frac{L_i^2 / M_i}{M_{total}} \quad (2.19)$$

where M_{total} is the total unrestrained mass of the system. Mass participation ratios are expressed as percentages. Mass participation ratios are very important as they give an indication as to how important a particular mode is by identifying what percentage of the overall mass of a structure takes part in any particular mode.

2.1.2.3 Damping

Damping plays an important role in the dynamic analysis of MDOF structures. The most common way of treating damping in a time history analysis is to use an equivalent Rayleigh damping in the form of:

$$\mathbf{C} = \alpha \mathbf{M} + \beta \mathbf{K} \quad (2.20)$$

where \mathbf{C} , \mathbf{M} and \mathbf{K} are the damping, mass and stiffness matrices of the physical system and α and β are pre-defined mass and stiffness damping constants.

Mass damping is linearly proportional to period and stiffness damping is linearly proportional to frequency.

The equivalent damping at a particular frequency is as follows:

$$\xi_n = \frac{\alpha}{2\omega_n} + \frac{\beta\omega_n}{2} \quad (2.21)$$

In order to damp a range of modes at a similar value, two modes at either end of the range, with frequencies ω_1 and ω_2 , can be chosen and assigned the same damping ratio, ξ .

The damping constants are then as follows:

$$\alpha = \xi \frac{2\omega_1\omega_2}{\omega_1 + \omega_2} \quad (2.22a) \quad \beta = \xi \frac{2}{\omega_1 + \omega_2} \quad (2.22b)$$

A typical plot of equation 2.21 is shown in Figure 2-4.

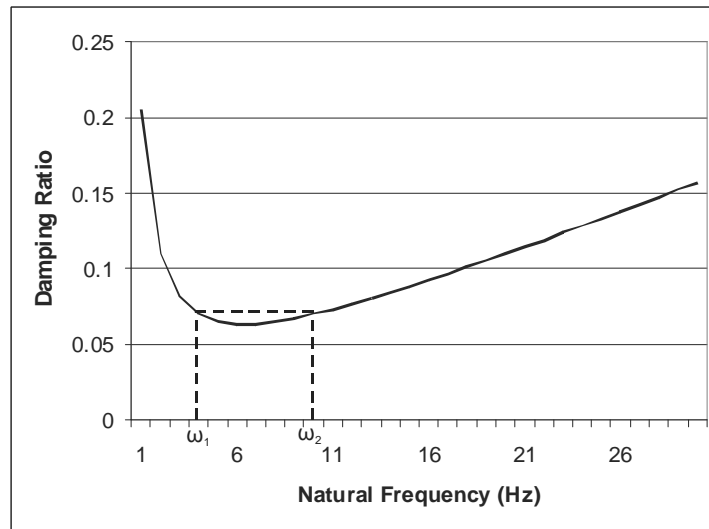


Figure 2-4 Typical plot of equation 2.21 for Rayleigh damping

Software packages (e.g. SAP2000) typically allow the user either to specify the damping coefficients directly, or to specify a damping ratio and two modal frequencies ω_1 and ω_2 as described above and shown in Figure 2-4. Unwanted vibrations or noise outside this range experience higher levels of damping.

2.1.3 Dynamic Analysis by Numerical Integration

The most general approach to determining the dynamic response of complex structural systems is to integrate the dynamic equilibrium equations directly. This usually involves the attempt to satisfy the dynamic equilibrium of the system at discrete time intervals, once the solution has been defined at time zero. Numerous techniques have been proposed, which can broadly be classified as either *explicit* or *implicit*. [24]

Explicit methods use the differential equation at time 't' to predict the solution at time 't+Δ', however the stability of the solution is very sensitive to the size of the time step and usually requires that very small time steps be used. Implicit methods require the solution to be solved at each time step 't', once the solution at 't-Δ' has been found. Larger time steps may be used and the system can be either conditionally or unconditionally stable. Wilson [24] recommends that only implicit, unconditionally stable methods be used for the step-by-step seismic analysis of structural systems.

The most commonly used method of analysis was developed by Newmark [15] and has been modified and improved by numerous researches. This method is used by SAP2000 and is used in this research.

The equilibrium equation, can be written as follows:

$$\mathbf{M}\ddot{\mathbf{u}}_t + \mathbf{C}\dot{\mathbf{u}}_t + \mathbf{K}\mathbf{u}_t = \mathbf{F}_t \quad (2.23)$$

where \mathbf{u} is a general displacement vector.

Newmark's equations are derived using a Taylor series and assume that the acceleration is linear within a time step. Newmark's equations in standard form are as follows:

$$\mathbf{u}_t = \mathbf{u}_{t-\Delta} + \Delta t \dot{\mathbf{u}}_{t-\Delta} + \left(\frac{1}{2} - \beta\right) \Delta t^2 \ddot{\mathbf{u}}_{t-\Delta} + \beta \Delta t^2 \ddot{\mathbf{u}}_t \quad (2.24)$$

$$\dot{\mathbf{u}}_t = \dot{\mathbf{u}}_{t-\Delta} + (1 - \gamma) \Delta t \ddot{\mathbf{u}}_{t-\Delta} + \gamma \Delta t \ddot{\mathbf{u}}_t \quad (2.25)$$

Equations 2.23, 2.24 and 2.25 are used iteratively at each time step to solve for each degree of freedom of the system. Wilson [25] formulated the method into a matrix form and eliminated the need for iteration.

Newmark's method is conditionally stable if:

$$\gamma \geq \frac{1}{2}, \beta \leq \frac{1}{2} \text{ and } \Delta t \leq \frac{1}{\omega_{\max} \sqrt{\gamma/2 - \beta}} \quad (2.26 \text{ a, b, c})$$

and is unconditionally stable if:

$$2\beta \geq \gamma \geq \frac{1}{2} \quad (2.27)$$

However, if γ is greater than 0.5, errors are introduced associated with 'numerical damping' and 'period elongation'.

Although the method may be stable if equation 2.27 is satisfied; if a particular structure contains natural periods smaller than the time step used, the response in these modes will not be computed. It is therefore essential that careful attention be paid to the time increment used, reducing this until no significant variations in the structure's response are evident.

2.2 Cable Theory

2.2.1 Static Analysis

One of the most important elements in correctly modelling guyed masts is a good understanding and modelling of the cable stays. Most of the nonlinearity in these types of structures stems from the nonlinear force–deflection relationship of the inclined cables. Under gravity loading, a flexible cable deforms into a catenary, and if the cable is taut this profile can be approximated as a parabola.

The length and typical forces of a free hanging cable subjected to uniform loading can be described by the following expressions reported in Buchholdt [26] and Irvine [28]. The expressions assume that the profile of the cable is flat, i.e. the ratio of sag to span is less than 1:8, and that the profile of the cable is therefore approximately parabolic. Independent finite element analyses have since shown that the expressions retain their validity with ratios as high as 1:5 or 1:4. [28]

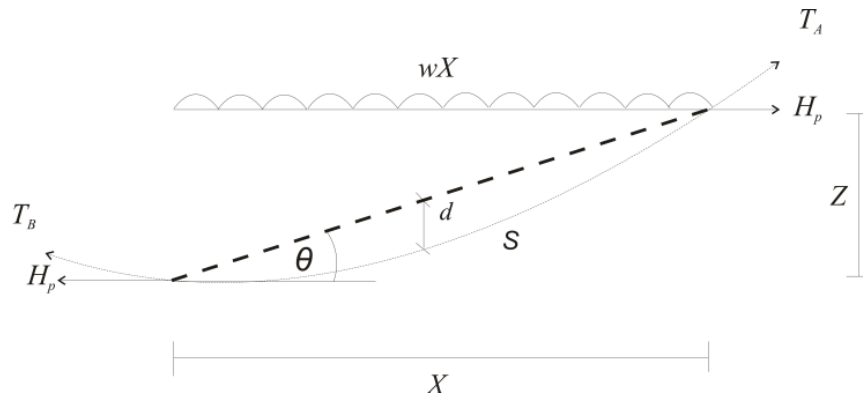


Figure 2-5 Simply supported cable with uniformly distributed load

$$S = X \left\{ 1 + \frac{8}{3} \left(\frac{d}{X} \right)^2 - \frac{32}{5} \left(\frac{d}{X} \right)^4 + \frac{1}{2} \left(\frac{Z}{X} \right)^2 - \frac{1}{8} \left(\frac{Z}{X} \right)^4 - \frac{4}{3} \left(\frac{d}{X} \right)^2 \left(\frac{Z}{X} \right)^2 \right\} \quad (2.28)$$

$$H_p = \frac{qX^2}{8d} \quad (2.29)$$

$$Q_A = H_p \left\{ 1 + \left(\frac{Z}{X} + \frac{4d}{X} \right)^2 \right\}^{1/2} \quad (2.30)$$

$$Q_B = H_p \left\{ 1 + \left(\frac{Z}{X} - \frac{4d}{X} \right)^2 \right\}^{1/2} \quad (2.31)$$

The static horizontal stiffness of cables primarily depends on two mechanisms:

- 1) changes in cable profile
- 2) elastic stretching of the cable as its tension varies.

The tauter the cable becomes, the more linear the stiffness becomes as the cable tends to behave increasingly like a rod. Much research has been done analysing this behaviour. Irvine [28] presented a theory that uses the parameter λ^2 to account for geometric and elastic effects:

$$\lambda^2 = \left(\frac{wL_c \cos \theta}{\bar{Q}} \right)^2 \frac{AEL / \bar{Q}}{L[1 + 8(wL_c^2 \cos \theta / 8\bar{Q}L_c)^2]} \approx 12 \frac{k_e}{k_g} \quad (2.32)$$

where

A cross sectional area of cable

E elastic modulus of cable

L_c length of the chord line joining cable ends

\bar{Q} average tension in cable $H_p / \cos \theta$

w weight of the cable per unit length

k_e, k_g elastic stretching component and cable profile component [19] defined by equations 2.34 and 2.35

This parameter describes the ratio between geometric and elastic effects. Higher values for λ^2 imply that geometric effects (changes in cable profile) govern the stiffness of the cable, whereas lower values imply that elastic stretching of the cable governs its stiffness. For example:

heavy inextensible metal cable – high value of λ^2

light taut flat cable – low value for λ^2

This parameter is used extensively in both static and dynamic cable theory.

The varying stiffness and in particular the varying horizontal stiffness of a cable is of fundamental importance to the behaviour of guyed masts. This relationship has been investigated by a number of researchers.

Sparling and Davenport [19] approximate the static horizontal stiffness k_x of a flat parabolic cable by:

$$k_x \approx \frac{1}{1/k_e + 1/k_g} \quad (2.33)$$

where k_e and k_g are the elastic stretching component and the cable profile component given by:

$$k_e = \frac{AE}{L_c} \cos^2 \theta \quad (2.34)$$

and $k_g = \frac{12\bar{Q}^3}{w^2 L_c^3} \quad (2.35)$

This relationship has been investigated by Goldberg and Gaunt [6] who showed that under uniform loading a cable deforms into a catenary and the arc length, S , of an inclined cable can be described by:

$$S = \left[\frac{4H_p^2}{w^2} \sinh^2 \left(\frac{wL_c \cos \theta}{2H_p} \right) + L_c^2 \sin^2 \theta \right]^{1/2} \quad (2.36)$$

A change in mean tension produces a change in arc length. When the end supports are displaced, the new cable force can be found iteratively using the above equation, as well as the following expression for arc length of the following step:

$$S = S_m + \frac{S_m}{A_c E_c} \left[\frac{H_p}{\cos \theta} - \left(\frac{H_p}{\cos \theta} \right)_m \right] \quad (2.37)$$

where

S_m arc length from previous step

$(H_p/\cos\theta)_m$ mean cable tension from previous step.

Davenport [2] gives an expression based on Dean's formula [4] for a catenary showing that for small deflections the cable horizontal stiffness can be written as:

$$k = k_t \left[\left\{ 1 - (0.38 + 0.04 \cos^2 \theta) r^2 \right\} + \frac{w^2 L^3 k_t}{12T^3} \left\{ 1 - 0.1r^2 \right\} \right]^{-1} \quad (2.38)$$

in which k_t is the horizontal stiffness of a taut wire (zero sag) given by:

$$k_t = \frac{EA \cos^2 \theta}{L_c} \quad (2.39)$$

and r is the ratio of the average cable weight to the average tension $\frac{wL_c}{Q}$.

Eurocode 8: Part 6 requires careful modelling of the cable stiffness. If the sag of the cable is significant, this should be accounted for by the use of an equivalent modulus of elasticity, E_{eq} . An iterative solution is required to show the cable force–deflection relationship, based on the following formula:

$$E_{eq} = \frac{E_c}{1 + \frac{(vL_c)^2}{12\sigma^3} E} \quad (2.40)$$

where

v specific weight of cable per unit volume

σ tensile stress in cable

E Youngs modulus of cable material

E_c Youngs modulus of cable, usually the same as E , but can be adjusted to take into account the wrapping effect of the cable strands according to:

$$E_c / E = \cos^3 V \quad (2.41)$$

where V is the wrapping angle of the single chords.

A plot of the force–deflection relationship using the above methods by Sparling *et al* [19], Goldberg *et al* [6], Davenport [2] and the method proposed by Eurocode 8: Part 6 for a typical inclined cable is shown in Figure 3-4 (section 3.2), in comparison to that of a simple model produced using SAP2000.

2.2.2 Dynamic Analysis

Dynamic cable behaviour has been investigated extensively by Irvine and Caughey [10]. Irvine [11] presented analytical expressions for the natural frequencies and mode shapes of taut inclined cables.

Dynamic cable behaviour can be divided as follows:

- Out of plane modes
- In plane modes (antisymmetric)
- In plane modes (symmetric)

Out of plane motion or swinging is uncoupled from in plane motion. No additional tension is generated during vibration, in which the only easily excited mode is its first pendulum mode. This motion is of little importance to a guyed mast analysis.

In plane modes are categorised as either purely geometrically symmetric or antisymmetric about the cable midpoint.

The lowest natural frequency of a perfectly taut elastic wire is given by Irvine [11] as:

$$\omega_0 = \frac{\pi}{L_c} \sqrt{\frac{Q}{m}} \quad (2.42)$$

where m is the mass per unit length.

When the sag of the cable is meaningful, natural frequencies for the antisymmetric modes can be obtained from the above taut wire equation by using the following relationship [11]:

$$\omega_n = 2n\omega_0 \quad n = 1, 2, 3, \dots \quad (2.43)$$

The relationship between symmetric modes and the taut wire modes is not constant and depends on the degree of tautness.

According to Irvine [11], the natural frequencies of symmetric modes can be found by finding the roots of the following equation:

$$\tan\left(\frac{\omega_n L_c}{2} \sqrt{\frac{m}{Q}}\right) = \left(\frac{\omega_n L_c}{2} \sqrt{\frac{m}{Q}}\right) - \frac{4}{\lambda^2} \left(\frac{\omega_n L_c}{2} \sqrt{\frac{m}{Q}}\right)^3 \quad (2.44)$$

Antisymmetric modes do not generate significant axial strain or changes in dynamic tension in the cable. They therefore interact very little with the structure and are generally ignored.

Figures 2-6 and 2-7 show the first two symmetric and antisymmetric cable mode shapes of a typical inclined cable.

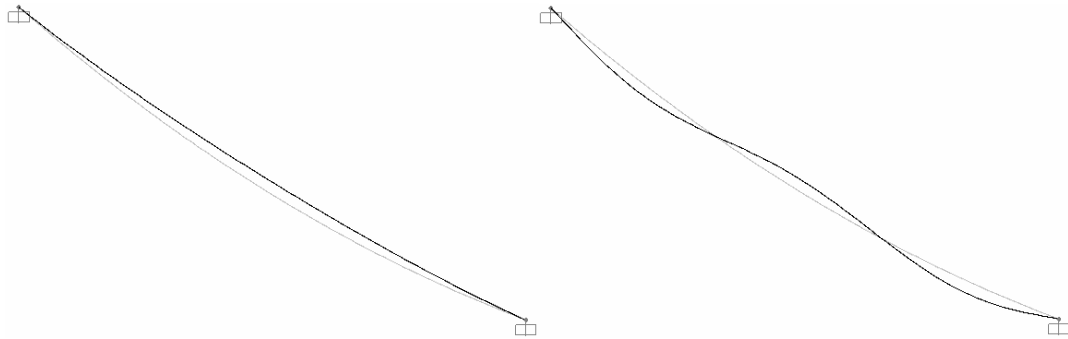


Figure 2-6 First two symmetric cable mode shapes

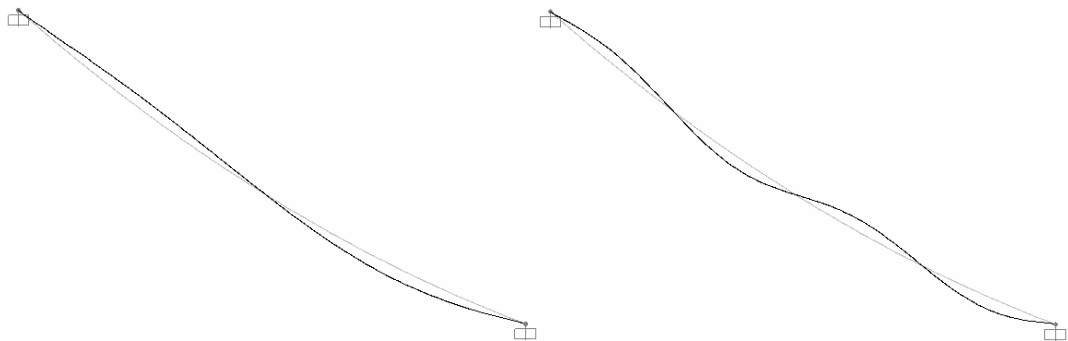


Figure 2-7 First two antisymmetric cable mode shapes

2.3 Earthquake Ground Motion and Spatial Variation of Motion

The measurement of seismic waves is fundamental to seismology and seismic analysis of structures. Three main types of waves propagate from the source of an earthquake:

- Primary waves – the fastest type of wave causing volumetric changes in the earth
- Secondary waves – shear the earth perpendicular to the direction of travel
- Love and Rayleigh waves – surface waves creating horizontal motion (Love waves) and horizontal and vertical motion (Rayleigh waves).

The interaction of these waves at the surface is extremely complicated, but the result is strong ground motion (i.e. accelerations, velocities and displacements). Earthquake locations and magnitudes are determined from measurements taken using seismographs installed all around the world. Engineering seismology is primarily concerned with motion that occurs up to 100km from the earthquake source (slightly more for large magnitude events), although there have been incidents where destructive motions have been caused at significantly larger distances, usually as a result of amplification by soft soil deposits.

Specifically designed seismographs, called accelerographs, produce records known as accelerograms which generally consist of three perpendicular components of motion (two horizontal, one vertical), registering the ground acceleration versus time. Large databases of these records are hosted by a number of websites (e.g. [33] and [34]) and individual records can be freely downloaded.

A number of parameters can be used to characterize earthquake ground motion. The peak ground acceleration (PGA) is the most commonly used and is simply the largest acceleration value in the time series. The corresponding peak ground velocity (PGV) and peak ground displacement (PGD), as well as the duration of motion and frequency content of motion are also important parameters. The energy content of ground motion can be described by the Arias intensity, which is the integral over time of the square of the acceleration:

$$AI = \frac{\pi}{2g} \int a(t)^2 dt \quad (2.45)$$

where $a(t)$ is the acceleration time history in units of g .

The software package Seismosignal (freely available from [36]) can be used to analyse all of these parameters. Different structures are excited by earthquakes in different ways, depending on the characteristics of each. However the peak ground acceleration and the duration of high amplitude ground motion are good indicators as to how destructive an earthquake will be.

Earthquake accelerograms measured at different positions within large engineering structures that occupy significant ground areas can be appreciably different. This is known as the Spatial Variation of Earthquake Ground Motion (SVEGM) and its causes include: [7]

- 1) *Wave passage effect* – Seismic waves arriving at different stations at different times.
- 2) *Incoherent effect* – Differences in superposition of waves from an extended source caused by irregularities and inhomogeneities along the path of the wave.
- 3) *Local site effect* – Differences in local soil conditions at each station may alter the amplitude and frequency.

The underlying ground type of the site is very important as it affects the travelling shear wave speed, the amplitude and frequency of groundmotion and the amount of damping introduced at the supports points due by movement of the footings.

SVEGM can be important as differential movement of supports can lead to a lateral ‘stretching’ or ‘compressing’ of a structure. A detailed assessment of these effects is beyond the scope of this research; however the *wave passage effect* is modelled by the use of a time delay of the excitations at various supports (stage 2). This effect is likely to be significant for guyed masts as the large distances between stay support points on the ground can generate significant differential movement, leading to a ‘snap’ type loading caused by rapid tightening of the cables.

Table 2-1 shows an extract from *Eurocode 8 part 1, Table 3.1: Ground types*, and describes the various properties of the relevant ground types to be used for design. Significant to this research is the shear wave speed parameter which is used in stage 2.

Ground Type	Description of Stratigraphic Profile	Parameters		
		$V_{s,30}$ (m/s)	N_{SPT} (blows/30cm)	c_u (kPa)
A	Rock or other rock-like geological formation, including at most 5m of weaker material at the surface.	> 800	-	-
B	Deposits of very dense sand, gravel, or very stiff clay, at least several tens of metres in thickness, characterized by a gradual increase of mechanical properties with depth.	360 - 800	> 50	>250
C	Deep deposits of dense or medium-dense sand, gravel or stiff clay with thickness from several tens to many hundreds of metres.	180 - 360	15 - 50	70-250
D	Deposits of loose-to-medium cohesionless soil (with or without cohesive layers), or of predominately soft-to-firm cohesive soil)	< 180	<15	<70

Table 2-1 Extract from Eurocode 8 Ground types (Table 3.1-Eurocode 8:1)

2.4 Overview of Relevant Sections of Eurocode 8: Part 1 and Part 6

Eurocode 8 applies to the design and construction of buildings and civil engineering works in seismic regions. Its purpose is to ensure that in the event of earthquakes:

- Human lives are protected
- Damage is limited
- Structures important for civil protection remain operational.

The code adopts a probabilistic approach with regard to the likelihood of significant seismic action and classifies structures in terms of their importance, as well as identifying various classes of failure, before determining design loadings. The specific magnitude of loading is obtained from the national annexe of the country, specific to the level of seismic activity of the region. Part 1 of Eurocode 8 outlines general rules and seismic actions for buildings and parts 2 to 6 outline specific provisions made for specialist structures, including Eurocode 8 part 6: Towers, Masts and Chimneys.

Eurocode 8 is a detailed design code, most of which is not applicable to this research. This section introduces techniques used in Eurocode 8 and summarises sections applicable to this research.

2.4.1 Response Spectrum

A response spectrum is a tool that designers commonly use in the design of buildings and other linear structures. It does not reflect the detailed time history response of a structure during an earthquake, but rather plots the peak response (acceleration, velocity, displacement) of a single degree of freedom structure to a particular earthquake, as a function of natural frequency (or period) and can be plotted for various damping ratios. Response spectra are used in simplified design procedures that estimate the peak response of a structure during seismic loading.

For design, the response spectra of many different earthquakes are combined into a smooth elastic response spectrum. The spectrum is adjusted according to underlying soil types and is scaled according to peak design acceleration. Softer ground types tend to amplify the peak ground acceleration and lengthen the period of groundmotion, thus increasing response of higher period structures. Figure 2-8 shows the EC8 elastic response spectrum for soil type C (defined in Table 2-1), scaled to a design acceleration of 3m/s^2 and 5% damping.

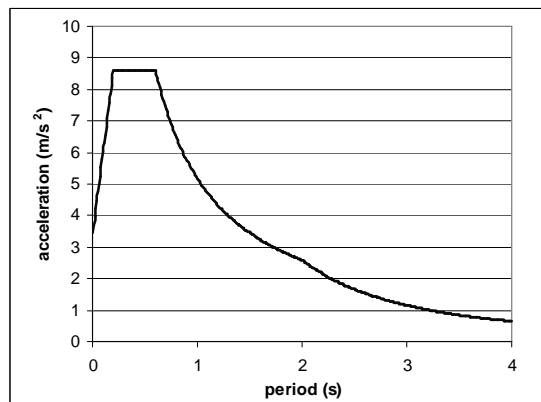


Figure 2-8 Type 1 elastic response spectrum for soil type C, design acceleration of 3m/s^2 , 5% damping

The use of an elastic response spectrum for design purposes is usually limited to linear structures whose response is governed by vibration in a small number of significant modes. Conventional structures in which failure occurs by distributed yielding are often designed using ductility modified spectra in which the response spectrum is reduced using a Q-factor to allow for energy dissipation during yielding. As most of the mass members operate

primarily under axial loading, any yielding that might take place is likely to lead to buckling, resulting in severe permanent deflections or even collapse. Yielding is therefore not usually allowed for in guyed masts, however a Q-factor of 1.5 is permitted by Eurocode8: part 6 for a response spectrum analysis of guyed masts which takes into account strain hardening and yield strength usually exceeding characteristic strength.

2.4.2 Modal Response Spectrum Analysis

This method is recommended by Eurocode 8 for every structure, with the seismic action defined by a response spectrum. The analysis is performed by applying horizontal forces to the lumped masses into which the structure has been divided and then calculating its response in each particular mode. The force applied to mass j , in mode i , calculated on the basis of a response spectrum is:

$$F_{ij} = \frac{L_i}{M_i} S(T)_i \phi_{ij} m_j \quad (2.46)$$

where

$S_d(T)_i$ the ordinate of the response spectrum for the period of vibration of mode i

L_i modal participating factor defined by equation 2.17

M_i modal mass defined by equation 2.18

The displacements for the i th mode can be calculated from:

$$u_{ij} = \frac{L_i}{M_i} S(T)_i \phi_{ij} m_j \frac{T_i^2}{4\pi^2} \quad (2.47)$$

where T_i is the period of the mode considered

Eurocode 8 requires that the following must be met:

- the sum of the effective modal masses for the modes taken into account amounts to at least 90% of the total mass of the structure.
- All modes with greater than 5% total mass participation must be taken into account.

The overall seismic response of any action shall be calculated by combining the response of the individual modes using the SRSS rule:

$$E_E = \sqrt{\sum E_i^2} \quad (2.48)$$

where

E_E is the seismic action effect under consideration (force, displacement etc.)

E_i is the value of the seismic action effect due to vibration mode i .

If modes are closely spaced such that their periods T_i and T_j (with $T_i < T_j$) do not satisfy the following condition:

$$T_i \leq 0.9T_j \quad (2.49)$$

more accurate combination procedures should be adopted, such as the Complete Quadratic Combination (CQC) (not detailed in EC8).

The CQC method of combination [23] is a relatively new method of modal combination based on random vibration theories and is used when coupling between closely spaced modes is likely and needs to be accounted for. The peak value of a response effect under consideration is estimated by the following double summation equation conducted across all modes:

$$E_E = \sqrt{\sum_n \sum_m E_n \rho_{nm} E_m} \quad (2.50)$$

where E_n is the modal response associated with mode n .

The cross modal coefficient ρ_{nm} with constant damping is:

$$\rho_{nm} = \frac{8\xi^2(1+f)f^{3/2}}{(1-f^2)^2 + 4\xi^2 f(1+f)^2} \quad (2.51)$$

where $f = \omega_n / \omega_m$ and must be equal to or less than 1.

2.4.3 Time History Representation

Eurocode 8 states that seismic motion may be represented by the use of ground acceleration time histories subject to a number of considerations stated in 3.2.3.1 of Eurocode 8. Artificial or recorded accelerograms can be used but need to be scaled accordingly to match the elastic

response spectrum for the particular soil type and design acceleration. The same accelerogram may not be used in both horizontal directions simultaneously.

2.4.4 Tension Limits

Eurocode 8: part 6 states that the stress in the cables due to the design seismic action shall be lower than the preload stress in the cable.

2.5 Guyed Mast Design Using BS8100-4:1995

At present British Standards require that guyed masts be designed according to BS8100-4, the code of practice for loading of guyed masts. The code covers dead, wind and ice loading and is applicable to bolted, riveted or welded metallic structures composed of leg members and triangular bracing. Portions of BS8100-4 are similar to BS6399-2, the code of practice for wind loading on buildings, in the determination of wind speeds, terrain factors etc.

The principles of limit state design are adopted throughout BS8100-4, and all dynamic loadings and response are approximated using an equivalent static load case. Factors of safety on wind and ice loading are applied to the design wind speed depending on the economic consequences of failure, or type of location. Additional factors of safety applied to design strength are based on a quality class described in BS8100-4. The following section summarizes the parts of BS8100-4 relevant to the wind loading analysis conducted in this research.

2.5.1 Overall Wind Resistance

The total resistance over a section of the mast is taken as:

$$\Sigma R_w = R_M + R_{AW} \quad (2.52)$$

where

R_M the wind resistance of the bare mast section

R_{AW} the wind resistance of the ancillaries

The resistance of the structure is calculated using drag coefficients for the lattice members that take into account the shielding effect of the windward members on the leeward members by the use of a solidity ratio.

The overall normal drag coefficient of a bare mast is given by:

$$C_N = C_{Nf} \frac{A_f}{A_F} + C_{Nc} \frac{A_c}{A_F} + C_{Nc'} \frac{A_{c'}}{A_F} \quad (2.53)$$

where

C_{Nf} , C_{Nc} , $C_{Nc'}$ are the overall normal drag coefficients for masts composed of flat sided, subcritical and supercritical circular members respectively, to be obtained from Figure 8 of BS8100-4

A_f the total projected area, when viewed normal to the face, of the flat-sided members in the face

A_c the total projected area, when viewed normal to the face, of the circular-sectioned members in the face in subcritical regimes

$A_{c'}$ the total projected area, when viewed normal to the face, of the circular-sectioned members in the face in supercritical regimes

A_F is the total projected area normal to the face

The resistance of a mast is given by:

$$R_M = K_\theta C_N A_s \quad (2.54)$$

where

A_s the total area projected normal to a face, of the structural components in the face within one section height of the mast at the level concerned

K_θ the wind incidence factor given in Figure 7 of BS8100-4

The resistance of linear and discrete ancillaries is calculated in a similar manner using drag coefficients and incidence angles. In addition a reduction factor K_A is used to take into account any shielding of the ancillary by the mast itself. The resistance of the guys is also calculated in a similar way.

2.5.2 Mean Load Effects

The wind load on the mast due to a mean hourly wind speed V_z in the direction of the wind should be taken as:

$$\bar{P}_{MW} = \frac{\rho_a}{2} V_z^2 \sum R_W \quad (2.55)$$

and the load on the guys in the plane containing the wind and the guy should be taken as:

$$\bar{P}_{GW} = \frac{\rho_a}{2} V_z^2 \sum R_G \quad (2.56)$$

where R_G is the resistance of the guys and ρ_a is the density of the air at the reference temperature and pressure ($\rho_a = 1.22\text{kg/m}^3$ for the UK).

2.5.3 Dynamic Loading

The dynamic response of the mast due to wind loading is simplified to a static analysis by the use of a series of successive patch loads. Each patch load is applied individually to the mast in its equilibrium position, under mean hourly wind load, and their effect is combined using the root sum of squares to calculate the effective dynamic response.

These successive patch loads are applied as follows:

- a) On each span of the mast between adjacent guy levels (separately)
- b) Over the cantilever if relevant
- c) From midpoint to midpoint of adjacent spans (separately)
- d) From the base to the mid-height of the first guy level
- e) From the mid-height of the span between the penultimate and the top guy and the top of the mast.

This arrangement of patch loads can mean that a typical mast with four stay levels could have as many as 10 patch load cases in addition to the mean load case.

The patch load is given by:

$$P_{MW} = \rho a i_0 V_z V_{10} \sum R_w \left[\frac{1}{1 + S_{h=10}} \right] \quad (2.57)$$

where

$S_{h=10}$ is the topography factor determined in accordance with section 3.2.4 (BS8100-4) for $h = 10$

V_{10} is the mean hourly wind speed at an effective height of 10m

i_0 is the turbulence intensity and is given in Figure 15 in BS8100-4 according to site terrain

For all patch loading cases the loading on each guy in the plane containing the wind and the guy should be calculated from:

$$P_G = \frac{p_a}{2} V_z^2 R_G \frac{[(1 + K_c K_T K_L)^{0.5} + S_h]^2}{(1 + S_h)^2} \quad (2.58)$$

where

K_c is a turbulence factor given in Figure 16 of BS8100-4

K_L is a length factor given in Figure 11 of BS8100-4

K_T is a terrain factor given in Figure 17 of BS8100-4

The response of the mast must be calculated under each successive patch load case. The overall response under patch loading is calculated by the root sum of squares of the mast's response under each individual patch load.

$$r_{PL} = \sqrt{\sum_{j=1}^N r_{PLj}^2} \quad (2.59)$$

where

r_{PL} is the load response from the jth load pattern

N is the total number of load patterns required

r_{PLj} is the total effective load effect of the patch loads

The equivalent dynamic load for design purposes is then calculated from:

$$F'_M = \delta r_{PL} \quad (2.60)$$

Where δ can either be calculated according to Annexe N of BS8100-4, or conservatively taken as 3.78.

2.5.4 Total Design Load Effect

The total load effect for each component of the mast column should be determined from:

$$\sum F_M = F_0 + \bar{F}_M \pm F'_M \quad (2.61)$$

where

F_0 is the still air load effect

\bar{F}_M is the hourly mean load effect

F'_M is the fluctuating load effect

3 Modelling Methods and Assumptions

In order to accurately model the masts a number of initial assumptions needed to be made and validated. The following chapter describes these assumptions with respect to the mast, cables and the model as a whole. The linear and nonlinear static and dynamic analysis finite element software, SAP2000, is used throughout this research. The analysis options were set to allow a large displacement, nonlinear geometric stiffness in all cases.

3.1 Mast Assumptions

Much research (described in section 1.2) has been undertaken into the modelling of a spatial lattice mast as an equivalent beam element. The self weight of a lattice truss is substantially different to that of a beam element with similar behavioural properties. In order to control the dead load and mass of the mast, the self weight and mass of the mast (calculated from section properties of the equivalent beam) were set to zero. The correct values, calculated from the original lattice mast were then applied as additional loadings and masses to the mast. All ancillary masses and loadings were applied in a similar manner.

The equivalent beam stiffnesses for the masts used in this research had already been calculated by ‘in house’ software at Flint and Neill Partnership (FNP) and were supplied to the author. Although a small amount of directional stiffness variation can be observed because of unsymmetrical bracing arrangements, it is generally considered negligible, and the stiffness in each direction is assigned the same value. A validation analysis was performed in order to verify the use of a beam model in preference to the more complicated lattice model, as well as to check the mast stiffnesses supplied by Flint and Neill Partnership.

3.1.1 Static Load case Comparison of Beam Model

A single section from the bottom span of mast A (100m mast with 3 stay levels introduced in chapter 4) was used for this comparison and modelled as both a cantilevered lattice (actual members) and a cantilevered beam (with section properties supplied by FNP). A load of 15kN was then applied at different heights and the corresponding displacement at that height

recorded. The bending stiffness was then calculated based on this deflection. Results are shown in Table 3-1 and Figure 3-1.

Load Height (m)	Unit Load (KN)	E	Lattice Model		Beam Model		% Difference	
			Deflection (m)	I (m ⁴)	Deflection (m)	I (m ⁴)		
15	15	2.E+08	0.013	6.30E-03	0.013	6.71E-03	6.12	
30	15	2.E+08	0.094	7.20E-03	0.093	7.27E-03	0.88	
45	15	2.E+08	0.309	7.38E-03	0.309	7.38E-03	0.09	
60	15	2.E+08	0.727	7.43E-03	0.728	7.42E-03	-0.15	
75	15	2.E+08	1.414	7.46E-03	1.418	7.44E-03	-0.26	
90	15	2.E+08	2.439	7.48E-03	2.447	7.45E-03	-0.31	
105	15	2.E+08	3.869	7.48E-03	3.882	7.46E-03	-0.34	
						FNP	7.51E-03	

Table 3-1 Results of static bending comparison for lattice and beam models

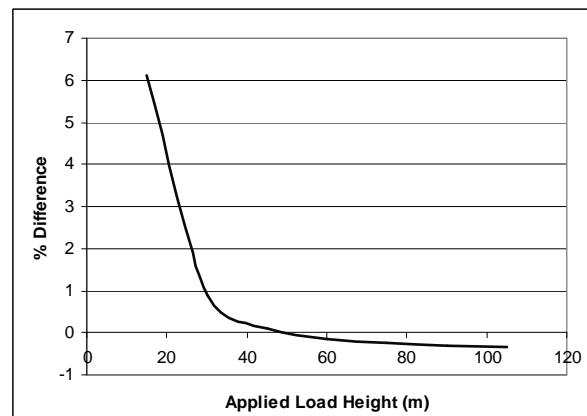


Figure 3-1 Percentage difference between the lattice and beam models

At heights below 15m it is likely that shear stiffness influences deflections and the bending stiffness calculated may not be entirely accurate. It also implies that the beam model may not be appropriate as deflection values differ by up to 6% and possibly more at lower heights. However, as the height of the applied load increases and bending stiffness of the model dominates its behaviour, the deflection values quickly converge to a difference of below 1%. The smallest span on a mast analysed in this research is 29.88m (implying a maximum difference of approximately 1% on Figure 3-1) and the shortest total mast height is 99.88m. In addition to the presence of long spans, cable supports that allow considerable movement provide additional flexibility in these regions. It can therefore be concluded that mast

behaviour in this research is likely to be governed by bending behaviour and the equivalent beam model is suitable for a static analysis.

3.1.2 Modal Comparison of Beam Model

A modal analysis was also undertaken on both the lattice and the beam cantilever models with a height of 105m. A comparison of the results is shown in Table 3-2.

Mode	Lattice Model			Beam Model			Difference (Hz)	% Difference
	Period (s)	Frequency (Hz)	% Mass Contribution	Period (s)	Frequency (Hz)	% Mass Contribution		
1	6.90	0.15	61.71	6.90	0.14	65.47	0.01	0.07
2	1.11	0.90	19.08	1.13	0.89	20.45	0.01	1.51
3	0.40	2.48	6.62	0.41	2.42	7.07	0.06	2.30
4	0.21	4.74	3.43	0.22	4.60	3.59	0.14	3.05
5	0.13	7.60	2.11	0.14	7.24	2.03	0.36	4.77

Table 3-2 Results of modal comparison for lattice and beam models

It can be clearly seen that for any important bending modes contributing more than 3% mass participation to the mode, there is little difference in the frequency of the vibration of the mode for the lattice and beam models.

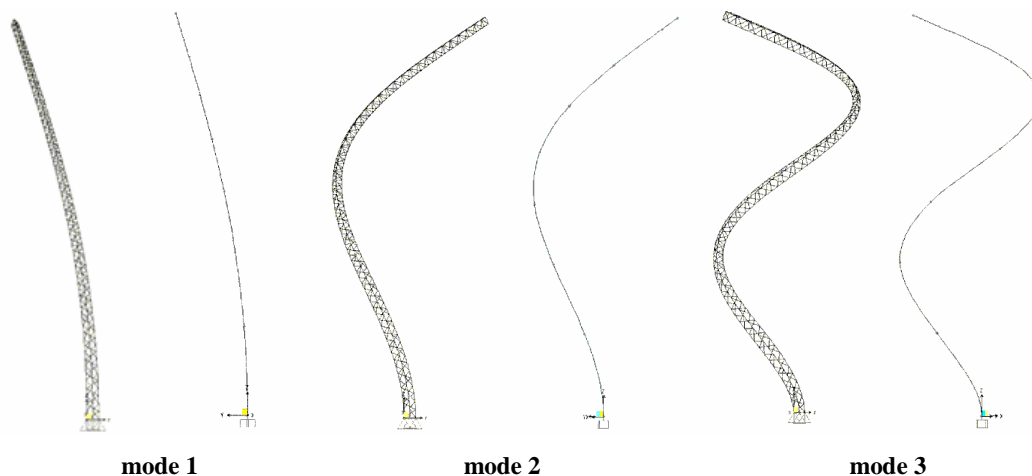


Figure 3-2 Lattice and beam cantilever mode shapes

Figure 3-2 shows that in addition to very similar natural frequencies, the mode shapes of the first three modes from the lattice and beam models are identical.

From the results of the static and modal validation analyses it was concluded that for this research, the mast lattice framework could be replaced by a beam element with similar properties.

3.2 Cable Modelling Methods and Assumptions

Much investigation was conducted into how cables were modelled using SAP2000, as their nonlinear behaviour is crucial in the modelling of guyed masts. SAP2000 analyses cables using a standard frame element with the following modifications.

- The bending stiffness of the ‘effective rod’ is reduced by a modification factor to accurately reflect the bending stiffness of the cables. Much research has been done by Raoof *et al* [16] in the area of bending stiffnesses of spiral strand cables, however this largely relates to the interaction between cable strands and the changing properties of the cable as it flexes. It is therefore of minimal use to this research as a single modification factor is needed by SAP2000.
- A compression limit can be set to zero, however this can lead to difficulties in convergence when running time history analyses. In practice, the use of this limit is unnecessary as the cable (with reduced cable stiffness) will simply buckle when compressed.
- The initial cable geometry is defined using standard cable formulae and was verified using equations 2.28-2.31 in section 2.2.
- The model is analysed using a full large displacement analysis to effectively model the geometric nonlinear effects. This implies that the stiffness matrix is recalculated at multiple stages during a static analysis; or at each time step during a time history analysis.
- To accurately model the cable profile, cables typically consisted of between 80 and 250 elements

The way in which SAP2000 models the force–deflection relationship of an inclined cable was investigated in comparison to a number of the analytical models introduced in section

2.2.1. A simple inclined cable (Figure 3-3) was modelled and its top support displaced horizontally. The results are plotted in Figure 3-4.

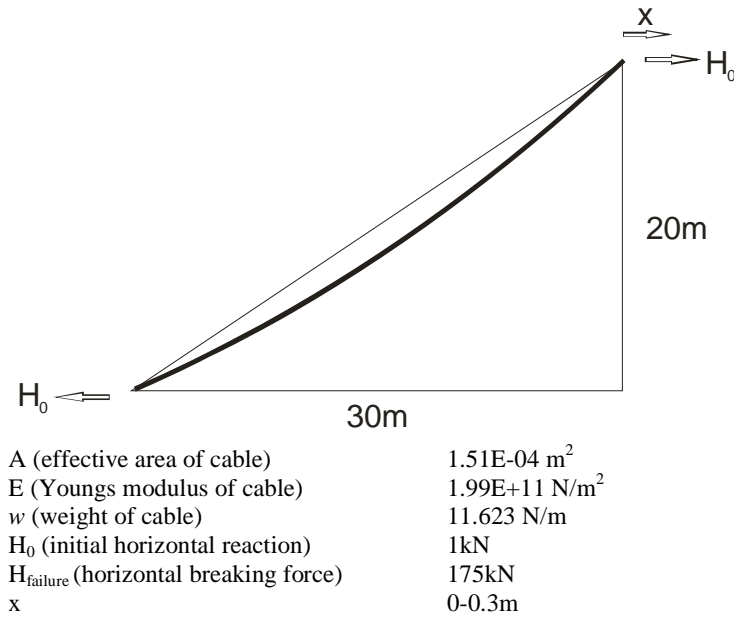


Figure 3-3 Simple inclined cable

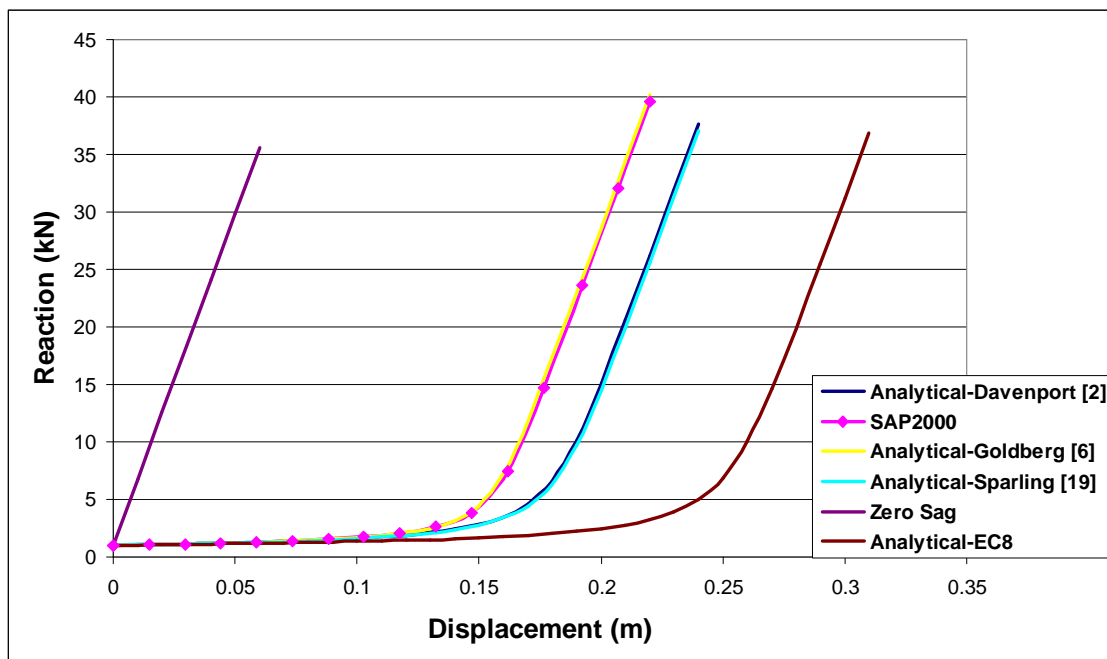


Figure 3-4 Plot of force–deflection relationship for an inclined cable using various models

It can be seen in Figure 3-4 that the SAP2000 model response is similar to that of the analytical method described by Goldberg and Gaunt [6]. This is the most accurate method that models the cable deformation as a catenary and not the usually assumed parabolic profile. It is also not limited to small deflections.

In all the methods the behaviour of a cable can be divided into three stages:

- 1) Almost linear behaviour up to a point, with very little increase in force. This stage is characterized by a flexible cable hanging in a catenary.
- 2) A period of marked nonlinearity with sharp increase in force as the cable starts to behave like a rod. The profile of the cable becomes straight.
- 3) A more linear behaviour similar to a taut rod i.e. zero sag.

All methods show reasonable agreement in the initial and final stiffnesses. What is of interest is that the onset of the nonlinear stage for the formulae described in Eurocode 8 part 6 is significantly later than the other methods. The significance of this is beyond the scope of this research, however is likely that when used in static analyses, deflection will be overestimated resulting in a conservative design. This certainly deserves investigation.

The above model was then analysed a number of times with different bending stiffness modification factors applied to the cable 'rod' properties, ranging from 0.1-1. It was found that even with this large range of modification factors, there was no appreciable change in the force–deflection relationship for the cable. A modal analysis was also performed on the model with the same range of modification factors. Again no appreciable change in natural frequencies for the first five modes was observed. A modification factor of 0.5 was chosen for all analyses, as this represented a substantial reduction in bending stiffness to encourage more 'cable like' behaviour, without reducing it too much so as to hinder the likelihood of convergence during analyses (early time history analyses suggested this).

3.2.1 Pretension

The cable geometry is chosen based on the initial pretension force and defined by SAP2000 using standard cable theory with corresponding forces described by equations 2.28-2.31. However, when the analysis is run, the self weight of the cable stretches it and the resulting increase in sag reduces the necessary tension. In addition to this loss of tension, the mast compresses under any loading and reduces the tension in the cables even further. It is therefore necessary to introduce an additional temperature load to control the tensile load of the cables effectively. The process of obtaining the correct pretension in all of the cables becomes an iterative one, in which the cable temperature loads are adjusted until the correct pretensions are reached in all cables.

3.3 General Assumptions

Cables are typically connected to the outer members of the lattice, producing an offset from the centre of the mast. It was found that this significantly complicated the analysis procedure and it was decided that the offset would be omitted and the cables assumed to be connected to the centroid of the mast. As the lateral bending and shear response are of primary interest it is unlikely that this assumption will have a significant effect on the overall behaviour of the mast; however the additional eccentric moment ($P-\Delta$ effect) introduced at stay connection points will not be accounted for. Early analyses that included this effect showed that the bending response was offset by the amount of the eccentric moment, however in relation to the overall bending in the masts was minimal.

A number of the mast models supplied had unsymmetrical cable anchor points (varying heights and radii), indicating that the mast was built on a slight slope. This also complicated the model considerably; in particular the iterative process of acquiring the correct cable pretensions, and it was decided to use an average value of radius and height for the anchor points of a particular stay level. In comparison to the scale of the masts these alterations in geometry of the structure are minor and their effect is likely to be insignificant.

The base of the mast was modelled as resistant to motion in all three directions, resistant to torsional rotation, but free to rotate about the X and Y axes. This assumption is in keeping

with the original mast design assumptions and due to its slenderness and relatively low lateral stability, is accurate in describing its behaviour.

All material is assumed to behave in the linear elastic range. A Q-factor of 1.5 is permitted by Eurocode8: part 6 for a response spectrum analysis of guyed masts, however as yielding is not allowed for in a BS8100-4 wind analysis, its allowance in the seismic analyses in this study would result in a futile comparison. Accurate modelling of this effect in a time history analysis in SAP2000 also has significant limitations.

4 Masts Used for Analysis

In order to assess the response of masts designed to current standards, existing masts in the UK were used for the analysis, rather than designing a generic mast, as these represented a more realistic representation of masts in the broadcasting industry. Data based on four existing guyed masts in the UK was supplied by Flint and Neill Partnership, a leading London based consultancy that has designed and analysed many masts in the UK and was largely involved in the development of BS8100-4, the code of practice for loading of guyed masts. Details relating to the original designer, owner or location of the masts were not supplied for confidentiality reasons, but all masts conformed to BS8100-4.

4.1 Mast Geometry

All four masts are triangular lattice in form, ranging in height from 99.88m to 313.6m. The geometry of the masts is summarised in Table 4-1. Guyed towers taller than 150m usually provide economical solutions over their free-standing counterparts. With three towers above this limit and one below, any changes in mast behaviour over this range can be assessed. Table 4-1 also gives an average panel width, along with the average mast mass (structure only) to give an indication of the relative member sizing (and number) of the masts. It should be noted that mast A, a more recent design, uses high strength steel (yield stress 355 N/mm²) and tubular members for the main mast members, whereas the remaining towers utilize solid rod members with yield stresses closer to 240 N/mm².

	Mast Height (m)	Type	No. of Stay levels	No. of Anchor Groups	Average Panel Width (m)	Average Mast Mass (kg/m)	Average Span (excluding cantilever) (m)	Outer Support Radius (m)
Mast A	99.88	Triangular Lattice	3	1	2.10	138.55	29.96	44.65
Mast B	245.00	Triangular Lattice	5	3	1.98	348.92	46.94	176.9
Mast C	239.30	Triangular Lattice	4	2	2.40	369.15	57.42	238.5
Mast D	313.60	Triangular Lattice	5	3	2.44	357.85	61.64	267.6

Table 4-1 Geometry of masts analysed

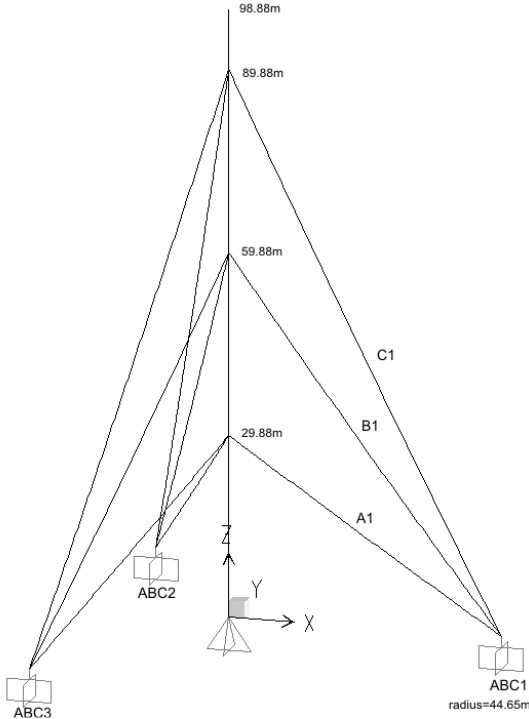


Figure 4-1 Mast A – geometry

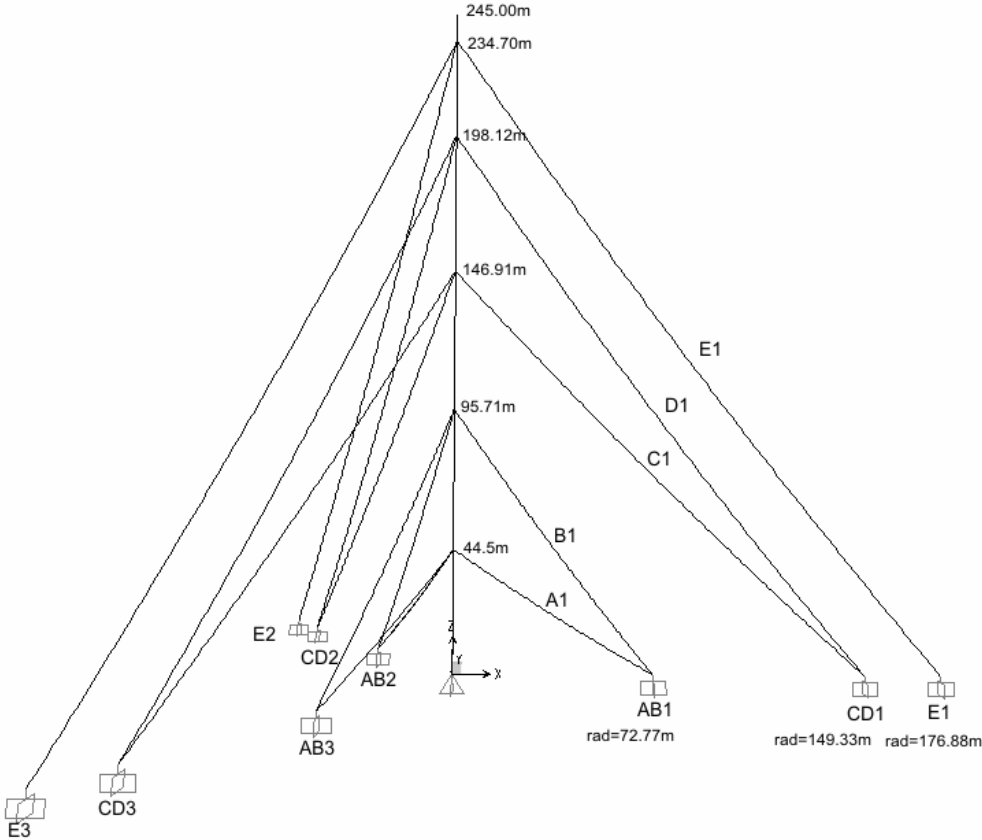


Figure 4-2 Mast B – geometry

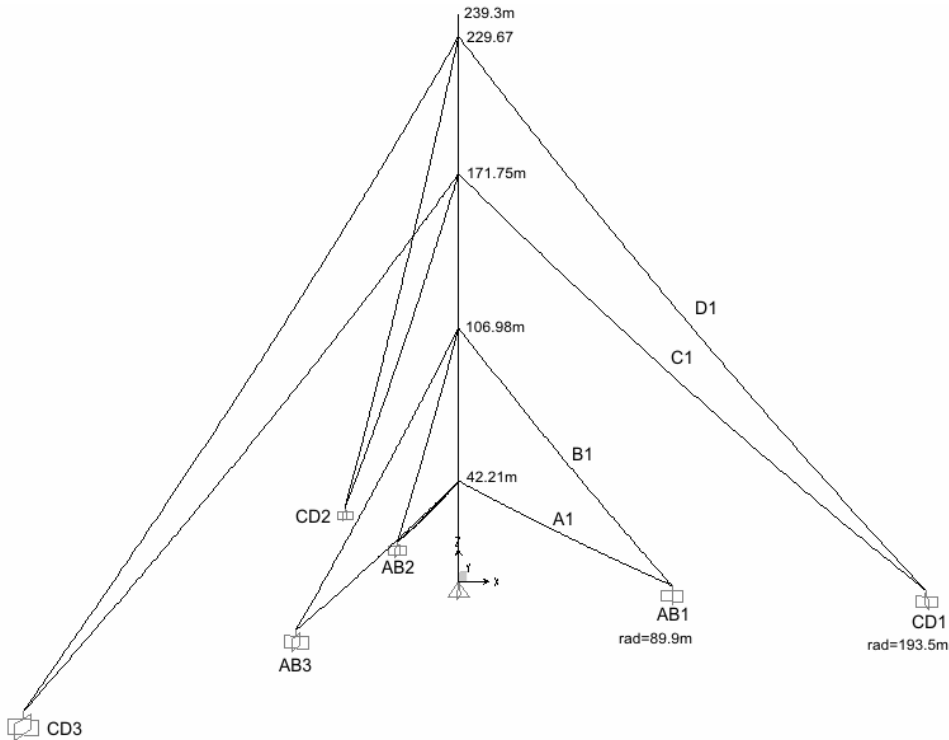


Figure 4-3 Mast C – geometry



Figure 4-4 Mast D – geometry

4.2 Mass Breakdown of Masts

In addition to the various static load cases to be considered for design, the distribution of mass is important in the determination of the various vibration modes of a structure. The primary reason for the existence of guyed masts is to support ancillaries for the telecommunications industry. It is therefore unwise to analyse these structures without this extra mass loading, as a number of previous studies have done. Hensely [8] showed that mast response is more susceptible to variations in mast mass than mast stiffness which further emphasizes this point.

A breakdown of the total mass for each mast is shown in Table 4-2.

Mast	Mass Component	Mass (kg)	Percentage of Total
A (99.88m)	Cable	5801	18.55
	Mast	13839	44.26
	Other	11628	37.19
	Total	31269	
B (245m)	Cable	20620	16.29
	Mast	85486	67.52
	Other	20508	16.20
	Total	126614	
C (239.3m)	Cable	18663	13.97
	Mast	88338	66.14
	Other	26567	19.89
	Total	133568	
D (313.6m)	Cable	46954	27.79
	Mast	112223	66.41
	Other	9804	5.80
	Total	168981	

Table 4-2 Mass breakdown of masts

The percentage of the total mass due to the cables ranges from approximately 14% to 28%. Generally this percentage increases with mast height, with the exception of mast A which has a relatively high cable mass. This might be explained by the relatively low mast mass (rather than high cable mass) due to the use of efficient high strength tubular members. As one would expect the percentage ancillary load carried by the shortest mast is the highest

(37%), whereas masts B and C are between 16% and 20%. Mast D (5%), at 313.6m, appears to be far less efficient carrying the least additional load of all the masts. As the tower height increases more of the member strength is needed to support the self weight of the structure and resist lateral loads due to increasing span lengths. Cable support radii need to be increased to be able to provide adequate lateral stiffness and consequently cable strengths (and therefore weights) need to be increased to support the self weight of the cable over such large spans. Mast D seems to be approaching some upper limit in the ability of the design to carry load.

A graphical representation of the mass distribution and breakdown over the length of each mast can be found in Figures 4-5 to 4-8 overleaf. It can be seen that most of the irregular distribution of mass is located at or near stay support levels (represented by dotted lines) and is caused by both the additional structural mass needed in these regions as well as ancillary point loads. In addition to these areas, the cantilevers of masts B, C and D have high concentrations of mass. The relatively low additional loading on mast D is clearly evident in Figure 4-8.

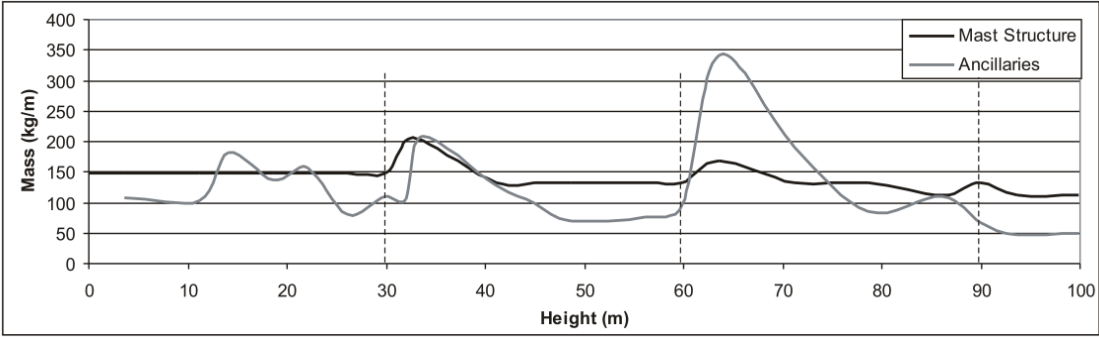


Figure 4-5 Mast A – mass distribution

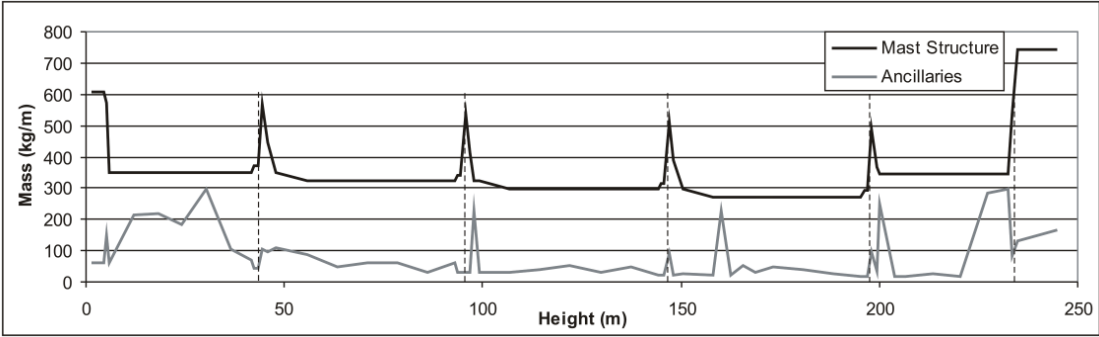


Figure 4-6 Mast B – mass distribution

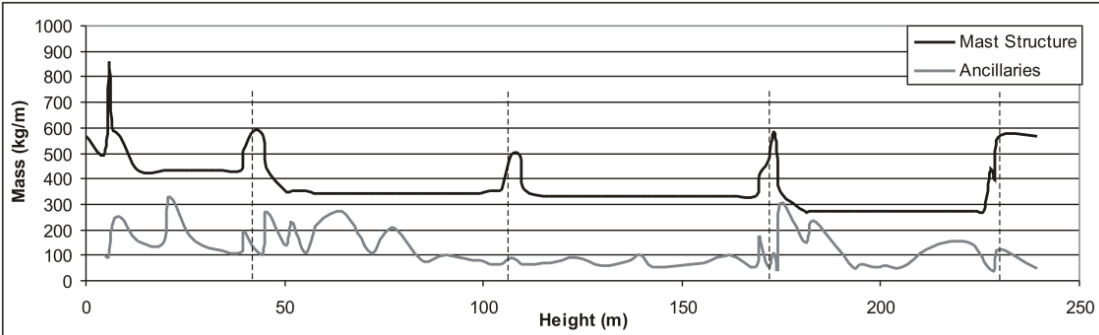


Figure 4-7 Mast C – mass distribution

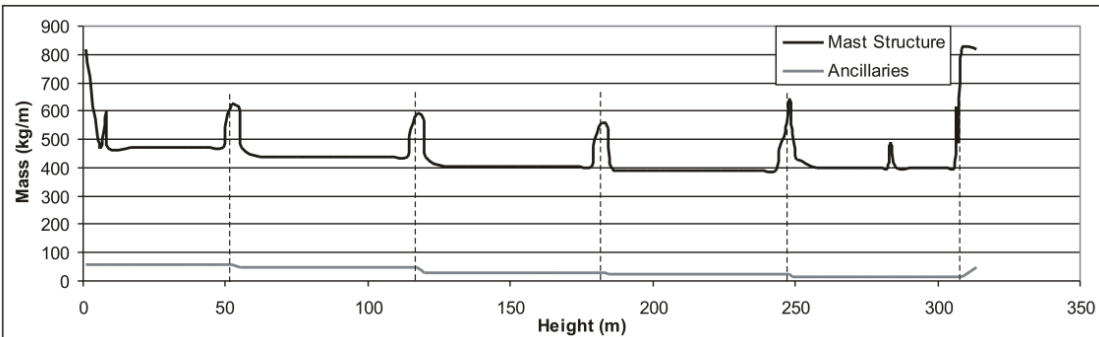


Figure 4-8 Mast D – mass distribution

4.3 Stay Pretension

A pretensile force of 10% of the breaking force of the cable is commonly used as a guideline for design. Previous studies by Amiri [1] used this threshold as a parameter to describe a ‘typical’ mast and suggested a formula to estimate the fundamental natural period of a mast, relative to its height, provided its initial cable tensions were close to this limit. It also showed that mast axial force was more susceptible to increases in dynamic tension (during a seismic analysis) if the initial tension was below this limit. This guideline design tension is low enough to ensure that the steel cables will not be prone to fatigue failure over time when subjected to repeated loading. All the masts considered are well below this limit and many may be considered slack if the above guideline was used, however the relative stiffness and stiffness utilization (described in section 4.4) is a far better description of relative cable tautness as it does not depend on the failure load of the cable. Table 4-3 shows the nominal cable diameters used and Table 4-4 shows the ultimate tensile load (UTL) and pretension force for the various mast stays.

Mast	Stay level				
	A	B	C	D	E
A	30.0	45.0	45.0	N/A	N/A
B	32.0	42.0	31.8	47.6	31.8
C	40.0	44.5	44.5	35.0	N/A
D	34.9	47.6	50.8	57.2	41.3

Table 4-3 Nominal cable diameters (mm)

		A (Level 1)	B (Level 2)	C (Level 3)	D (Level 4)	E (Level5)
Mast A	Pretension (kN)	78.48	98.10	127.53	N/A	N/A
	UTL (kN)	822.10	1957.00	1957.00	N/A	N/A
	% of UTL	9.55	5.01	6.52	N/A	N/A
Mast B	Pretension (kN)	41.69	65.55	76.27	142.25	84.33
	UTL (kN)	864.26	1446.98	847.19	1983.43	847.19
	% of UTL	4.82	4.53	9.00	7.17	9.95
Mast C	Pretension (kN)	88.83	107.03	152.06	103.01	N/A
	UTL (kN)	1393.02	1654.59	1654.59	1103.63	N/A
	% of UTL	6.38	6.47	9.19	9.33	N/A
Mast D	Pretension (kN)	100.71	112.99	147.38	222.44	108.08
	UTL (kN)	1036.56	1784.09	1943.56	2571.48	1435.24
	% of UTL	9.72	6.33	7.58	8.65	7.53

Table 4-4 Initial pretension force and UTL of stays

4.4 Relative Horizontal Stiffness of Stays

The correct modelling of the nonlinear lateral stiffness of the stays is fundamental in the analysis of guyed towers. In order to compare the equivalent lateral stiffness of each mast an equivalent linear stiffness was calculated for each stay based on equations 2.36 and 2.37 presented by Goldberg *et al* [6] for force displacement relationship of a cable (the same relationship as used by SAP2000). An initial displacement of 10mm was used to calculate an effective linear stiffness k under initial conditions. This was compared to the stiffness of a rod k_0 (i.e. with zero sag) under the same conditions, the ratio k/k_0 giving a comparable stiffness utilization for each cable.

Mast	Stay level	A (level 1)	B (level 2)	C (level 3)	D (level 4)	E (level 5)
Mast A (99.88m)	Anchor Point	Inner	Inner	Inner	N/A	N/A
	k (N/m)	1147600	791600	360000	N/A	N/A
	k_0 (N/m)	1192377	979166	403685	N/A	N/A
	$(k/k_0)\%$	96	81	89	N/A	N/A
Mast B (245m)	Anchor Point	Inner	Inner	Intermediate	Intermediate	Outer
	k (N/m)	347800	202200	122500	127700	62700
	k_0 (N/m)	842674	501705	211419	293054	107577
	$(k/k_0)\%$	41	40	58	44	58
Mast C (239.3m)	Anchor Point	Inner	Inner	Outer	Outer	
	k (N/m)	763300	309900	179800	80800	N/A
	k_0 (N/m)	1193960	508514	364405	150198	N/A
	$(k/k_0)\%$	64	61	49	54	N/A
Mast D (313.6m)	Anchor Point	Inner	Inner	Intermediate	Outer	Outer
	k (N/m)	397200	207000	101300	80000	28200
	k_0 (N/m)	569991	402609	290428	256764	101758
	$(k/k_0)\%$	70	51	35	31	28

Table 4-5 Cable horizontal stiffnesses

As expected the stiffness utilization tends to decrease with increased cable length and increased support radius. Horizontal stiffness tends to decrease with height, but increase with support radius. This generally means that the higher stays are less efficient and requires that anchor points for the higher stay levels are further away from the mast to generate significant stiffness.

Although the stiffness utilizations described by Table 4-5 indicate that most of the cables are initially in the nonlinear range described by Figure 3-4, the overall lateral stiffness of the masts is more linear than might be suggested by this. Movement of the stay support points involves the loading (stiffening) of cables on the side away from the direction of movement,

and unloading (reducing stiffness) on the side in the direction of movement. The nonlinear effect of loading and unloading of individual cables is somewhat balanced by the unloading and loading of cables on the opposite side of the mast. Figures 4-9 and 4-10 show the overall force–deflection relationship of the stay level points in the X direction for the various masts. Included on the graphs for comparison are the effective linear force–deflection relationships based on the stiffness after pretension.

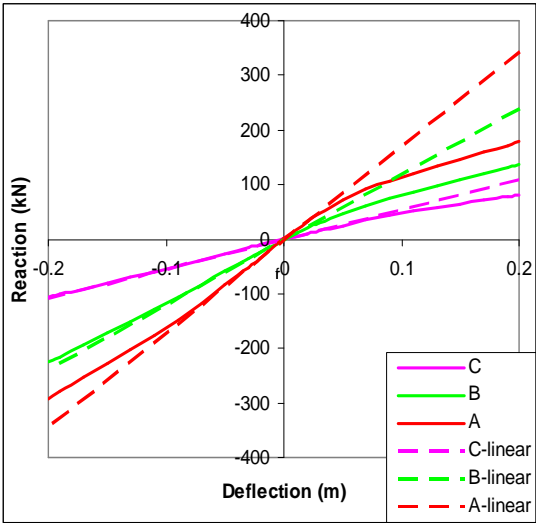


Figure 4-9 Mast A Stay level force–deflection

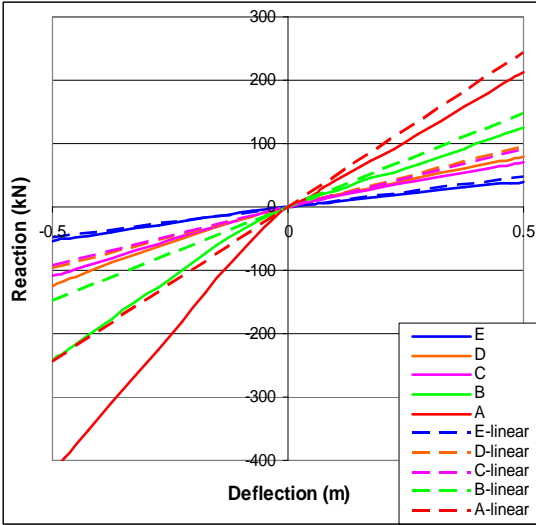


Figure 4-10 Masts B Stay level force–deflection

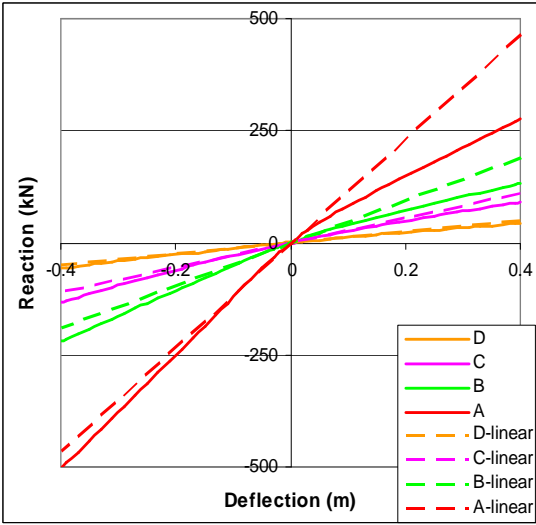


Figure 4-11 Mast C Stay level force–deflection

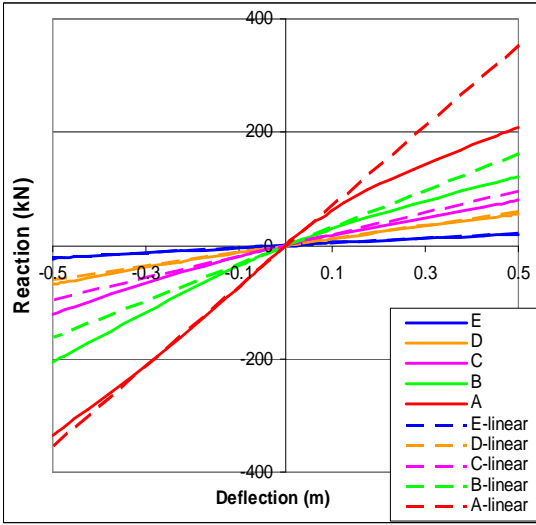


Figure 4-12 Mast D Stay level force–deflection

5 Modal Analysis

5.1 Introduction and Methodology

A linear modal analysis was performed on each model based on the stiffness at the end of the nonlinear pretension load case. Although the mode shapes and frequencies would be different if the analysis was conducted with the mast in a deformed position, this is still a useful analysis as it gives some insight into the initial behaviour of the mast before any nonlinear cable effects are induced.

The mass of the cables contributes between 15% and 30% to the overall mass of the structure and thus has a significant effect on its vibration modes. It also makes it extremely difficult to differentiate between ‘mast modes’, ‘cable modes’, and modes that are a combination of the two. By running analyses with the cable mass set to zero, it is possible to get a feel for which modes are essentially ‘mast’ modes and therefore of interest. The percentage contribution of total mass to the mode is also a key feature in determining which modes are of interest to the behaviour of the mast. SAP2000 calculates the mass participation of each mode using the method described in section 2.1.2.2. The user sets the number of modes (in order of increasing frequency) to be calculated and the percentage mass participation to be achieved (typically 99%). During the analysis SAP2000 calculates modes until one of these conditions has been satisfied.

Bending modes typically occur in orthogonal pairs (as the initial stiffness is the same about both the X and Y axes). The presence of the cables makes it necessary for a large number of modes to be calculated in order to achieve 99% mass participation (usually between 100 to 200 modes). With the large number of modes calculated, it was necessary to identify a percentage mass contribution, below which a mode was not deemed significant. A mass participation ratio of 5% was identified as a suitable minimum limit as this was deemed low enough to cover major modes, and excluded a large number of minor modes below this ratio, particularly in the 3% to 5% range. Eurocode 8 part 1 also identifies 5% mass participation as a cut-off, above which modes should be considered for a response spectrum analysis. This identified between three and eight modes for the masts analysed.

5.2 Results and Discussion

5.2.1 Lateral Modes

Table 5-1 lists all lateral modes that have close to, or more than 5% mass participation when both orthogonal bending modes are considered as a single mode. The modes are listed in order of increasing frequency, with their relative importance shown by their percentage mass participation.

Mast	Mode	Frequency (Hz)	Period (s)	% Mass Participation
A (99.88m) Cables % 18.55	1 (A&B)	1.67	0.60	20.90
	2 (A&B)	1.81	0.55	9.70
	3 (A&B)	2.06	0.49	4.62
	4 (A&B)	2.18	0.46	33.80
	5 (A&B)	2.48	0.40	7.38
	6 (A&B)	2.59	0.39	6.34
	Other			17.27
B (245m) Cables % 16.29	1 (A&B)	0.52	1.91	11.90
	2 (A&B)	0.78	1.29	28.71
	3 (A&B)	1.27	0.79	15.84
	Other			43.56
C (239.3m) Cables % 13.97	1 (A&B)	0.63	1.59	20.34
	2 (A&B)	0.69	1.45	4.92
	3 (A&B)	0.83	1.21	19.00
	4 (A&B)	0.99	1.01	14.69
	5 (A&B)	1.30	0.77	4.68
	6 (A&B)	1.90	0.53	6.73
	Other			29.63
D (313.6m) Mast D Cable % 27.79	1 (A&B)	0.51	1.96	13.60
	2 (A&B)	0.57	1.76	5.54
	3 (A&B)	0.62	1.62	5.15
	4 (A&B)	0.64	1.55	15.66
	5 (A&B)	0.77	1.30	13.67
	Other			46.37

Table 5-1 Mast modes with greater than 5% mass participation

It can be seen that the taller the mast, and the more cables that contribute to the structure, the more modes occur that contribute less than 5% mass participation overall to the vibration of the structure. In mast B (245m) and mast D (313.6m), which both have five stay levels, approximately 45% of the mass is not accounted for if only significant modes (> 5% mass participation) are considered, whereas mast A (99.88m) and mast C (239.3m) with three and four stay levels respectively, approximately 20% and 30% of the mass is not accounted for.

The presence of a large number of flexible cables may serve to ‘split’ what is essentially a single mast mode. Slight variations in the mode shape of a particular set of cables can occur without significantly altering the deformed shape of the mast. This causes a slight change in natural frequency and introduces a new mode. Difficulties in understanding the vibration of such structures are clearly illustrated here.

The dynamic behaviour of most structures can usually be described by a small number of natural frequencies, one of which is the most dominant and described as the fundamental natural frequency. Although this is not the case with guyed masts, investigation of the most significant flexural mode is a useful starting point. Figure 5-1 below shows a plot of the most significant flexural period (highest mass participation ratio) versus mast height for the four masts. A linear trend line has been added showing the increase in flexural period with height. The trend line identified by Amiri [1] in a similar study has also been added to the graph for comparison.

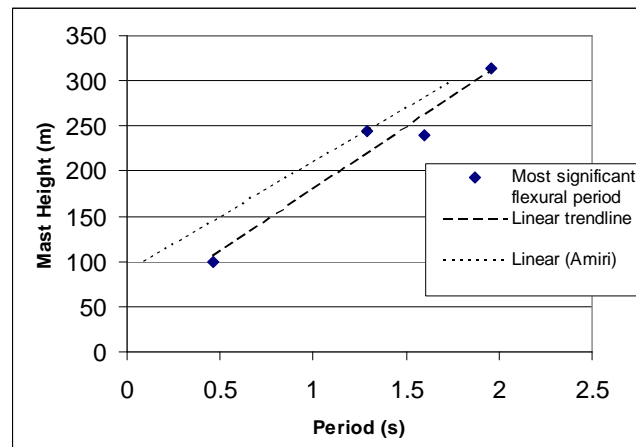


Figure 5-1 Plot of the most significant flexural periods against mast height

The study by Amiri [1] did not include the mass of any ancillaries in the analyses of the towers. The added mass of the ancillaries considered in this research would cause increases in the natural period of the structure, and explains the rightwards shift of the graph. Amiri [1] suggested that his formula could be used to estimate the fundamental natural period of guyed towers in the range 150m to 350m and then be used for a design check to assess the

importance of lateral effects. Evidence produced in this research suggests that a large number of significant modes exist with varying levels of mass participation and the author would not recommend the use of such an equation for anything more than an initial estimate of natural period. The governing formula for the above trendline to estimate natural period is as follows:

$$T = 0.007H - 0.2347 \tag{5.1}$$

where

T natural period in s

H tower height in m.

5.2.2 Mode Shapes

Figures 5-2 to 5-5 show the mode shapes of modes with more than 5% mass participation. The modes are shown in order of increasing frequency and their frequencies and mass participation shown in Table 5-1. As the deformed mast shape is of primary interest, the cables have been omitted.

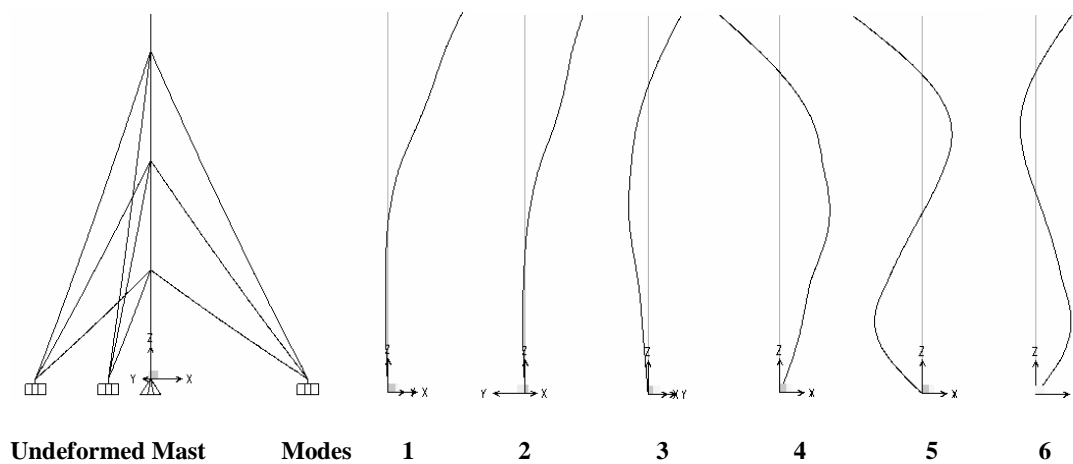


Figure 5-2 Mast A – mode shapes

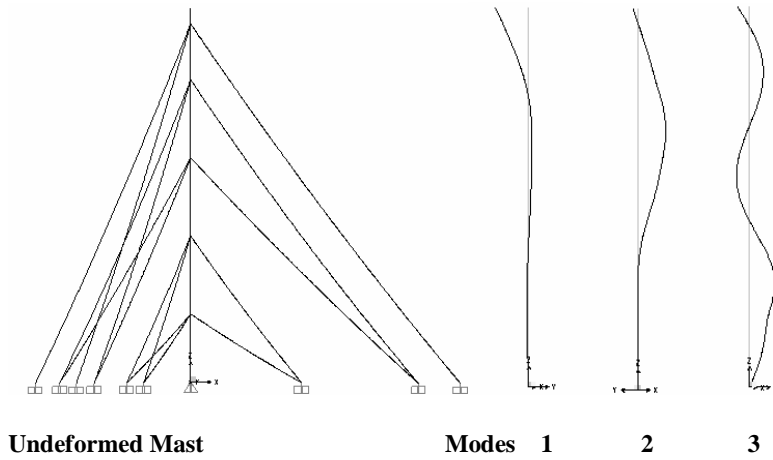


Figure 5-3 Mast B – mode shapes

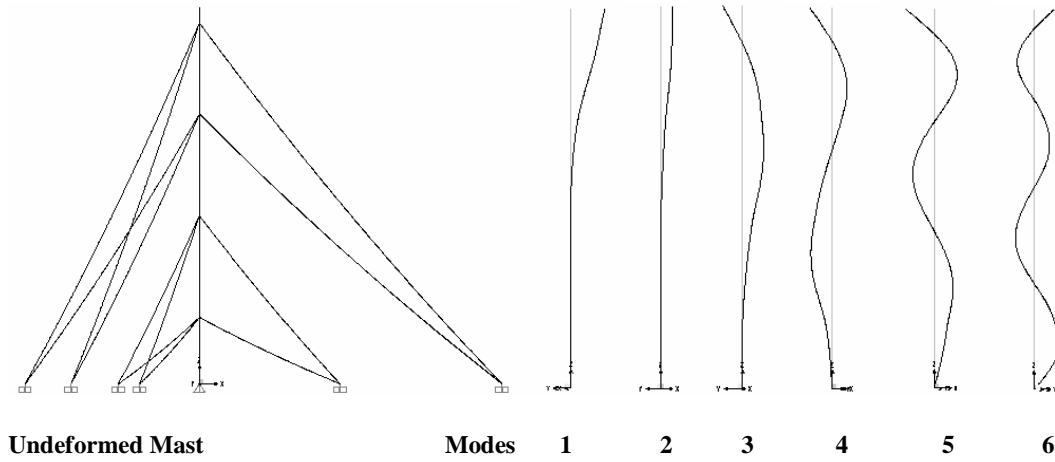


Figure 5-4 Mast C – mode shapes

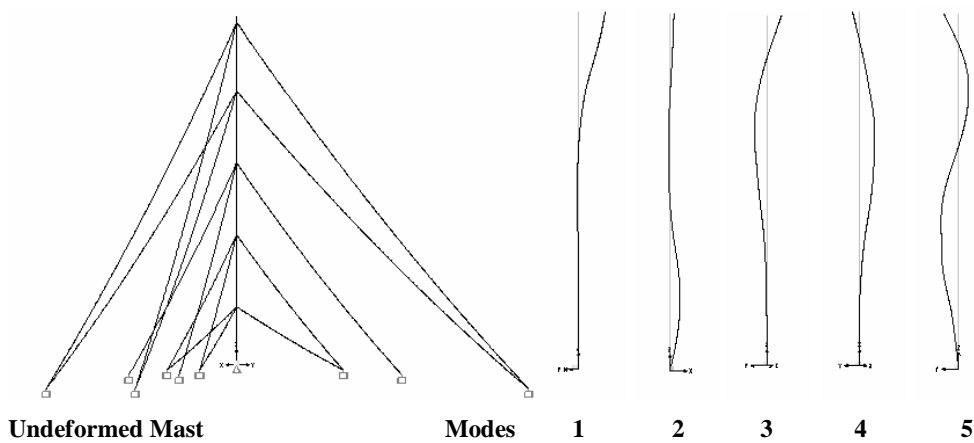


Figure 5-5 Mast D – mode shapes

The distribution of mass is largely uniform along the length of the masts with local areas of increased mass, usually at the stay attachment points due to ancillary loading and strengthening in these areas (see Figures 4-5 to 4-8). The top section (including any small cantilever) of masts B, C and D also shows a higher concentration of mass. The shapes of the significant modes generally appear to be closer to that of a cantilever or propped cantilever rather than those of a continuous beam with multiple supports. This characteristic was also observed by Amiri [1] when describing the first few fundamental mast mode shapes and can be explained by the fact that the horizontal stiffness of the stays reduces with increases in height (see Figures 4-9 and 4-10), resulting in a more fixed support closer to the base, while allowing more flexibility further up the mast. It is apparent that local variations in mass distribution (usually at stay levels) have minimal effect on the significant mode shapes, which are primarily governed by cable stiffness.

5.2.3 Vertical Modes

The lateral seismic behaviour of guyed masts (and most other structures) is usually considered more important than the vertical response, and consequently a vertical modal analysis is often not undertaken. Part of this research investigates the effect of vertical ground motion on mast response and thus vertical vibration and the analysis of the vertical natural frequencies is essential in understanding the importance of this effect. Table 5-2 lists the most significant modal frequencies of the masts (above 5% mass participation).

Mast	Frequency (Hz)	Period (s)	% Mass participation
A	7.63	0.131	9.7
	7.78	0.129	58.7
	Other		90.3
B	3.89	0.257	38.4
	3.91	0.256	22.0
	Other		39.6
C	4.30	0.233	36.0
	4.32	0.232	9.3
	4.34	0.231	15.0
	4.36	0.229	5.3
	Other		34.4
D	0.27	3.638	3.6
	3.42	0.293	57.2
	Other		42.8

Table 5-2 Mast vertical natural frequencies

Table 5-2 shows that the vertical modes occur at much higher frequencies than lateral modes; of the order of 3 to 4 times higher. As expected, there is a strong correlation between mast height (and therefore mass) and natural frequency, with increasing frequencies shown for shorter masts. Analysis of the mode shapes shows that for the most part, important vertical modes involve extension and contraction of the mast rather than vertical cable vibration.

6 Wind Analysis

6.1 Introduction and Methodology

In order to assess the importance of a seismic analysis it was necessary to undertake a wind loading analysis to be able to compare the design forces, produced during a wind loading design, with the forces produced during the seismic analysis. BS8100-4 was chosen as a suitable design code to give an indicative design wind response because:

- The masts had already been designed/checked to BS8100-4
- Eurocode 3 part 3: Towers, Masts and Chimneys is not yet available in the UK, but is due for publication in June 2006 (without the national annexe)
- Both codes are similar and both use the Patch Load method.

It should be noted that BS8100-4 is based on a mean hourly wind speed, and EC3-3 is based on a 10 minute average. Both are given at a reference height of 10m with a return period of 50 years. A factor of approximately 1.07 can be used to convert mean hourly wind speed to 10 minute average².

A full wind loading analysis using BS8100-4 was undertaken on all four masts from one direction only, along the line of a mast leg. The wind direction was chosen with the worst direction factor (i.e. the closest to 1) and should represent the worst wind loading condition, although this would have to be verified as the effective area of mast in another direction may be the dominating factor in determining the structure's response. It was decided that as only an indicative wind loading assessment was needed, loading from this single direction was sufficient.

All the loading area calculations to be used had already been carried out by Flint and Neill Partnership and were supplied to the author in the form of distributed areas (i.e. in m²/m), and point areas (i.e. in m²).

² Obtained from Figure 4.2 of [29]

6.2 Wind Speeds and Loading Profiles

The analysis was undertaken using the general method described in BS 8110-4 and summarised in section 2.5. It should be noted that all the masts have been analysed fully according to BS8100-4 by Flint and Neill Partnership and all of the masts fulfil its requirements.

Mast	Mean Hourly Wind Speed V_b (m/s)	Direction factor, S_d	Equivalent 10 minute average Speed (m/s)	Partial factor on wind speed, γ_v	Site altitude factor, S_a
A	23.0	0.97	24.6	1.4	1.2
B	24.0	0.92	25.7	1.1	1.3
C	22.5	0.93	24.1	1.1	1.05
D	23.5	0.91	25.1	1.1	1.15

Table 6-1 Mast design wind speeds

Figures 6-1 to 6-4 show the mean wind loading profiles for the four masts. Point loads have been ‘smoothed’ into the data to give a visual representation of the mean loading. Stay levels are indicated by dotted lines.

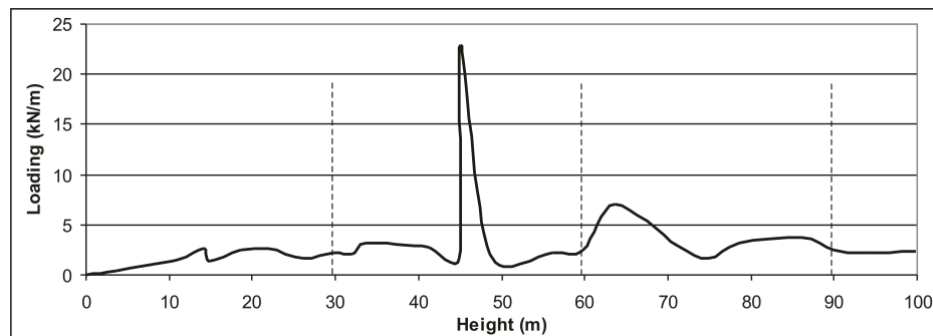


Figure 6-1 Mast A – mean wind load profile

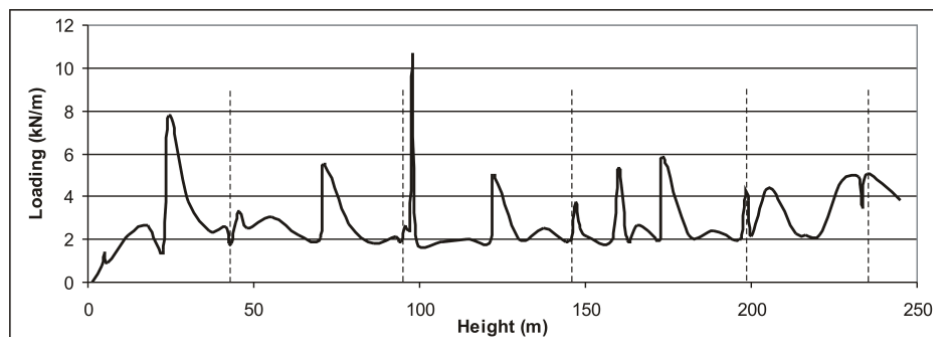


Figure 6-2 Mast B – mean wind load profile

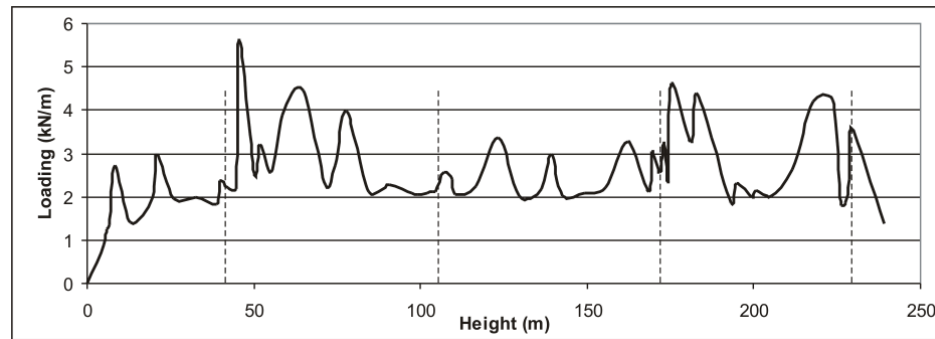


Figure 6-3 Mast C – mean wind load profile

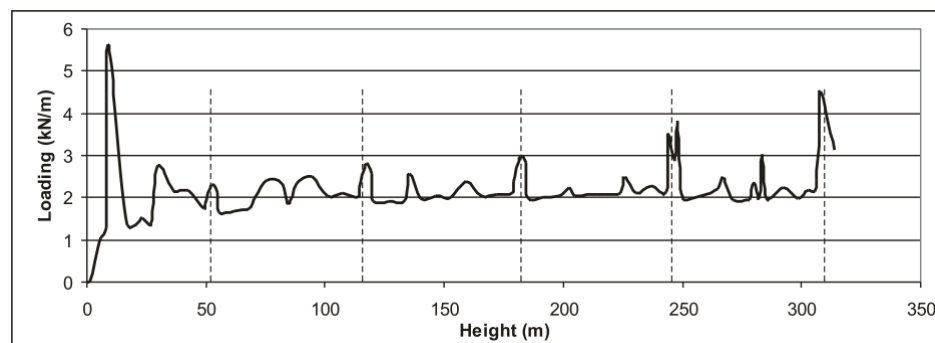


Figure 6-4 Mast D – mean wind load profile

Mast	Height (m)	Average mean load (kN/m)
A	99.88	2.54
B	245.00	2.64
C	239.30	2.49
D	313.60	2.11

Table 6-2 Mast average wind loading

The average mean loading on the four masts is relatively similar (between 2.11 and 2.64 kN/m). Although mast D is the tallest, its relatively low additional loading leads to a lower overall wind resistance.

Both the mean wind loading and patch loading are proportional to V^2 . In order to understand the relative significance of seismic loadings in areas with more or less wind than that used for the design of masts used in this research, an indicative wind analysis was also conducted with mean hourly wind speeds of 20m/s and 28m/s respectively (21.4m/s and 30m/s equivalent 10 second average). Mast forces produced in these analyses are shown in section 8 in comparison to those produced during the seismic analyses.

6.3 Results and discussion

The results of the wind loading analysis are shown in the form of force diagrams (moment, shear and axial). Both the mean response and the design envelope (F_{M+} and F_{M-}) and are shown in Figures 6-5 to 6-16 for all masts. Table 6-3 shows the mean and design tensions for the stays from the wind loading analysis, as well as the ultimate tensile load (UTL), and design tension as a percentage of the ultimate tensile load, indicating the utilization of the cable under wind loading.

		Stay Level				
		Lowest				Highest
		A	B	C	D	E
Mast A	Unloaded (kN)	79.8	104.1	136.5	xx	xx
	Wind (mean) (kN)	141.5	239.7	254.4	xx	xx
	F_{M+} (design load) (kN)	211.1	351.7	344.9	xx	xx
	UTL (kN)	822.1	1957.0	1957.0	xx	xx
	% utilization	25.7	18.0	17.6	xx	xx
Mast B	Unloaded (kN)	44.1	73.8	83.4	164.7	95.7
	Wind (mean) (kN)	136.9	239.7	190.4	394.0	244.4
	F_{M+} (design load) (kN)	283.1	380.7	256.2	483.1	306.3
	UTL (kN)	864.3	1447.0	847.2	1983.4	847.2
	% utilization	32.8	26.3	30.2	24.4	36.2
Mast C	Unloaded (kN)	92.0	116.7	167.6	116.3	xx
	Wind (mean) (kN)	203.3	280.3	346.4	234.1	xx
	F_{M+} (design load) (kN)	370.4	451.4	458.7	300.6	xx
	UTL (kN)	1393.0	1654.6	1654.6	1103.6	xx
	% utilization	26.6	27.3	27.7	27.2	xx
Mast D	Unloaded (kN)	80.5	120.8	152.7	267.7	136.3
	Wind (mean) (kN)	190.3	325.0	364.5	485.5	286.3
	F_{M+} (design load) (kN)	304.7	459.0	463.8	562.2	335.2
	UTL (kN)	1036.6	1784.1	1943.6	2571.5	1435.2
	% utilization	29.4	25.7	23.9	21.9	23.4

Table 6-3 Cable tensions from wind analysis

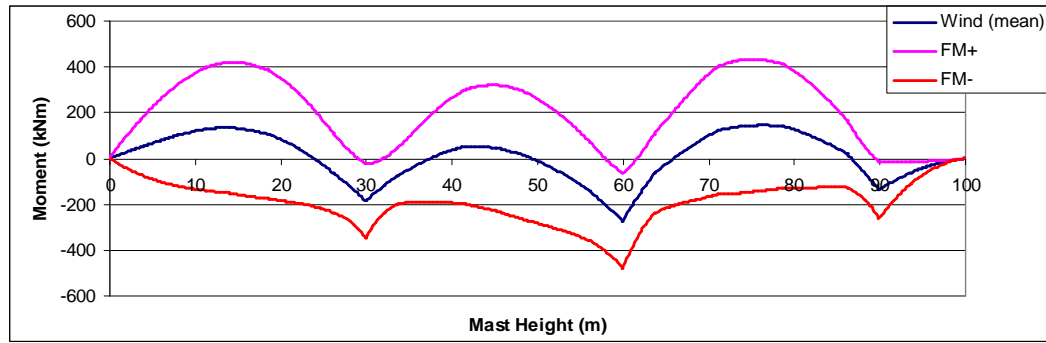


Figure 6-5 Mast A – design wind moments

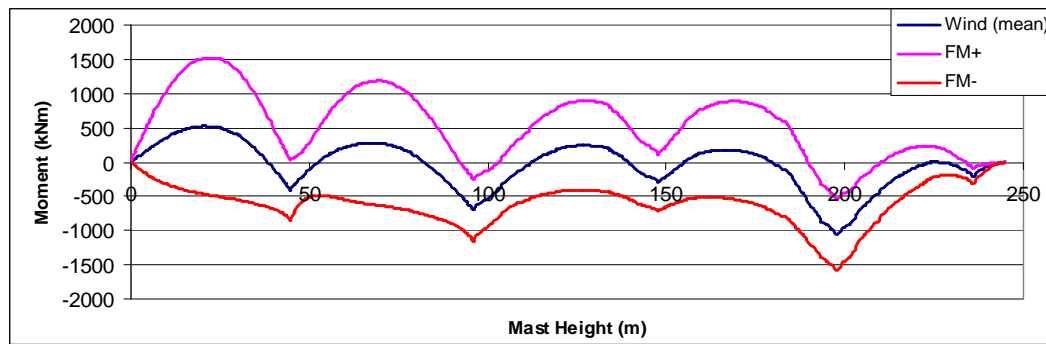


Figure 6-6 Mast B – design wind moments

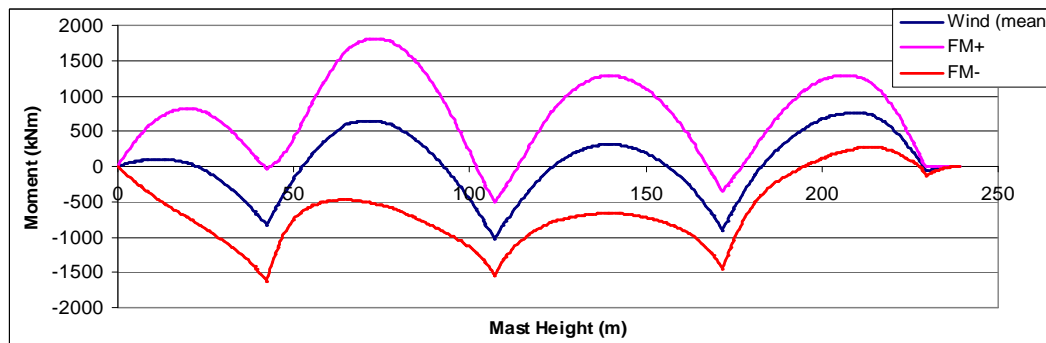


Figure 6-7 Mast C – design wind moments

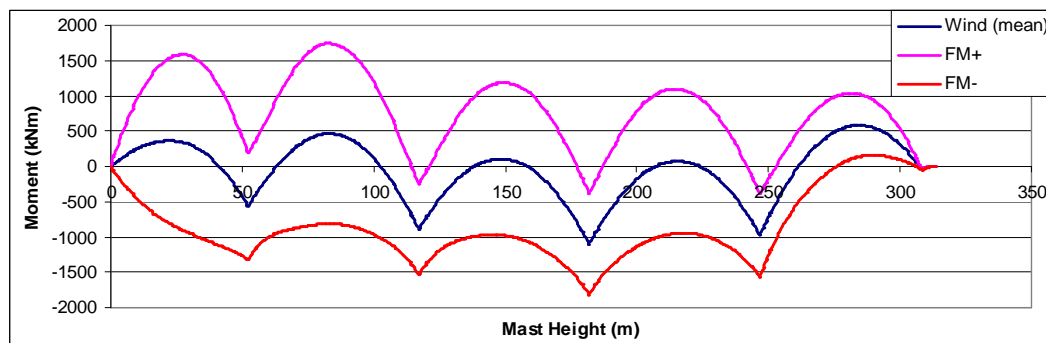


Figure 6-8 Mast D – design wind moments

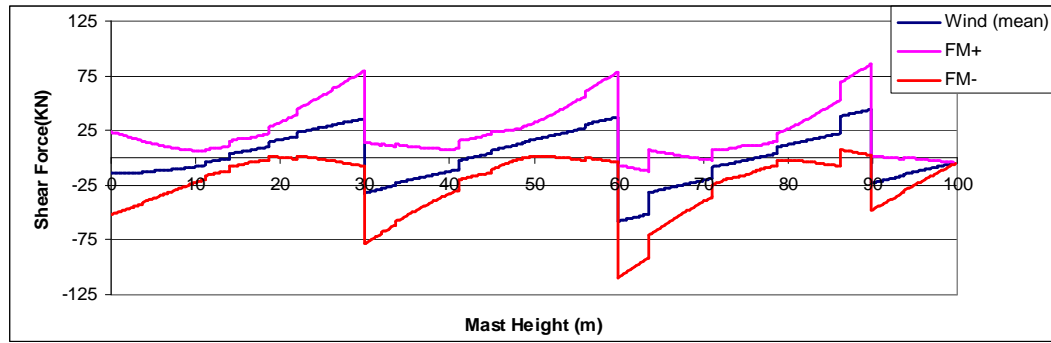


Figure 6-9 Mast A – design wind shear

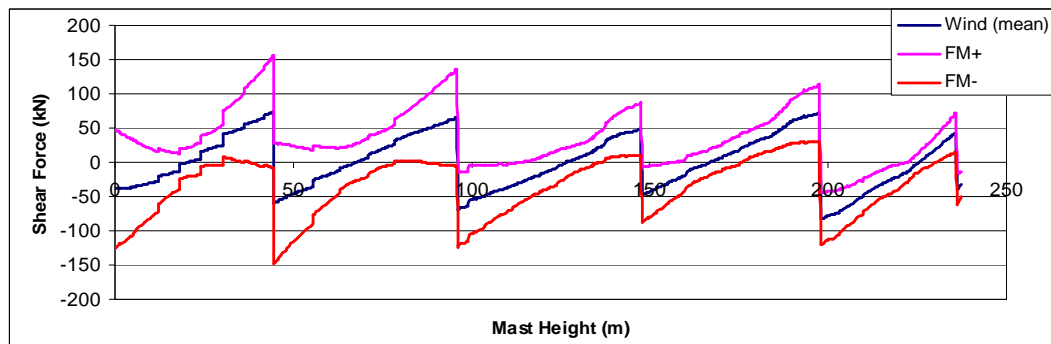


Figure 6-10 Mast B – design wind shear

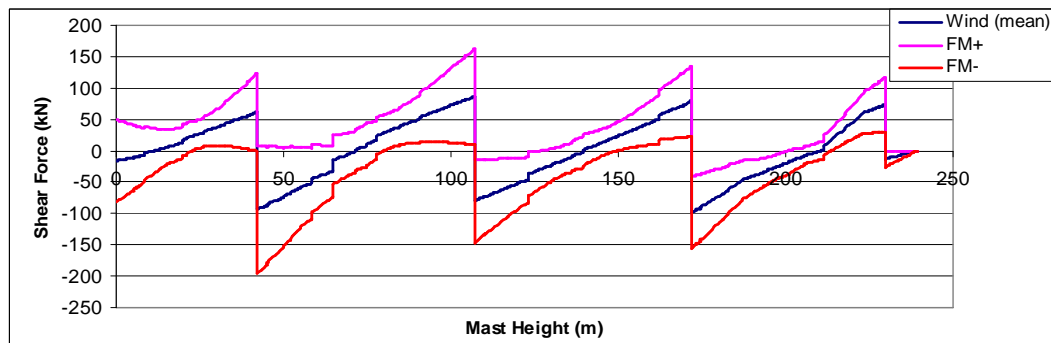


Figure 6-11 Mast C – design wind shear

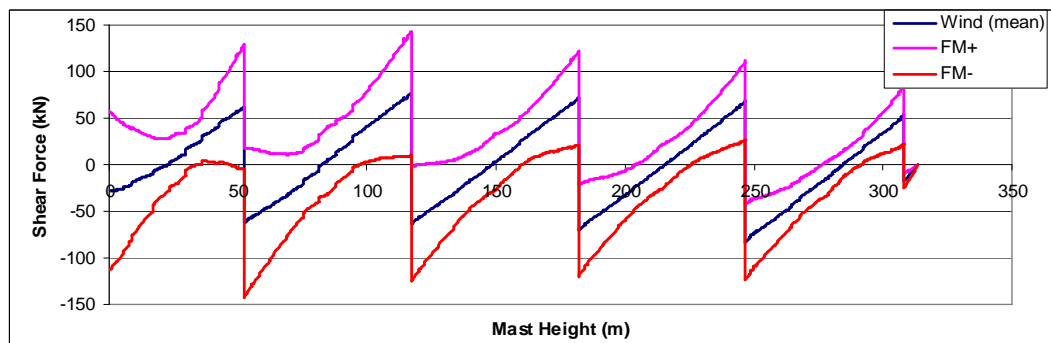


Figure 6-12 Mast D – design wind shear

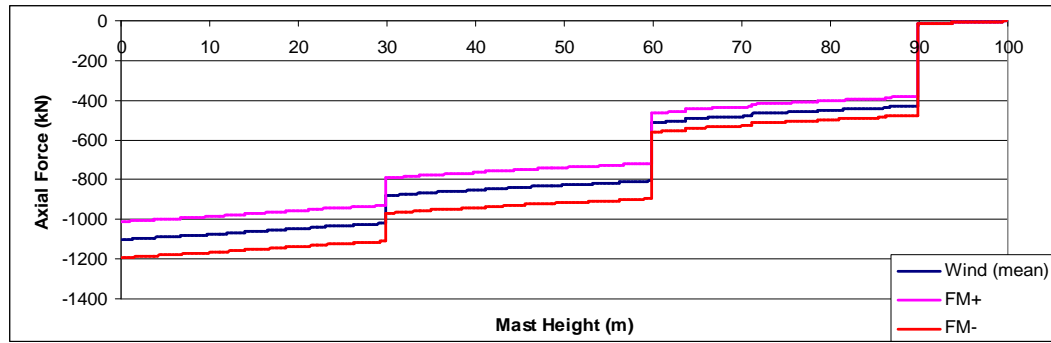


Figure 6-13 Mast A – design wind axial forces

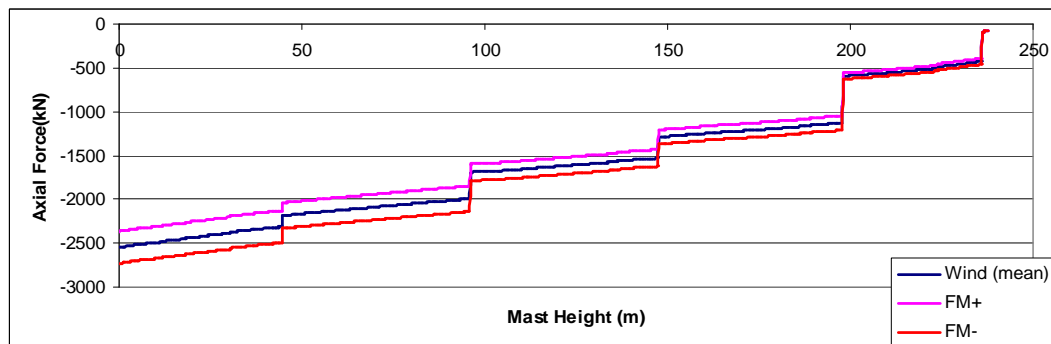


Figure 6-14 Mast B – design wind axial forces

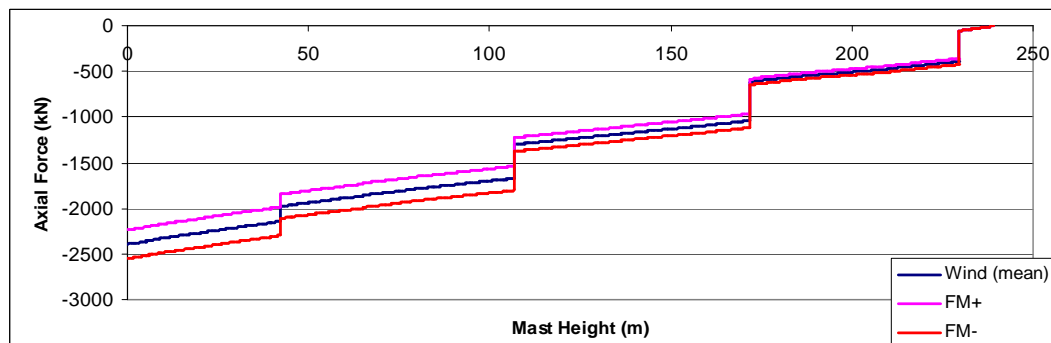


Figure 6-15 Mast C – design wind axial forces

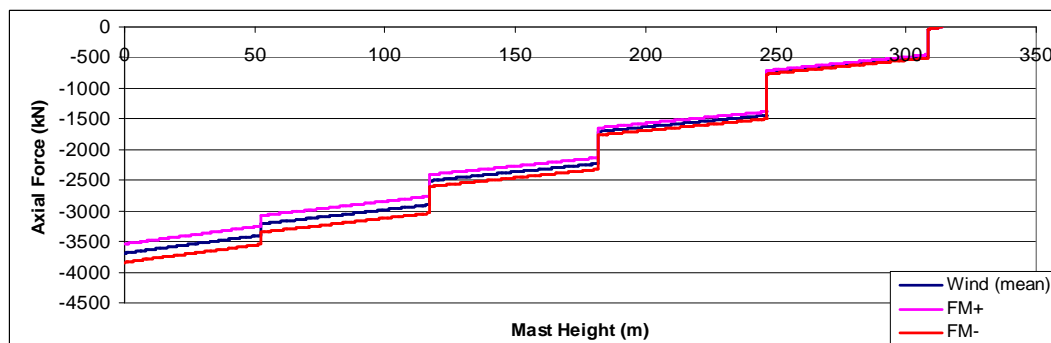


Figure 6-16 Mast D – design wind axial forces

It can be seen in Figures 6-5 to 6-12 that the shape of the bending moment and shear force diagrams closely resembles that of a continuous beam, with sagging moments in the spans and hogging moments at the stay supports. The balance of sagging and hogging moments depends on the span lengths and the relative stiffness of the stays. It can be seen that a better balance seems to have been obtained for masts A and C with relatively similar maximum sagging and hogging moments along the length of the mast. Masts B and D have large differences between these sagging and hogging moments and mast D in particular has maximum hogging moments generally twice the value of sagging moments under mean wind loading. This is likely to indicate an inefficient design as it is unlikely that significant variations in section sizes would be employed at adjacent spans and supports. A much higher design bending moment (produced at the supports) would therefore need to be used throughout. Increasing the span length in these regions could serve to redistribute the bending moment, creating a more efficient design. The profile of the design loading case F_M^+ and F_M^- with patch loading (described in section 2.5), generally follows the same trend as the mean loading diagrams, with values usually 200% or 300% of the mean loading case.

The axial force distribution is typical for that of a column with point loads at repetitive intervals. The self weight of the mast and its ancillaries produce a gradual increase in axial load down the mast and the prestress cable supports add large loads where they are attached. The effect of the patch loading increases the design loading by a maximum of 10% at the base of the towers.

Table 6-3 shows that all stay tensions are well within limits under the wind design loading case. In most cases they are approximately 30% or less of the ultimate tensile load.

7 Seismic Analysis

The nonlinear seismic response of the masts was assessed using a series of time history ground motions applied at the base of the masts and at the stay supports. The following sections describe the main objectives of each set of analyses and outline the assumptions and methodology used.

7.1 Details of Analyses

7.1.1 Stage 1 – Uniform Ground Motion

The major part of this research assessed the response of the four masts to time history ground motion based on three different earthquake accelerograms. The scale of the accelerograms was increased through a range typically used in earthquake design until some of the forces produced were similar to those produced during an indicative wind loading assessment using BS8100-4. Analyses at four different levels of peak ground acceleration were conducted to gain an understanding into the magnitude and distribution of forces produced during different seismic events and to assess how nonlinear the peak response of the masts was to increases in the scale of the accelerograms. In addition results were also used to assess how vulnerable masts designed primarily for wind loading would be to a typical seismic event. A total of 48 time history analyses were conducted during this stage.

7.1.2 Stage 2 – The Travelling Wave Effect

The distance between support points of a guyed mast can be substantial, particularly with taller masts (up to 401m for the masts in this study). A simplified approach was adopted to allow for the travelling effect of earthquake waves, by means of a delayed onset of ground motion at the different supports, according to different shear wave speeds. Although earthquake groundmotion consists of a number of different types of waves travelling at different speeds, the shear wave speed was used to characterize this effect. As this is the slower of the two most destructive types of wave (P and S waves), it is likely that this effect will be exaggerated. However a more detailed analysis of the combine effect of both P and S waves is beyond the scope of this research. Analyses were conducted based on shear wave

speeds of 270m/s, 580m/s, 800m/s (corresponding to ground types A, B and C in EC8). The direction of the travelling wave was applied along the X axis (Figures 4-1 to 4-4), in line with a line of stays. Table 7-1 shows a breakdown of the delay times at the various supports of each mast subjected to the various travelling waves.

Mast A		Support Point						
	Wave Speed (m/s)	ABC1	Mast	ABC2&3				
Distance from 1st support in wave path (m)		0.00	44.65	66.98				
Time delay (s)	800 m/s	0.00	0.06	0.08				
	580 m/s	0.00	0.08	0.12				
	270 m/s	0.00	0.17	0.25				
Mast B		E1	CD1	AB1	Mast	AB2 & 3	CD2 & 3	E2 & 3
Distance from 1st support in wave path (m)		0.00	27.55	104.11	176.88	213.27	251.55	265.32
Time delay (s)	800 m/s	0.00	0.03	0.13	0.22	0.27	0.31	0.33
	580 m/s	0.00	0.05	0.18	0.30	0.37	0.43	0.46
	270 m/s	0.00	0.10	0.39	0.66	0.79	0.93	0.98
Mast C		CD1	AB1	Mast	AB2 & 3	CD2 & 3		
Distance from 1st support in wave path (m)		0.00	103.60	193.50	238.45	290.25		
Time delay (s)	800 m/s	0.00	0.13	0.24	0.30	0.36		
	580 m/s	0.00	0.18	0.33	0.41	0.50		
	270 m/s	0.00	0.38	0.72	0.88	1.08		
Mast D		DE1	C1	AB1	Mast	AB2 & 3	C2&3	DE2 & 3
Distance from 1st support in wave path (m)		0.00	116.10	169.87	267.65	316.54	343.42	401.47
Time delay (s)	800 m/s	0.00	0.15	0.21	0.33	0.40	0.43	0.50
	580 m/s	0.00	0.20	0.29	0.46	0.55	0.59	0.69
	270 m/s	0.00	0.43	0.63	0.99	1.17	1.27	1.49

Table 7-1 Delay times for each support during travelling wave analyses

Although the accelerograms were scaled (or synthesized) to match a soil type C design spectrum (which corresponds to a specific shear wave velocity of 180m/s to 360 m/s), in order to assess the effect of asynchronous ground motion, the same accelerograms were analysed whilst adjusting the effective shear wave speed (accelerograms and scaling procedures are defined in section 7.3). Stage 1 analyses identified that the masts responded far more to the EC8 and El Centro accelerograms than the Parkfield accelerogram, and thus the Parkfield accelerogram was not used during this phase. A total of 24 time history analyses were conducted during this stage.

7.1.3 Stage 3 – Uniform Ground Motion without Vertical Motion

The relatively recent Northridge earthquake (1994) identified significant vertical motions that suggested that more careful attention should be paid to seismic loading in this direction. Accelerations in this direction were previously given minimal consideration as it was commonly believed that lateral behaviour governed mast response. By running a set of analyses without the inclusion of vertical motion, the effect of this loading on the masts will be assessed. As with stage two, the Parkfield accelerogram was not used during this stage. A total of twelve time history analyses were conducted during this stage.

7.2 Modelling Methods and Assumptions for Seismic Analyses

7.2.1 Time Integration Method

The nonlinear dynamic analysis is done by a step-by-step integration of the equilibrium equations in the time domain. SAP2000 offers a number of standard direct integration methods. Newmark's method [15] of numerical integration (described in section 2.1.3) was used with $\gamma = 0.5$ and $\beta = 0.25$. With these parameters, the method is equivalent to the average acceleration method and is unconditionally stable with no energy dissipation. Full geometric nonlinearity is allowed for by the selection of a large displacement nonlinear setting, thus allowing for the stiffness matrix to be computed at each time step in the deformed position of the current step. Mass and stiffness proportional damping (Rayleigh damping) was used to damp both high and low frequency modes outside of the range significant to mast response. All convergence problems were solved by increasing the number of cable elements in each cable, which resulted in 80 to 250 elements per cable. The maximum time step used was reduced until no significant variation in mast response was evident; this was typically 0.0025s for mast A, and 0.005s for masts B, C and D. The time step was usually automatically reduced by SAP2000 for the travelling wave analyses to approximately 0.001s. A data sampling time step was chosen for each mast to accommodate at least 20 data points from each significant natural period identified during the modal analyses. More information on the time integration and its use in SAP2000 can be found in the CSI Analysis reference manual [27].

7.2.2 Damping

Eurocode 8: part 6 states that if a reduced design spectrum is not used for analysis, damping ratios other than 5% may be used. A ratio of 1% to 4% is suggested for steel elements. For this research a value of 2% was used, the same value employed by Amiri [1]. The range of important natural frequencies was identified during the modal analysis and was used to identify the two frequencies needed for SAP2000 to calculate Rayleigh damping coefficients as described in 2.1.2.3. These coefficients were then used throughout the time history analyses.

7.3 Accelerograms and Time Histories

Three earthquakes were chosen for the analysis, each exhibiting different characteristics. ‘Classic’ time histories from the 1940 El Centro earthquake, exhibiting a wide range of frequencies and numerous episodes of strong ground motion, and the 1966 Parkfield earthquake, exhibiting a single pulse type loading with dominant lower frequencies. Both of these earthquakes occurred in the vicinity of the San Andreas Fault in California. Time histories in all three directions were available for these two earthquakes from [33] and [34]. The third time history was synthesized using SIMQKE-1 (software package) to match the Type 1 European horizontal elastic response spectrum for soil type C. Eurocode 8 states that identical time histories may not be used to characterize motion about two axes simultaneously, thus a total of three time histories were synthesized for loading along respective axes. As loading in one direction is usually dominant the EC8 time histories used to load the Y and Z directions were scaled down by a factor of 5/6 and 3/4 respectively, an approach similar to that adopted by Amiri [1], based on the Building Code of Canada 1995–Commentary J. It should be noted that future research could improve slightly on this treatment of vertical motion by utilizing a vertical accelerogram corresponding to the EC8 vertical elastic response spectrum.

Figures 7-1 to 7-3 show the accelerogram with the highest accelerations (i.e. dominant direction) from each of the earthquakes to be used. The remaining directions are shown in Appendix 1.

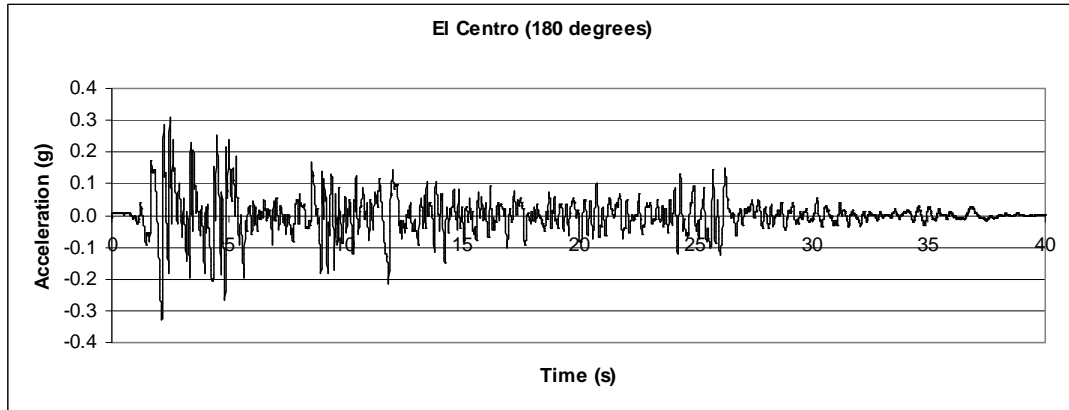


Figure 7-1 El Centro accelerogram in dominant (X) direction for $3m/s^2$ scaling

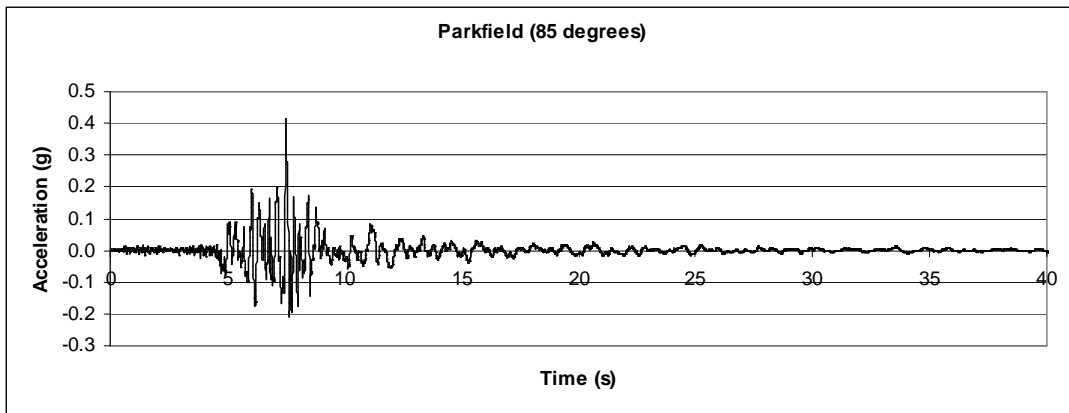


Figure 7-2 Parkfield accelerogram in dominant (X) direction for $3m/s^2$ scaling

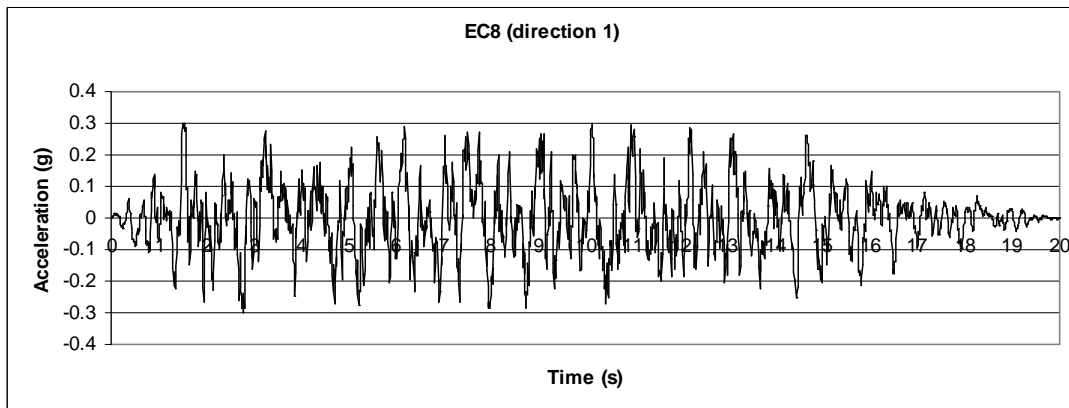


Figure 7-3 EC8 accelerogram in dominant (X) direction for $3m/s^2$ scaling

7.3.1 Scaling and Comparison of Time Histories

Typically buildings are designed for earthquake resistance by means of a response spectrum (described in section 2.4.1). A software package called Seismosignal (available from [36]) was used to calculate the elastic response spectrum from the various accelerograms. The amplitude of all of the response spectra (and thus accelerograms) was then scaled linearly to ‘best fit’ the response spectrum for a type 1, soil type C earthquake as stipulated by EC8. The scaling approach used was not strictly in accordance with the design requirements of EC8 part 1, which requires that the mean of the zero period spectral response (calculated from the individual component time histories) be greater than that of the site in question. The requirement that in the significant period range of the structure ($0.2T$ to $2T$) that the peak elastic spectrum value, calculated from the individual time histories be no less than 90% of the EC8 elastic response spectrum of the ground type is also not strictly adhered to. Compliance with these requirements is necessary for design to ensure that all possible ranges of seismic loading are covered for any particular structure. However as this study was not strictly a design exercise and undertakes to model the realistic response of a range of masts to different types of loading with the aim of developing new response trends, increasing the scale of the accelerograms to such an extent would not have been appropriate. Soil type C was chosen as it represented a ‘middle range’ EC8 response spectrum, defining a reasonably stiff ground type. It is closest to the ‘average’ EC8 response spectrum and thus should yield the most applicable set of results; however analyses based on other soil types would be needed to cover all ranges of mast response. Figure 7-4 shows the three corresponding response spectra (after scaling – worst direction only) relative to the EC8 design spectrum. Table 7-2 shows the significant natural frequency ranges for the four masts.

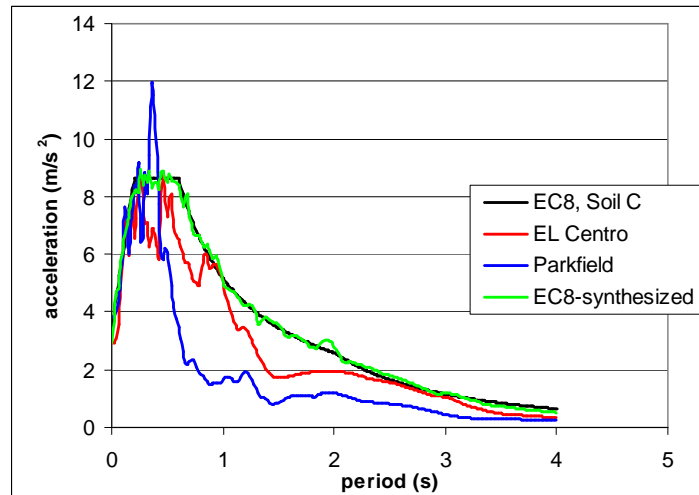


Figure 7-4 Response spectra (5% damping) for accelerograms in dominant direction at 3m/s^2 scaling

Mast	Significant Frequency Range (modes with > 5% Mass Participation)	Equivalent Period Range
A	1.75Hz-2.55Hz	0.39s - 0.57s
B	0.5Hz-1.3Hz	0.77s - 2.0s
C	0.6Hz-1.9Hz	0.53s - 1.66s
D	0.5Hz-0.8Hz	1.25s - 2.0s

Table 7-2 Significant frequency ranges of masts

The EC8 synthesized accelerogram clearly has the widest range of vibration frequencies and is likely to interact more with all of the masts. Although of lower response amplitude, the El Centro accelerogram also consists of a wide range of frequencies, however the duration of high amplitude ground motion is significantly shorter than that of EC8. The Parkfield response is particularly high for lower periods ($<0.5\text{s}$) with minimal response shown for higher periods ($>1\text{s}$). It is likely that the Parkfield ground motion will only excite significant response from mast A.

To assess the response of the masts to increases in accelerogram amplitude, analyses were conducted with various scale factors applied to the time histories corresponding to the ‘best fit’ EC8 (type 1, soil type C) response spectrum with design acceleration set at 2.5m/s^2 , 3m/s^2 , 3.5m/s^2 , 4m/s^2 . Table 7-3 shows a breakdown of the accelerogram properties.

Accelerogram (worst direction only)	EC8 Design acceleration (m/s ²)	Peak Ground acceleration (m/s ²)	Peak Ground velocity (m/s)	Peak Ground displacement (m)	Scale from Original Record
EC8-synthesized	2.5	2.59	0.28	0.09	0.25
	3	3.11	0.34	0.11	0.30
	3.5	3.63	0.40	0.12	0.35
	4	4.15	0.46	0.14	0.40
EL-Centro	2.5	2.43	0.29	0.08	0.88
	3	2.91	0.35	0.09	1.05
	3.5	3.40	0.31	0.08	1.23
Parkfield	4	3.89	0.56	0.15	1.4
	2.5	3.20	0.18	0.06	0.75
	3	3.84	0.21	0.07	0.90
	3.5	4.48	0.25	0.08	1.05
	4	5.12	0.28	0.09	1.2

Table 7-3 Scaled accelerogram properties

7.3.2 Input for SAP2000

SAP2000 allows for acceleration time histories to be applied to all supports simultaneously, but in order for differential movement to be applied to the various supports, a displacement time history must be applied to a unit displacement load at each individual support. As part of the analyses to be performed required differential movement, displacement time histories were used throughout. Seismosignal was also used to accurately convert the acceleration time histories into displacement time histories. In order to eradicate unwanted noise and simplify the analysis the time histories were band filtered between 0.1Hz to 10 Hz for mast A and 0.1Hz to 5Hz for the remaining masts. These ranges represent the frequencies that have any significant effect on the masts. This assumption was verified by doing a number of different analyses, varying the filter bands. A visual representation of the displacement time histories is shown in Figure 7.5.

The earthquake direction was chosen to coincide with the X and Y axes shown in Figures 4-1 to 4-4, i.e. the X direction coincides with a line of stays. The dominant component of vibration was therefore applied along the X axis, in plane with a line of stays.

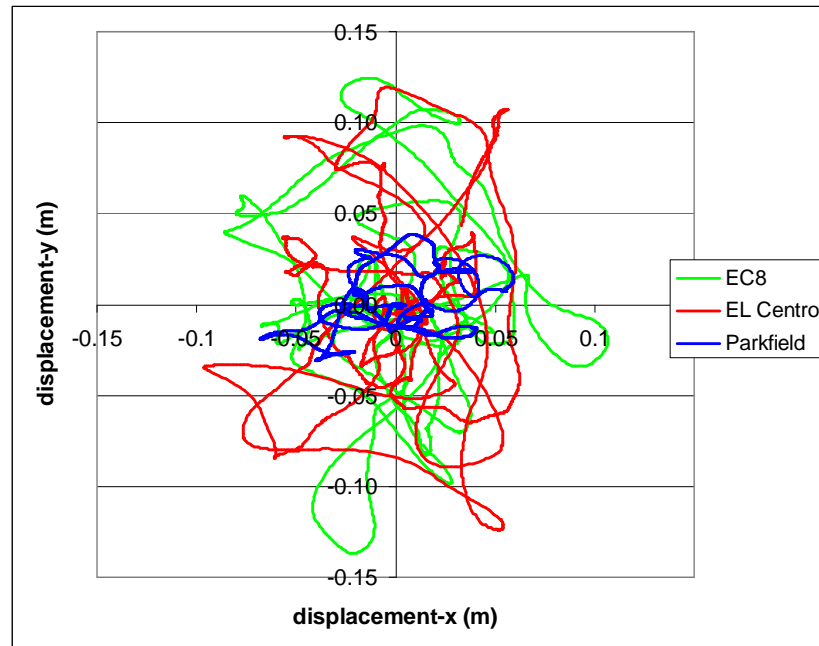


Figure 7-5 Horizontal displacement time histories (3m/s^2 scaling)

The total times shown in Figure 7-5 for EC8, Parkfield and El Centro are 20s, 25s and 30s respectively. The relatively high long period content of the EC8 and El Centro time histories allow for a larger range of displacements than the Parkfield accelerogram.

8 Stage 1: Uniform Ground Motion – Results and Discussion

This section presents and discusses the response of the four masts to time history ground motion from the three sets of accelerograms at four different scale factors. All displacement loads at the supports were applied simultaneously.

8.1 Mast Bending Moments

Figures 8-1 to 8-8 show the peak bending moment envelopes about the Y and X axes for each mast in response to the three earthquakes at $4m/s^2$ scaling. Bending about the Y axis represents bending in the dominant direction of the earthquake.

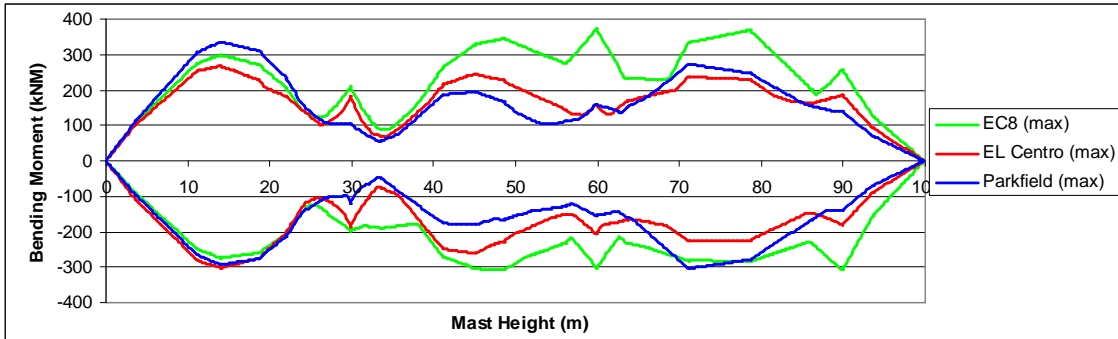


Figure 8-1 Mast A – bending moment envelopes (about Y axis) for $4m/s^2$ scaling

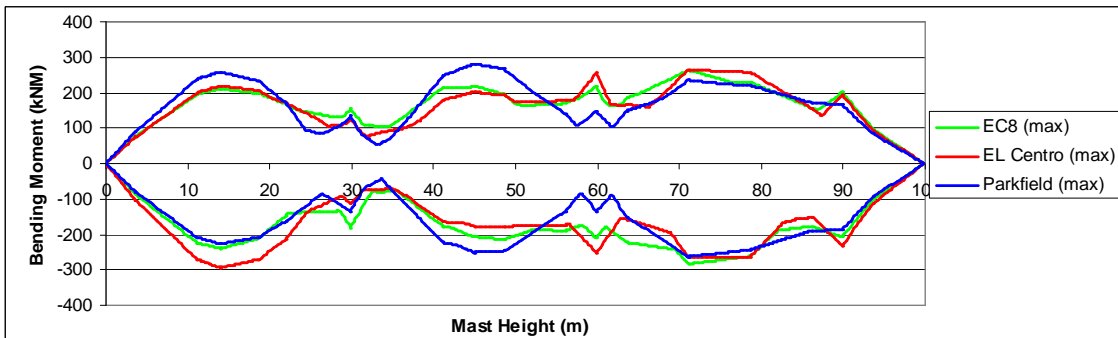


Figure 8-2 Mast A – bending moment envelopes (about X axis) for $4m/s^2$ scaling

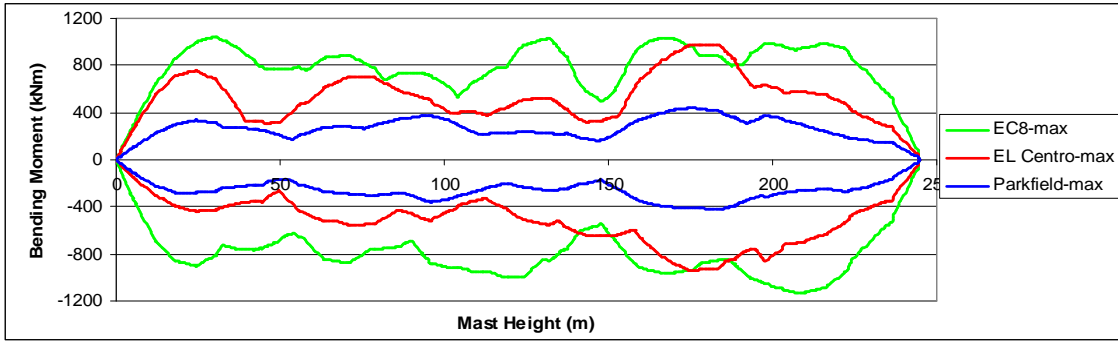


Figure 8-3 Mast B – bending moment envelopes (about Y axis) for 4m/s^2 scaling

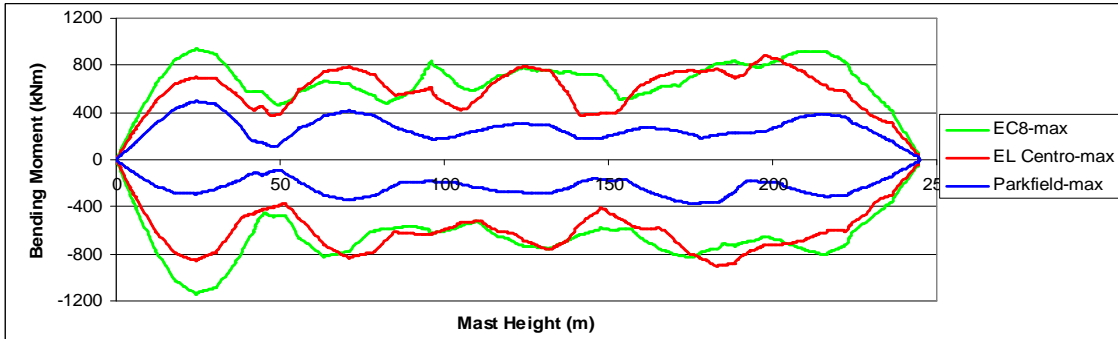


Figure 8-4 Mast B – bending moment envelopes (about X axis) for 4m/s^2 scaling

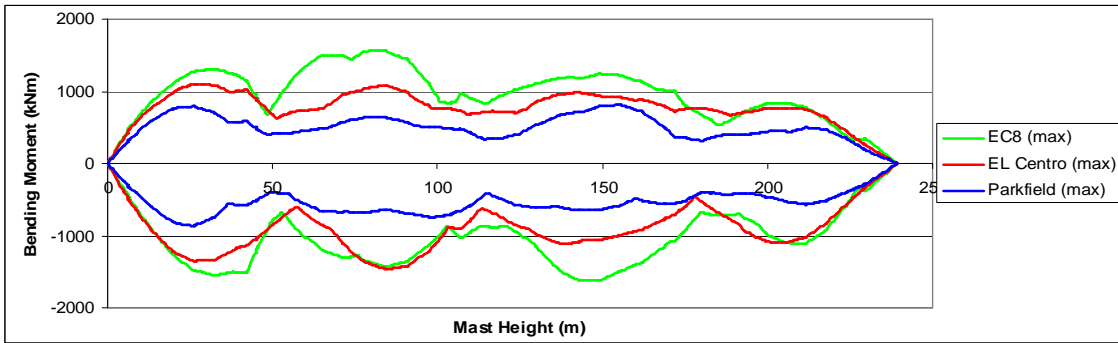


Figure 8-5 Mast C – bending moment envelopes (about Y axis) for 4m/s^2 scaling

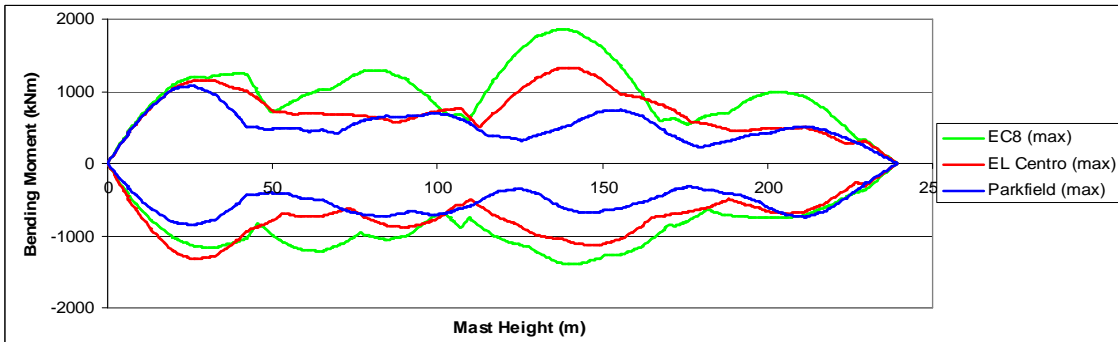


Figure 8-6 Mast C – bending moment envelopes (about X axis) for 4m/s^2 scaling

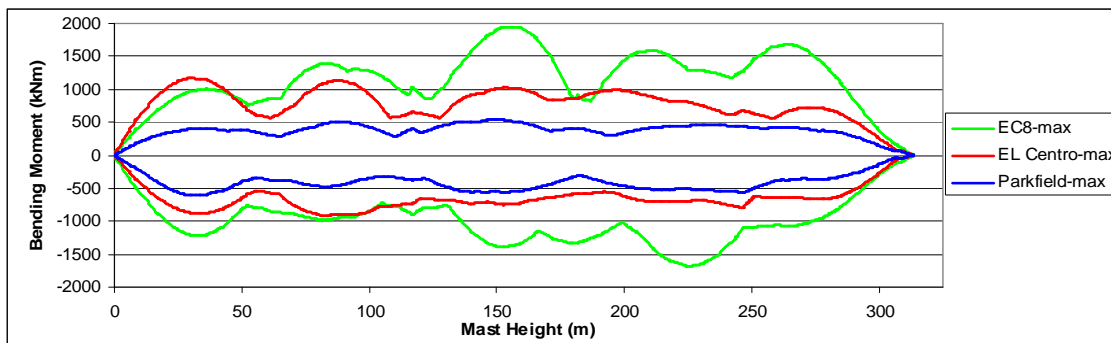


Figure 8-7 Mast D – bending moment envelopes (about Y axis) for $4m/s^2$ scaling

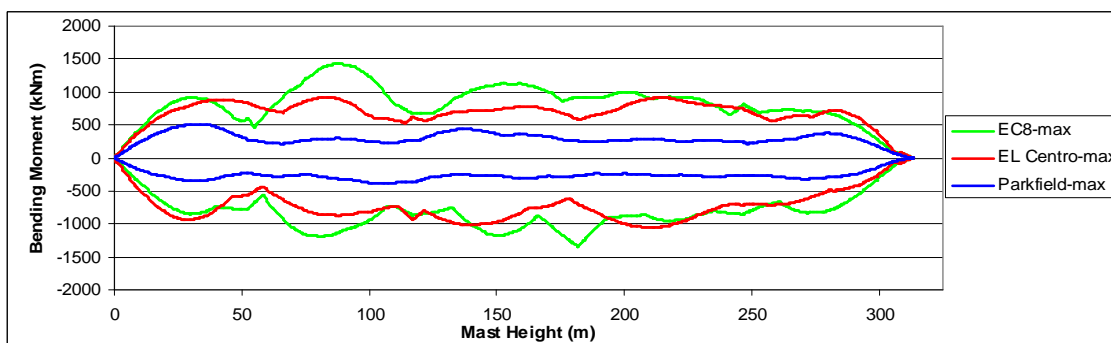


Figure 8-8 Mast D – bending moment envelopes (about X axis) for $4m/s^2$ scaling

Mast A responded significantly to all three ground motions, whilst masts B, C and D responded more to the EC8 ground motion, and less to the Parkfield motion. This spread of results is consistent with the frequency content of the respective accelerograms and natural frequency ranges of the masts, and it seems likely that the longer duration of ground motion in the EC8 accelerograms contributed to the appreciable difference between the EC8 and EL Centro results.

Although similar, the distribution of bending moments across the masts shows notable differences. Mast A, with relatively high cable support stiffness and stiffness utilization shows sharp hogging moments at the stay connection points of similar magnitude to the bending moments in the spans. This response is similar to that of a continuous beam. However masts B, C and D, with much lower cable stiffness utilization and horizontal stiffnesses, show considerable bending in the spans with insignificant or isolated bending at

the stay connection points. This indicates that the stay supports behave more like a spring than a fixed support.

A comparison between the distribution of bending forces in similar sized masts B (five stay levels) and C (four stay levels) also shows interesting, although explicable results. Typical variations in midspan to support point moment are in the region of 2:1 for mast B, whereas the longer spans of mast C increase this ratio to approximately 3:1 with significantly higher midspan moments. It is interesting to note that the peak response and distribution about the Y and X axes can be appreciably different, although higher bending is usually shown about the Y axis (consistent with dominant direction of earthquake loading).

It should be noted that Figures 8-1 to 8-8 show peak bending moment values across the masts which do not all occur at the same point in time. Determining the peak bending moment in the X and Y directions and designing for their vector sum is therefore very conservative as the peak moments at different locations and directions do not occur simultaneously. By analyzing the vector sum of the bending response in the X and Y directions in the time domain, the magnitude of the peak bending moment can be determined. Figures 8-9 to 8-16 show the magnitudes of the peak bending moments for the EC8 and El Centro analyses generated in this way for all PGA scale factors. Four envelopes from a particular earthquake are shown in the same colour with increasing magnitudes corresponding to PGA scale factors of 2.5, 3, 3.5 and 4m/s^2 . The magnitude of the design wind bending moment is also shown, as well as an indicative design moment produced from analyses with mean hourly wind speeds of 20m/s and 28m/s respectively.

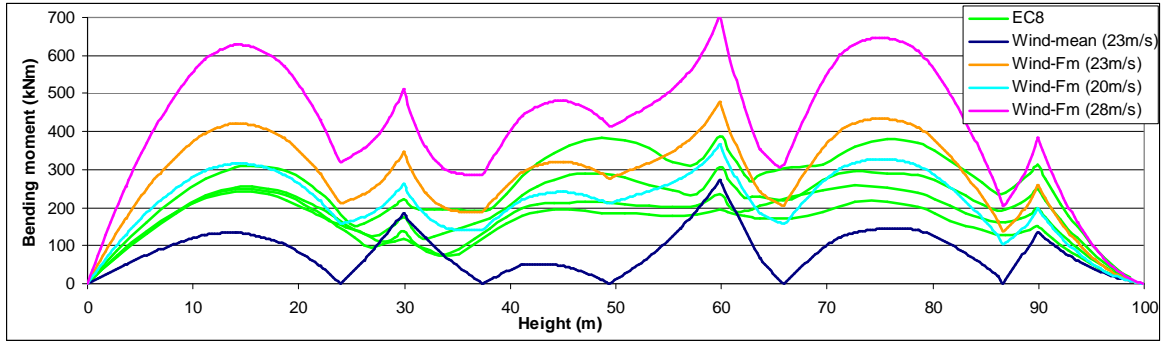


Figure 8-9 Mast A – absolute bending moments for EC8 time histories

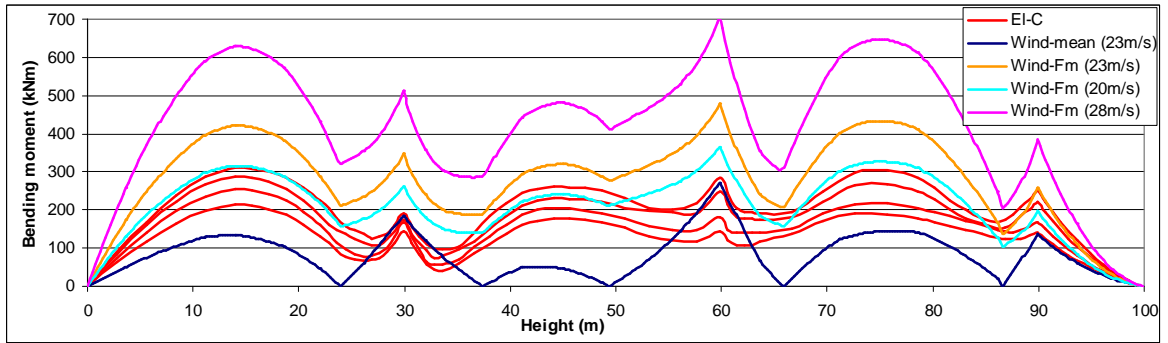


Figure 8-10 Mast A – absolute bending moments for El Centro time histories

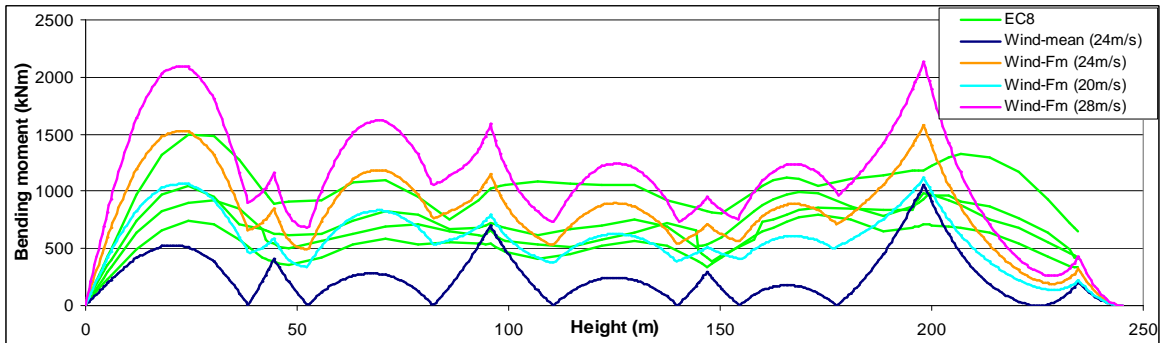


Figure 8-11 Mast B – absolute bending moments for EC8 time histories

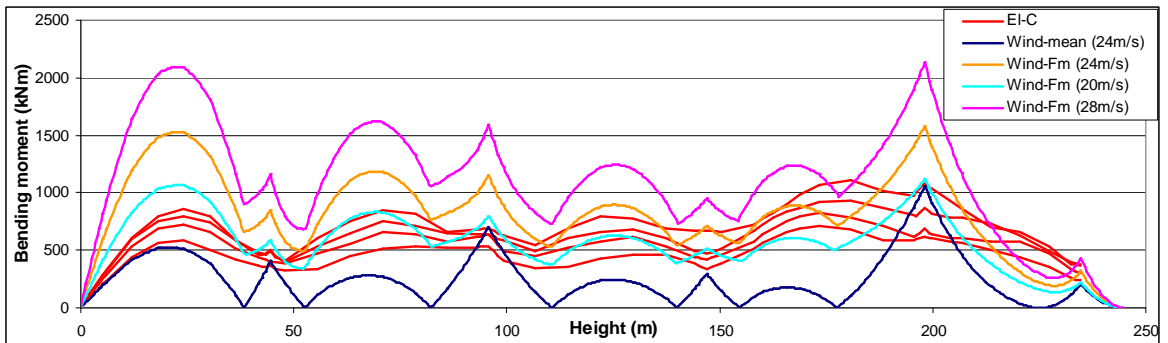


Figure 8-12 Mast B – absolute bending moments for El Centro time histories

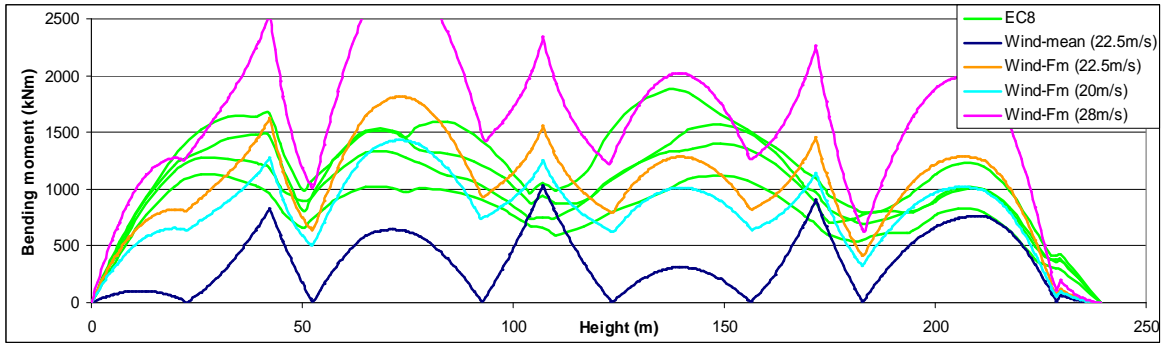


Figure 8-13 Mast C – absolute bending moments for EC8 time histories

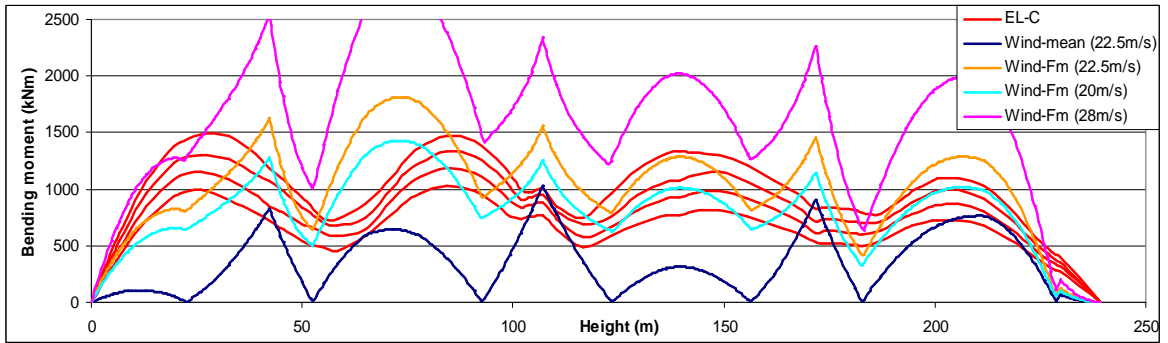


Figure 8-14 Mast C – absolute bending moments for El Centro time histories

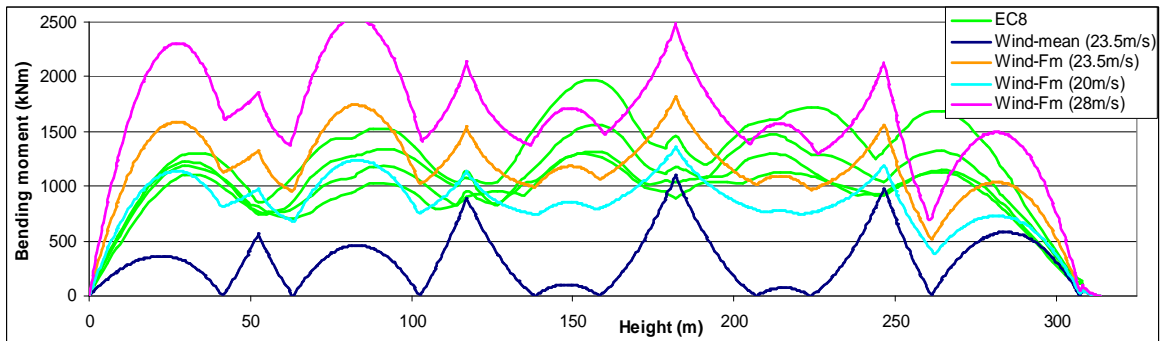


Figure 8-15 Mast D – absolute bending moments for EC8 time histories

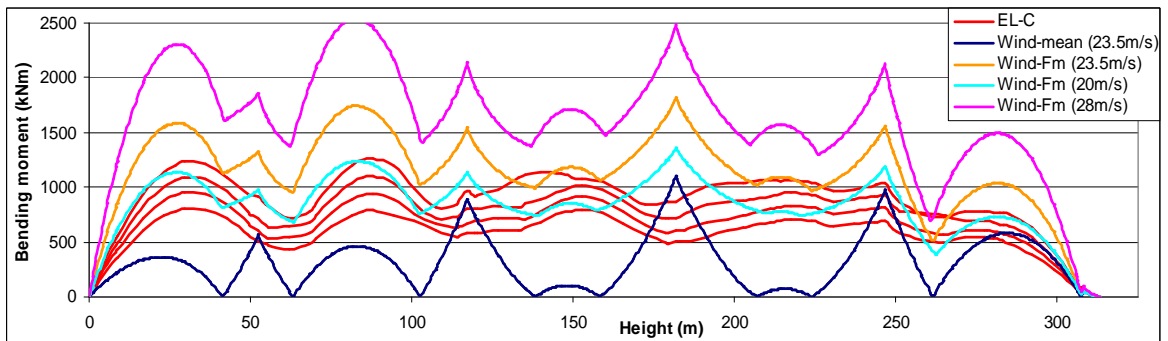


Figure 8-16 Mast D – absolute bending moments for El Centro time histories

The consistent spacing of the El Centro peak moment envelopes show that the peak bending–PGA relationship is relatively linear for all masts. However, the peak response to the EC8 accelerograms exhibits significant nonlinear characteristics, particularly at the higher PGA scale factors. The response of mast B with a PGA scaling of 4m/s^2 shows the most severe increase in bending magnitude. This nonlinearity is for the most part limited to certain regions of the masts and is usually caused by the response at one PGA scale factor not fitting the trend produced by the other three analyses which are largely linear. The nonlinear response to the EC8 analyses can largely be accounted for by the broad frequency content, and the longer duration of high amplitude ground motion of the EC8 accelerograms. This enables the excitation of numerous vibration modes, that when combined can produce irregular results.

Generally the El Centro seismic moments are within the wind design moments of these masts; although in some regions of masts B and C the design wind forces are slightly exceeded at the higher PGA scale factors. The EC8 bending response, however, exceeds the design wind response in some regions of all of the masts at the higher scale factors. Regions where this is most apparent include sagging in the top three spans of mast B and D and spans one and three in mast C. Although these are regions of high seismic bending, the wind design analyses have produced relatively low bending forces in these regions and an imbalance in regions of hogging and sagging is apparent. The mean wind loading analysis has produced areas of low midspan bending that are flanked by areas of high hogging at support points, and consequently a relatively low midspan design moment is exceeded by some of the seismic analyses. Slightly longer spans in these regions could serve to redistribute these moments, producing a more efficient design for wind. This redistribution could bring the wind design envelope closer to the seismic envelope. Although there are regions of susceptibility, the magnitude of adjacent hogging moment (wind) is usually of similar magnitude to that of the peak seismic midspan moment and if minimal variations in mast capacity were designed for, between stay connection points and midspan, it is likely that the masts would have sufficient capacity to withstand the seismic load.

Indicative design bending envelopes produced for mean hourly wind speeds of 20m/s and 28m/s show that in this range the design wind moment can be doubled with an increase in design wind speed of 8m/s (this is because design loads are proportional to V^2). In areas with significant seismic activity and low design wind speeds close to 20m/s, it is very likely that seismic loading will be the dominant load case. Conversely if design wind speeds are nearer the 26m/s to 28m/s range the likelihood of a seismic response (caused by seismic loading in the region of $3m/s^2$ to $4m/s^2$) exceeding that of a design wind response is slim.

In order to compare the peak bending moments produced across the four masts, and identify possible trends, a simple method has been used to normalize the moments. Amongst other factors, mast vibration behaviour is related to mast mass and span length, and as static bending behaviour can be derived from its weight (+additional load) and span length, the following equation was adopted in an attempt to normalize peak bending moments:

$$NMR = \frac{M}{PGA \times \bar{m} \bar{L}^2} \quad (8.1)$$

where *NMR* is a Normalized Moment Ratio, *M* is the peak bending moment in the mast, and \bar{m} and \bar{L} are the average mass per unit length and average span length of the mast.

Mast	EL Centro					EC8				
	2.5	3	3.5	4	average	2.5	3	3.5	4	average
A	0.00069	0.00068	0.00066	0.00063	0.00066	0.00080	0.00069	0.00070	0.00078	0.00074
B	0.00037	0.00036	0.00035	0.00036	0.00036	0.00042	0.00042	0.00039	0.00049	0.00043
C	0.00034	0.00033	0.00031	0.00030	0.00032	0.00037	0.00038	0.00037	0.00038	0.00038
D	0.00024	0.00023	0.00023	0.00023	0.00023	0.00038	0.00032	0.00033	0.00036	0.00035

Table 8-1 Normalized Moment Ratio for peak bending moments

Table 8-1 shows normalized moment ratios across the four masts subject to the El Centro and EC8 analyses. Due to the frequency content of the El Centro time history, the four masts behaved differently with the shorter masts interacting significantly more. The EC8 time history contains a wide range of frequencies and therefore excited all four masts considerably. A relatively small spread is shown between ratios for a particular mast. Figure 8-17 shows a plot of the normalized moment ratios versus mast height and average span. A power function trend line has been added to the EC8 data.

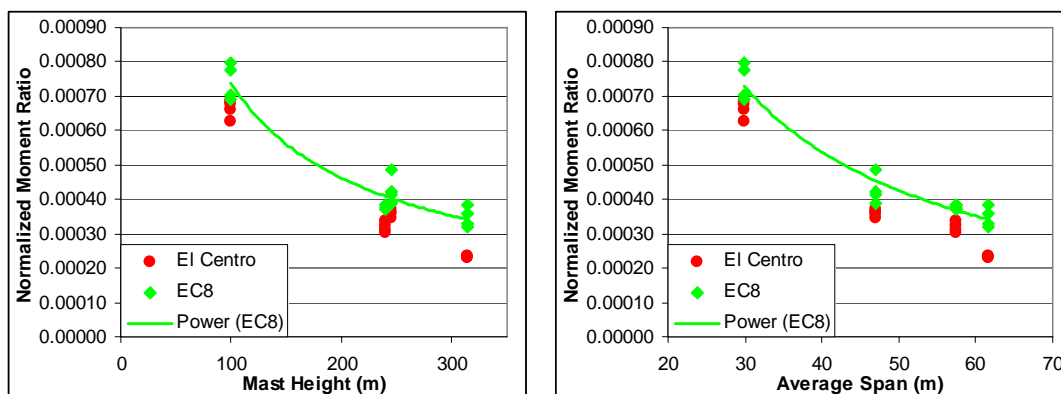


Figure 8-17 Average *NMR* vs mast height and average span

Although both plots show good correlation to a power function, a better fit is shown when *NMR* is plotted against average span length. The shape of the plots is consistent with much of the mast response, particularly the shear response and is consistent with the trends observed by Amiri for base shear. This method of normalization could be developed significantly to apply to individual spans, masses etc, however for the purposes of this study is sufficient in showing common behaviour between masts.

The average peak normalization ratio (from EC8 analyses) can be estimated using the following equation:

$$NMR = 0.03\bar{L}^{-1.05} \quad (8.2)$$

where \bar{L} is the average span length of the mast.

8.2 Mast Shear

Figures 8-18 to 8-25 show the peak shear force envelopes in the X and Y directions for each mast in response to the three earthquakes at 4m/s^2 scaling. Shear force in the X direction represents the response in the dominant direction of the earthquake.

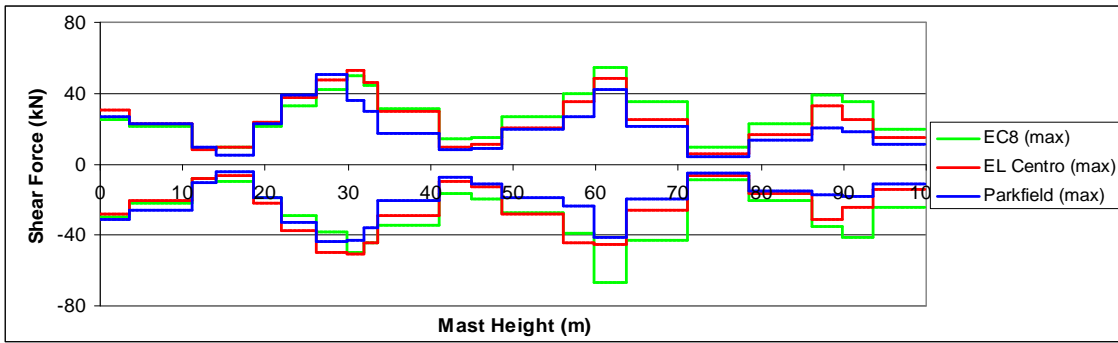


Figure 8-18 Mast A – shear force envelopes (X direction) for 4m/s^2 scaling

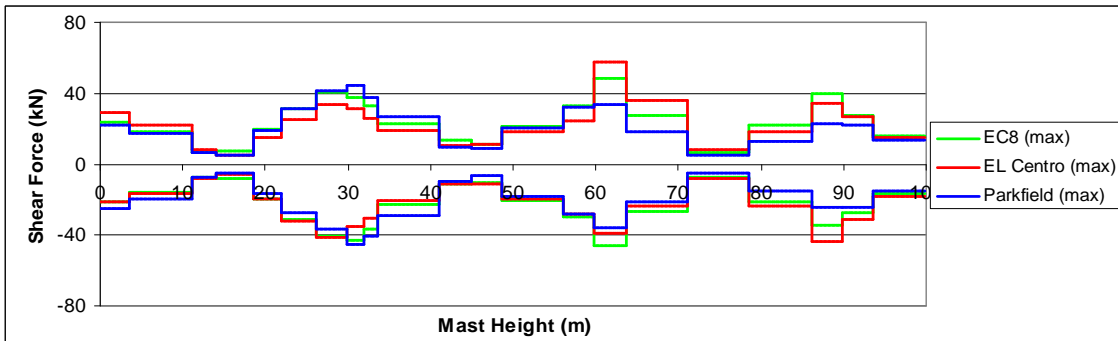


Figure 8-19 Mast A – shear force envelopes (Y direction) for 4m/s^2 scaling

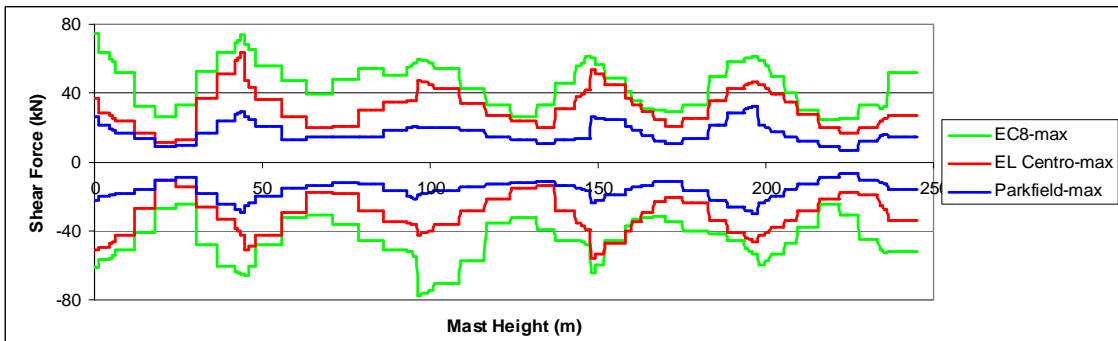


Figure 8-20 Mast B – shear force envelopes (X direction) for 4m/s^2 scaling

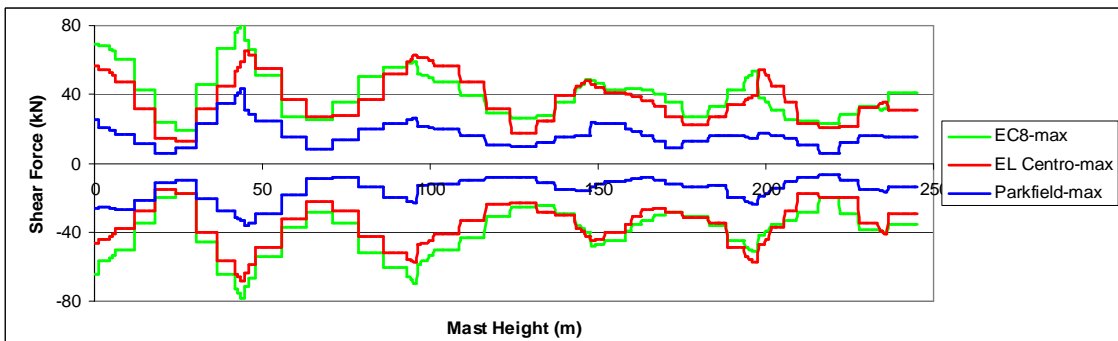


Figure 8-21 Mast B – shear force envelopes (Y direction) for 4m/s^2 scaling

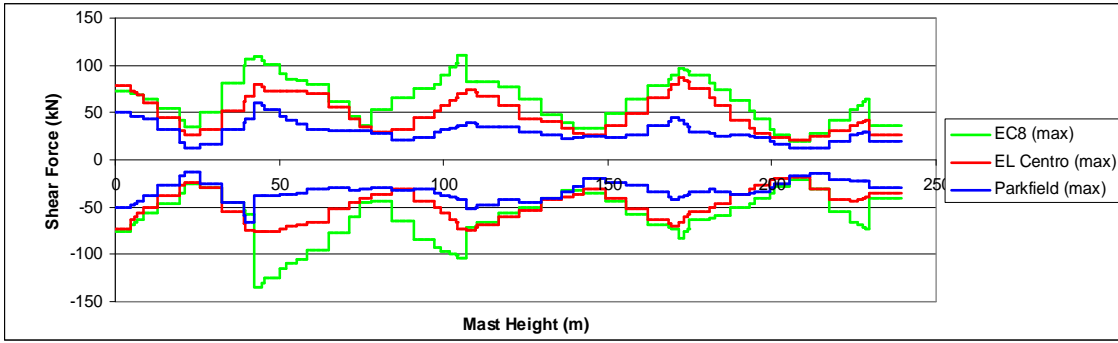


Figure 8-22 Mast C – shear force envelopes (X direction) for 4m/s^2 scaling

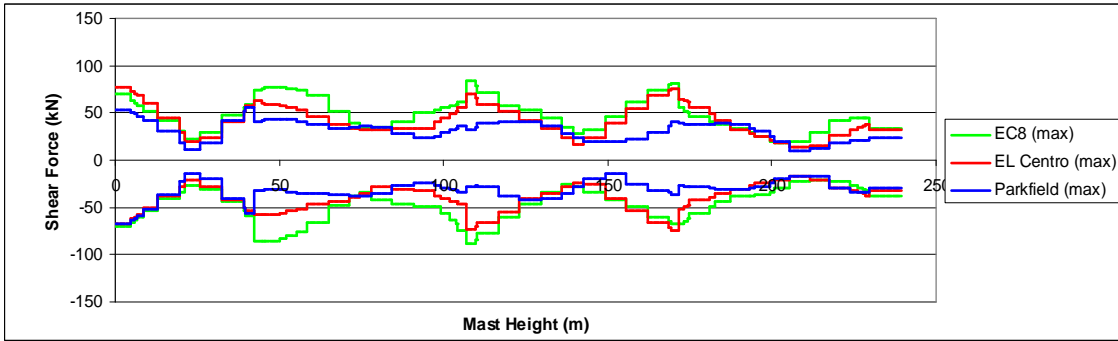


Figure 8-23 Mast C – shear force envelopes (Y direction) for 4m/s^2 scaling

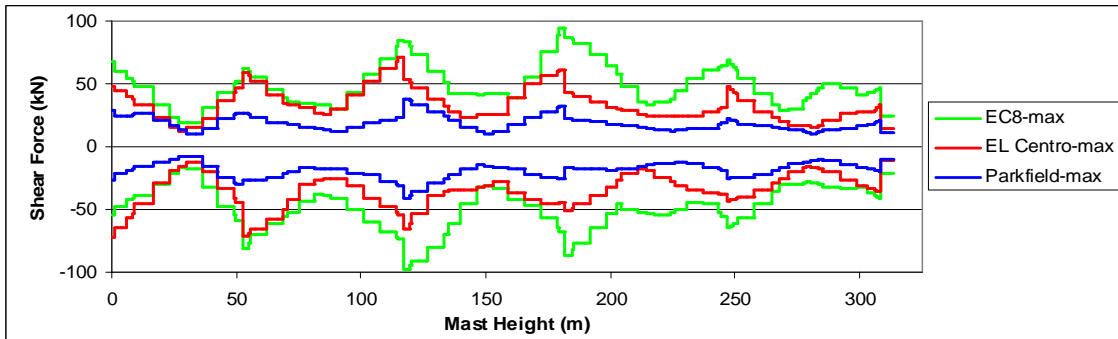


Figure 8-24 Mast D – shear force envelopes (X direction) for 4m/s^2 scaling

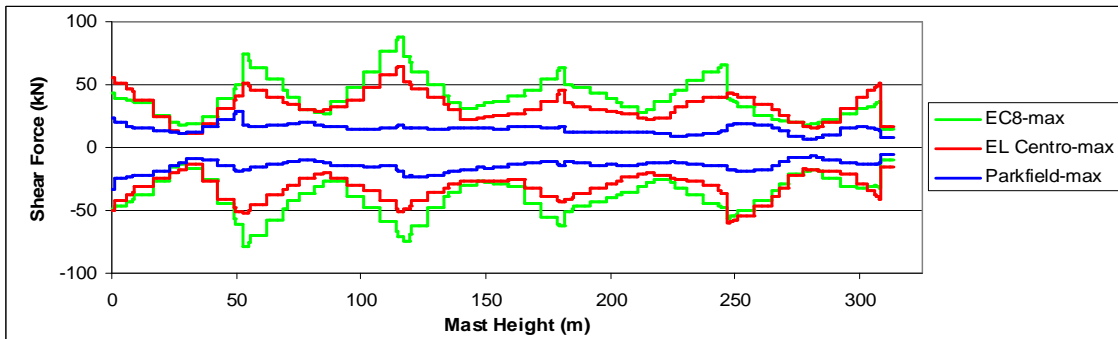


Figure 8-25 Mast D – shear force envelopes (Y direction) for 4m/s^2 scaling

Shear force envelopes for the masts show a distribution in all masts similar to that of a continuous beam with high shear forces produced at stay connection points and reduced shear produced at midspan. As with the bending response, mast A generated significant shear forces in response to all three ground motions, whilst masts B, C and D responded more to the EC8 ground motion, and less to the Parkfield motion. This is consistent with the natural frequency content of the masts and accelerograms. Also consistent with the bending response, the longer spans of mast C generated significantly higher shear forces than those of mast B; as much as twice those of mast B at support points. The distribution of shear force shows appreciable differences in the X and Y direction, with higher forces generally developing in the X direction, in response to the dominant direction of vibration. It is interesting to note that the response of mast A to the Parkfield ground motion appears more severe at the base of the mast and is generally lower than the other analyses in the upper regions. This is because the ‘pulse’ contained in the Parkfield motion is primarily resisted at the base of the mast with all of the mast and cable mass in the lower regions oscillating together. The ‘pulse’ provides less repetitive ground motion that might cause excitation of the upper regions of the mast.

As with the bending response, determining the peak values of shear force in the X and Y directions and designing for the vector sum is very conservative as peak forces at different locations and directions do not occur simultaneously. Figures 8-26 to 8-33 show the magnitudes of the peak shear forces for the EC8 and El Centro analyses generated using the vector sum of the X and Y shear components in the time domain. Four envelopes from a particular earthquake are shown in the same colour with increasing magnitudes corresponding to PGA scale factors of 2.5, 3, 3.5 and 4m/s². The magnitude of the design wind shear force is also shown as well as an indicative design shear force produced from analyses with mean hourly wind speeds of 20m/s and 28m/s respectively.

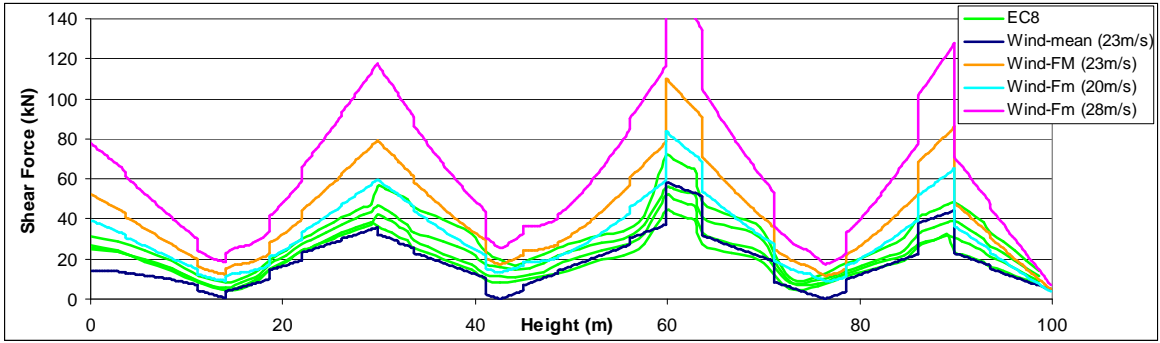


Figure 8-26 Mast A – absolute shear force envelopes for EC8 time histories

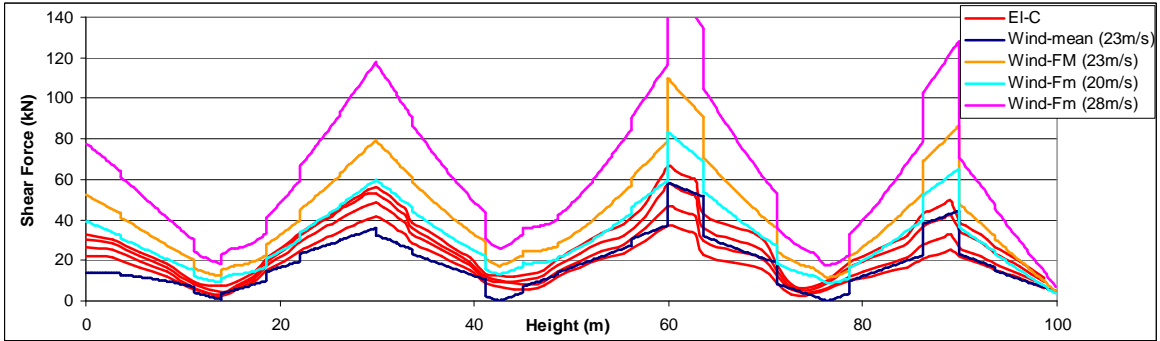


Figure 8-27 Mast A – absolute shear force envelopes for El Centro time histories

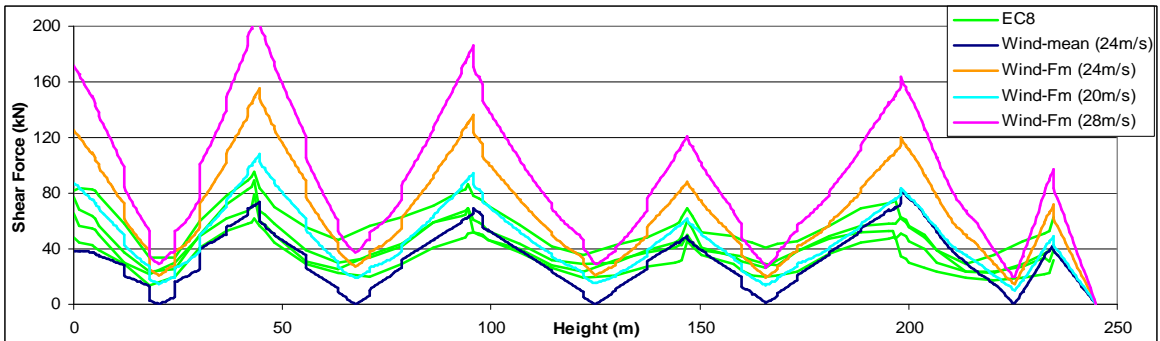


Figure 8-28 Mast B – absolute shear force envelopes for EC8 time histories

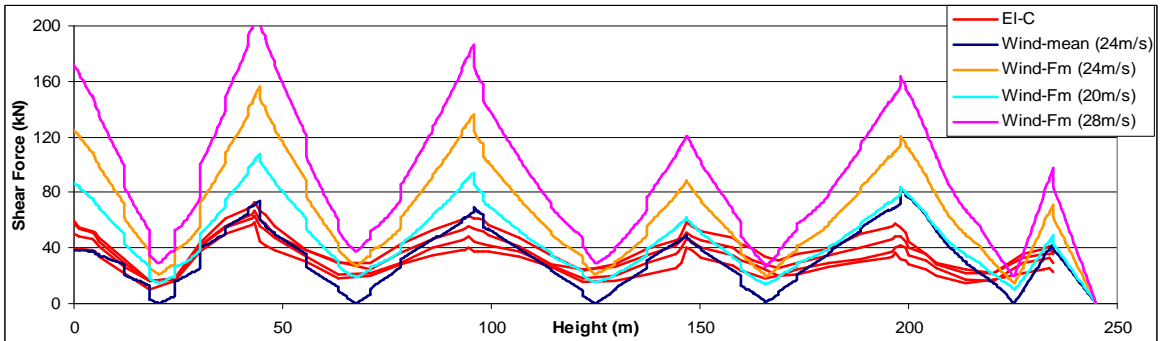


Figure 8-29 Mast B – absolute shear force envelopes for El Centro time histories

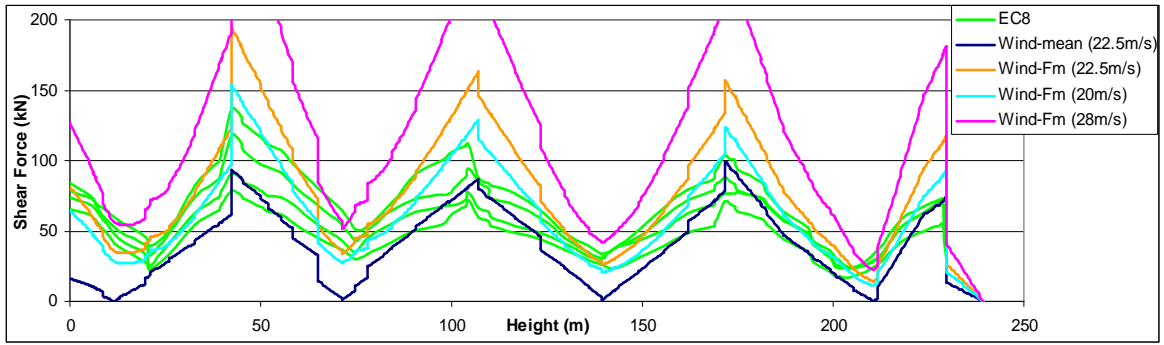


Figure 8-30 Mast C – absolute shear force envelopes for EC8 time histories

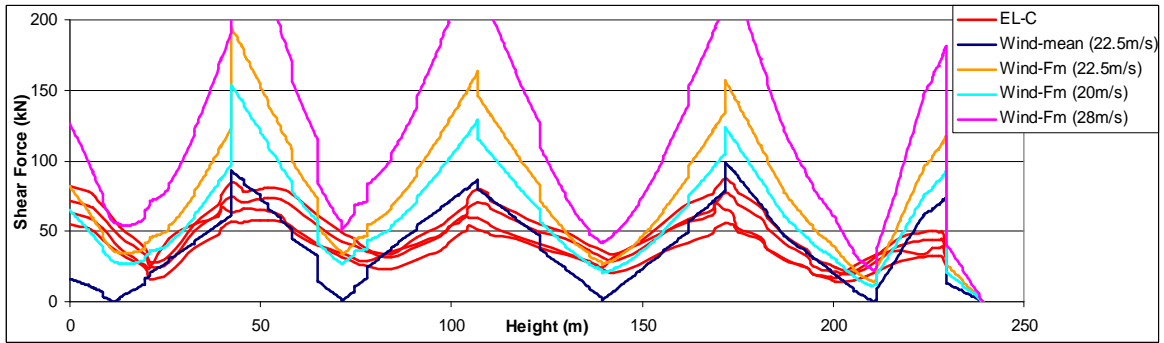


Figure 8-31 Mast C – absolute shear force envelopes for El Centro time histories

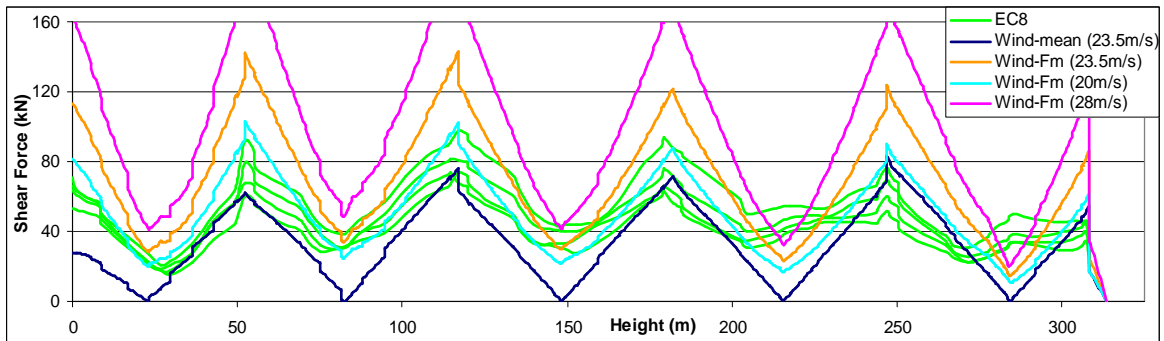


Figure 8-32 Mast D – absolute shear force envelopes for EC8 time histories

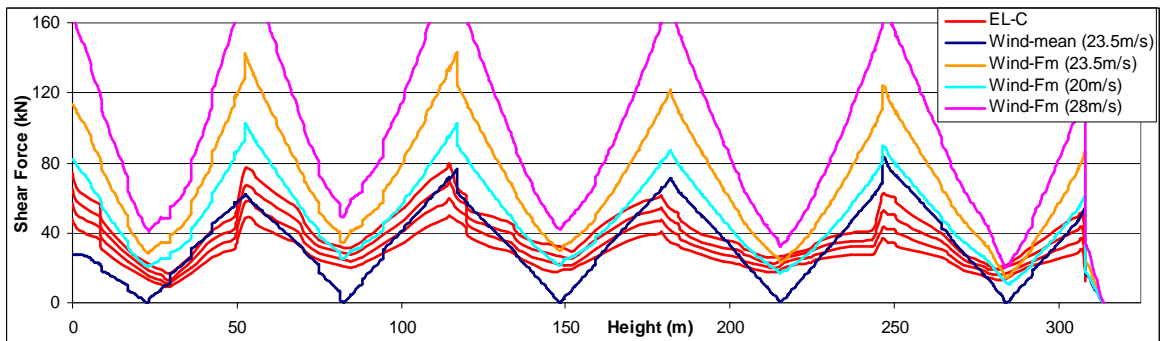


Figure 8-33 Mast D – absolute shear force envelopes for El Centro time histories

The peak shear force response show similar characteristics to the bending response with regard to linearity in comparison to PGA. The peak shear response of all of the masts is reasonably linear to the El Centro time histories. More irregularities and nonlinearities are shown in response to the EC8 time histories, particularly in mast B when PGA is increased from 3.5m/s^2 to 4m/s^2 .

Unlike the bending response, the shear response (apart from base shear for mast C and isolated midspan regions) is well within the design forces produced from the wind analysis. During a static or equivalent static analysis such as a BS8100-4 wind analysis all loading is applied in one direction and the whole load needs to be resisted by the cables. During a dynamic seismic analysis, it is unlikely that adjacent spans will oscillate in the same direction simultaneously and thus part of the overall force generated by a particular span is opposed, to some extent, by the force generated by the adjacent span. The restraint force provided by the cable supports is therefore lower than might be expected when considering the vibration of each span independently. The opposing bending in adjacent spans reduces the hogging moment at the supports and increases the sagging moment in each respective span. The shear force response in the mast is not affected to the same extent and consequently the seismic bending response described in section 8.1 is comparable to the design wind analyses, whereas the shear response is not.

Indicative design shear force envelopes produced for mean hourly wind speeds of 20m/s and 28m/s show that in this range the design wind shear force can be doubled with an increase in design wind speed of 8m/s (this is because design loads are proportional to V^2). However even with a design wind speed as low as 20m/s, it is unlikely that design wind shear forces will be exceeded by a seismic response caused by seismic loadings similar to those used in this research.

As with the bending response a simple method has been used to normalize the peak shear force across the four masts. The following equation was adopted in an attempt to normalize peak shear forces:

$$NSR = \frac{V}{PGA \times \overline{mL}} \quad (8.3)$$

where *NSR* is a Normalized Shear Ratio, *V* is the peak shear force in the mast, and \overline{m} and \overline{L} are the average mass per unit length and average span length of the mast.

Mast	EL Centro					EC8				
	2.5	3	3.5	4	average	2.5	3	3.5	4	average
A	0.00401	0.00390	0.00397	0.00398	0.00396	0.00427	0.00413	0.00385	0.00430	0.00414
B	0.00144	0.00128	0.00116	0.00112	0.00125	0.00150	0.00161	0.00155	0.00146	0.00153
C	0.00108	0.00110	0.00104	0.00103	0.00106	0.00148	0.00142	0.00158	0.00161	0.00152
D	0.00091	0.00090	0.00090	0.00090	0.00090	0.00134	0.00112	0.00105	0.00111	0.00115

Table 8-2 Normalized Shear Ratio for peak shear forces

As with the bending ratios, a relatively small spread of results is shown between the difference ratios of any particular mast. Figure 8-34 shows the normalized shear ratios plotted against mast height and average span length.

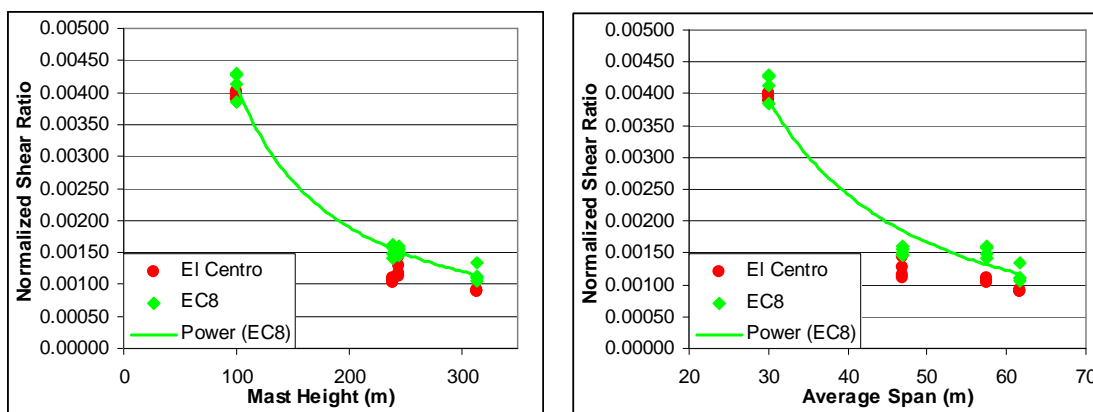


Figure 8-34 Average normalized shear ratio versus mast height and average span

Again the shape of the curve indicates a similar trend to that observed for bending and total base shear (reported later in this section for this research and that of Amiri’s). Unlike bending however, a better fit is observed when *NSR* is plotted against mast height than against average span length.

The following equation can be used to estimate the average *NSR* for the masts subject to the EC8 ground motion:

$$NSR = 0.712H^{-1.119} \tag{8.4}$$

where *H* is the total height of the mast.

Figures 8-35 to 8-38 show plots of the peak mast base shear and total base shear for the four masts subjected to three different time histories, each at four different scale factors. The total base shear is the sum of all the horizontal reactions at support points.

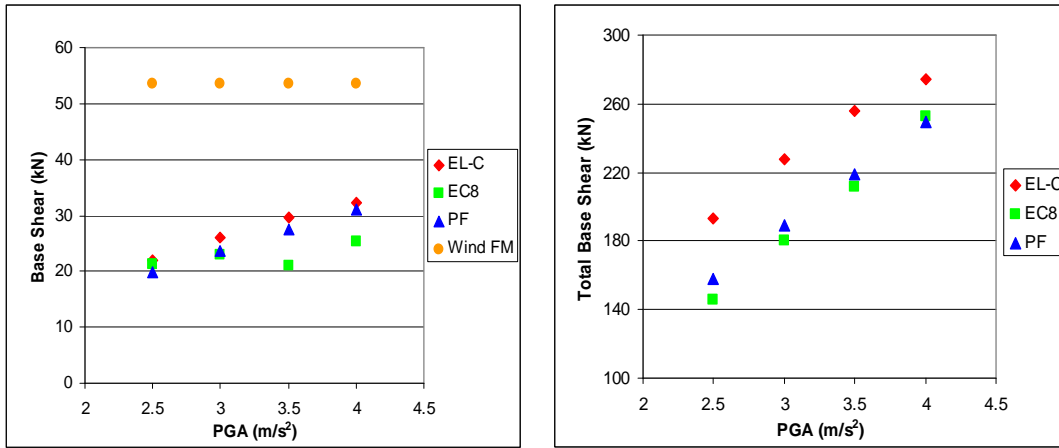


Figure 8-35 Mast A – peak mast base shear and total base shear vs PGA scale factor

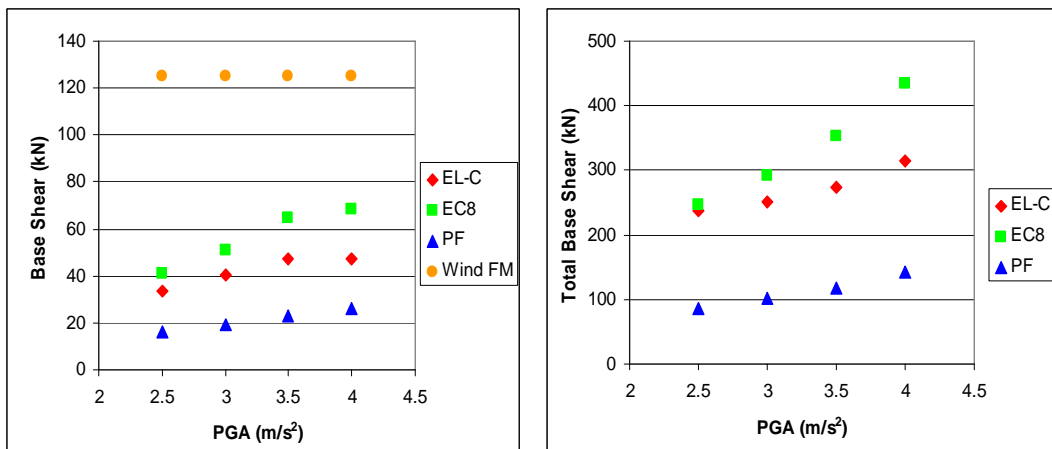


Figure 8-36 Mast B – peak mast base shear and total base shear vs PGA scale factor

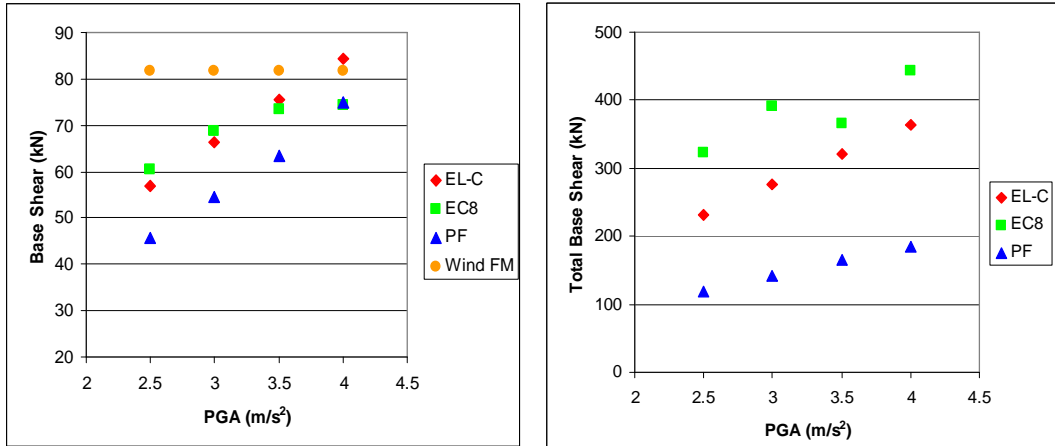


Figure 8-37 Mast C – peak mast base shear and total base shear vs PGA scale factor

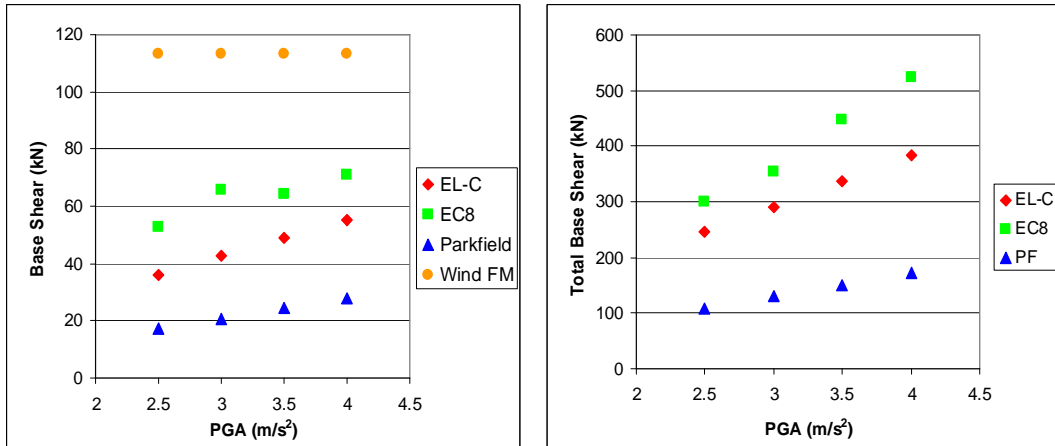


Figure 8-38 Mast D – peak mast base shear and total base shear vs PGA scale factor

The peak base shear and total base shear response to the El Centro and Parkfield time histories show an approximately linear response to variations in PGA scale factor. Close investigation showed that even when the peak response occurred at different time steps, the overall response was close to linear. This could have a significant impact on the development of an equivalent static method, as the overall response to increased design PGA is linear.

The base shear response of the masts to the EC8 accelerogram exhibits significant nonlinearity. Generally an increase in the scale of the input accelerogram leads to an increase in peak base shear (mast or total), however isolated peak responses (e.g. mast C total base shear) show decreases in this value (usually with a PGA scale factor of 3.5 or 4). This

nonlinear response is not usually reflected in both the mast base shear and the total base shear for a particular mast which suggests that there is either a shift to a different vibration mode or that a particular part or span of the structure becomes more excited at particular amplitudes.

Figure 8-39 shows the total base shear response as a time history for mast C for the EC8 accelerograms. The overall response of the mast appears relatively similar for each of the four scale factors with similar oscillation patterns appearing throughout. The magnitude of the peak response for the four accelerograms is generally consistent with the scale factor applied to the accelerogram, apart from a few isolated regions where this order is not apparent. At approximately 16.5s an inconsistent peak is shown in the EC8-3 analysis, causing a magnified peak base shear in Figure 8-37 and an apparent reduction in total base shear at 3.5m/s^2 .

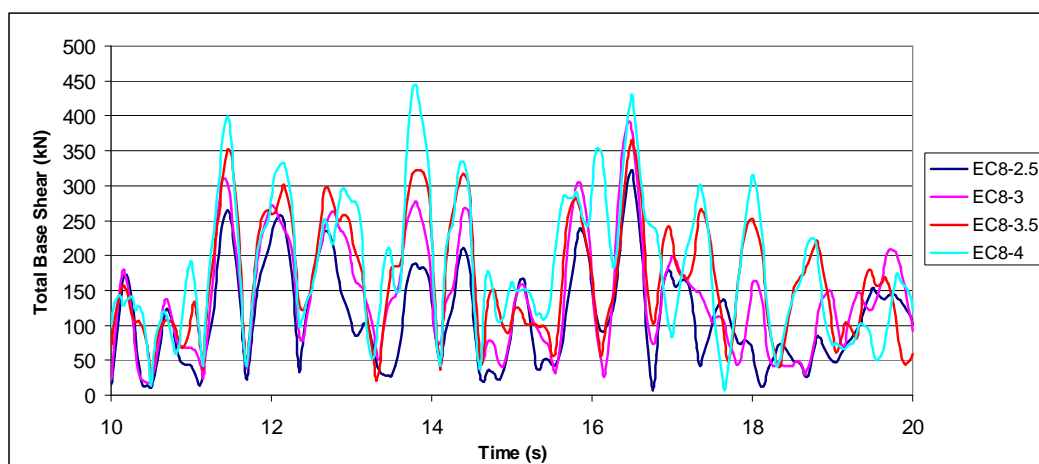


Figure 8-39 Mast C – total base shear magnitude for EC8 analyses (time 10s–20s)

Mast base shear was identified during early analyses as being an area that may be susceptible to earthquake loading when only design wind loading was considered. Wind design mast base shear was only exceeded in mast C with the highest scale factor of 4m/s^2 . This seems to be due to low wind design forces rather than high seismic forces as the arrangement of wind loading, mast geometry and cable stiffnesses lead to a mean wind loading of close to zero at the base of mast C, and thus a relatively low design force in this area.

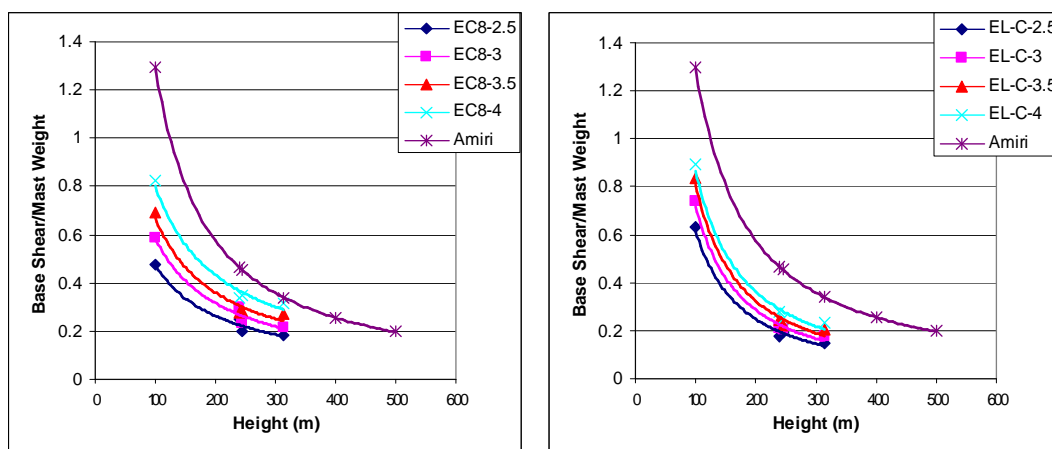


Figure 8-40 Peak total base shear/mast weight vs mast height for EC8 and El Centro analyses

Figure 8-40 shows a representation (initially shown by Amiri [1]) of maximum total base shear as a function of total mast weight against mast height for the four masts for the EC8 and El Centro analyses. The trend observed by Amiri, with input accelerograms scaled at $0.34g$ ($3.34m/s^2$), has been added to the graph for comparison. A similar trend is observed for the masts in the current analyses. Part of the offset from the trend observed by Amiri could be explained by the fact that additional ancillary loads were included in the current study, and were omitted in Amiri's research. This is substantiated by the fact that mast A, with the highest percentage ancillary loading, is furthest from Amiri's trendline, and mast D, with the lowest percentage ancillary load, is closest. The consistent shape of the curve for both studies is a positive sign for the development of an equivalent static method for seismic design. The following equation describes the peak base shear shown by this study (for both EC8 and El Centro accelerograms at $4m/s^2$ scaling) as a function of mast height (correlation factor of 0.97).

$$BS = 7523H^{-0.97} \quad (8.5)$$

where

BS Peak Total Base Shear (kN) as a percentage of total mast weight (including ancillaries)

H Mast height (m)

8.3 Mast Deflections

The following Figures 8-41 to 8-44 show the peak deflections relative to the ground of the masts to the EC8 accelerogram with increasing scale factors. The vector sum of the X and Y components has been calculated in the time domain and the peak value identified and plotted. The direction of the deflection is therefore not specified. As the EC8 analyses exhibited the worst and most consistent response across the four masts, the deflection responses from these analyses are shown.

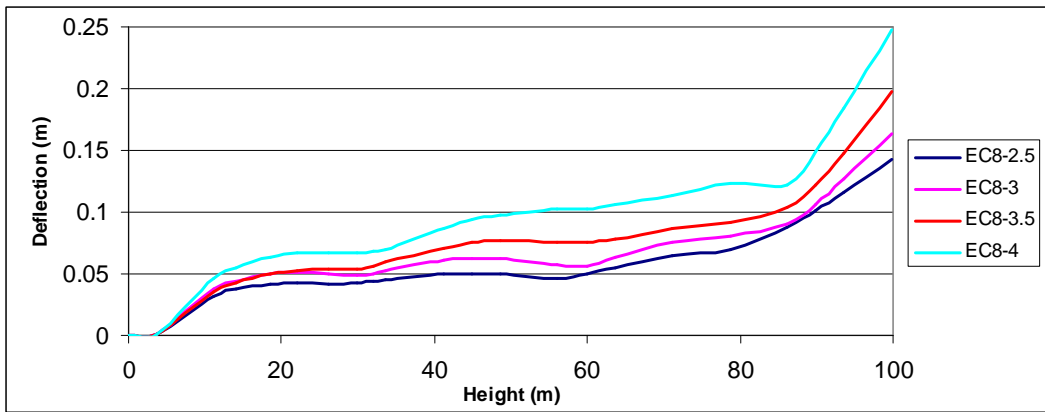


Figure 8-41 Mast A – peak deflection for EC8 time histories

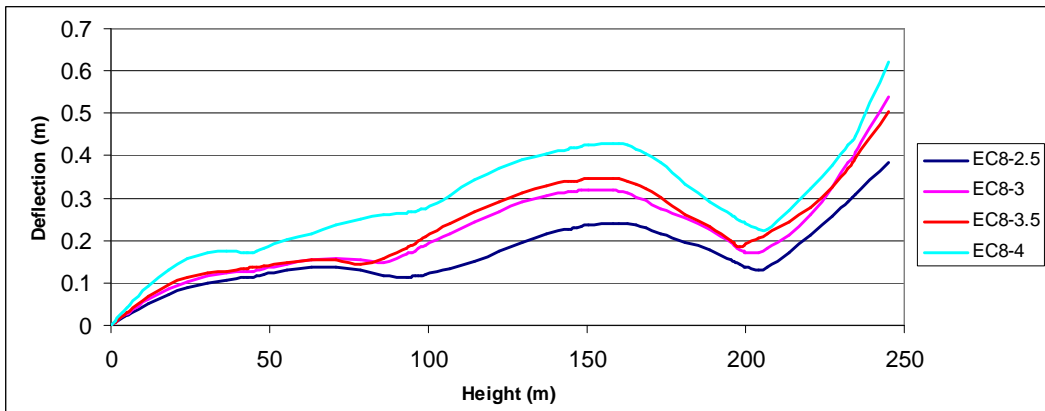


Figure 8-42 Mast B – peak deflection for EC8 time histories

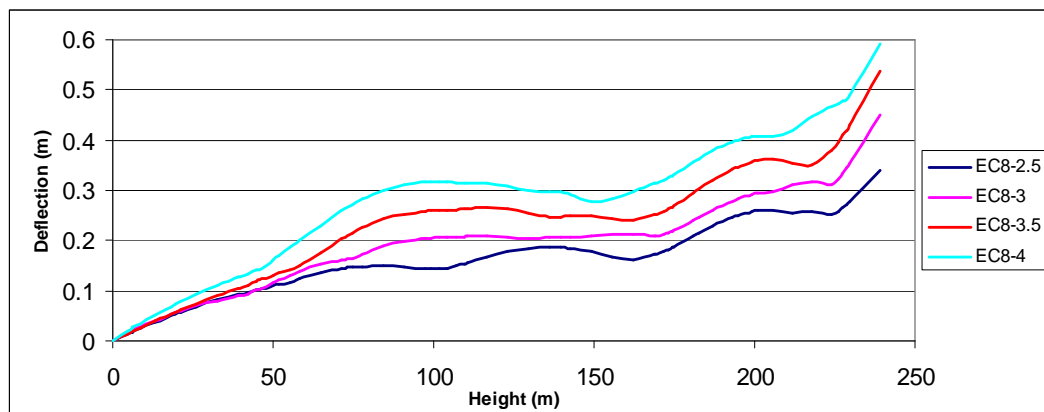


Figure 8-43 Mast C – peak deflection for EC8 time histories

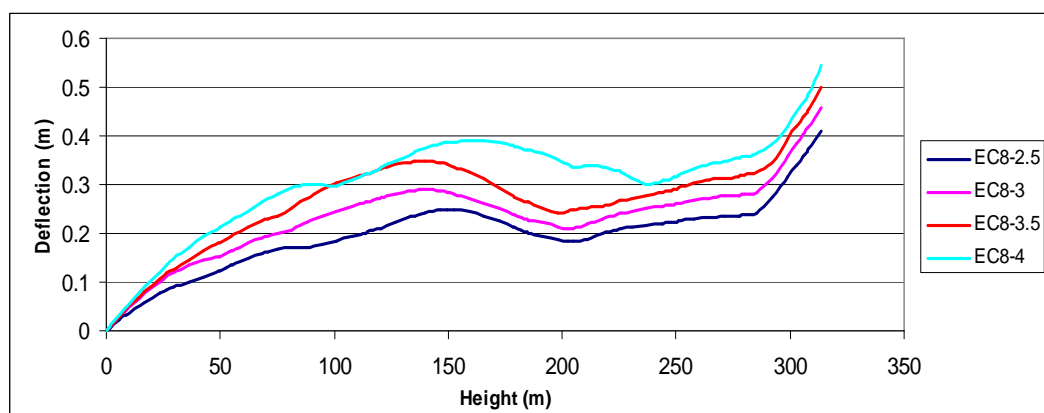


Figure 8-44 Mast D – peak deflection for EC8 time histories

The peak deflection in any particular mast generally increases with height, apart from bulges that are shown in the middle part of mast B and mast D. This general increase is consistent with an overall reduction in horizontal stiffness of the stays with increased height (see Table 4.5). The bulge in the mast B profile is explained by the comparatively low cable stiffness at level C. It is interesting to note that the peak deflection/mast height ratio for masts A, B, and C is approximately equal to 1/400. This ratio for mast D is 1/575. The relatively low deflection at the top of mast D can be explained by the absence of any significant cantilever, and relatively stiff cable stay supports at level 4. In addition to this a much lower ancillary load is present in mast D causing the mast to interact less, in proportion to its height, than the other masts.

The time history deflection response at each stay level is shown in the following Figures 8-45 to 8-48 for the four masts in response to the EC8 accelerogram with $4m/s^2$ scaling.

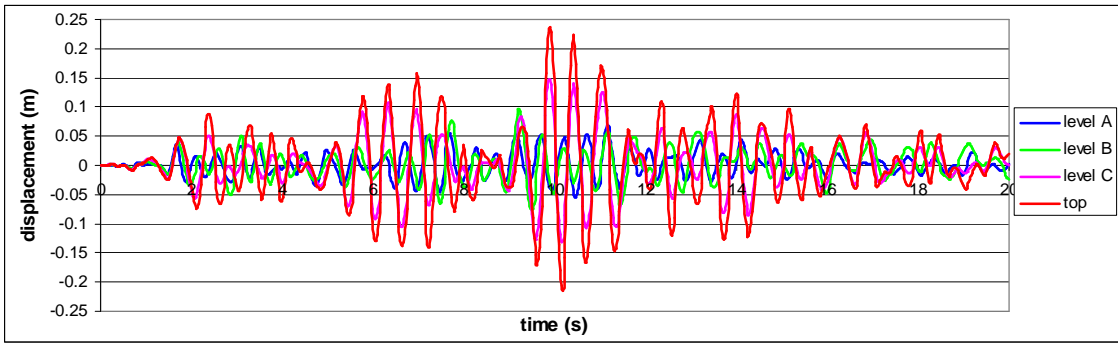


Figure 8-45 Mast A – EC8-4 stay level deflection, X-direction (time history)

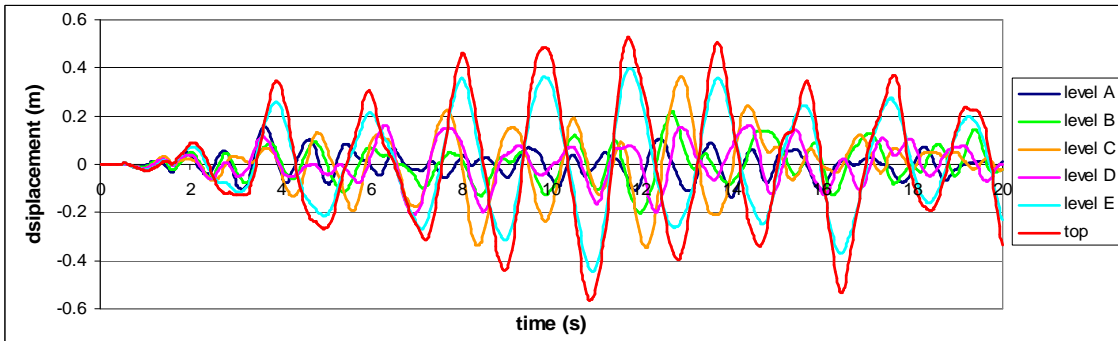


Figure 8-46 Mast B – EC8-4 stay level deflection, X-direction (time history)

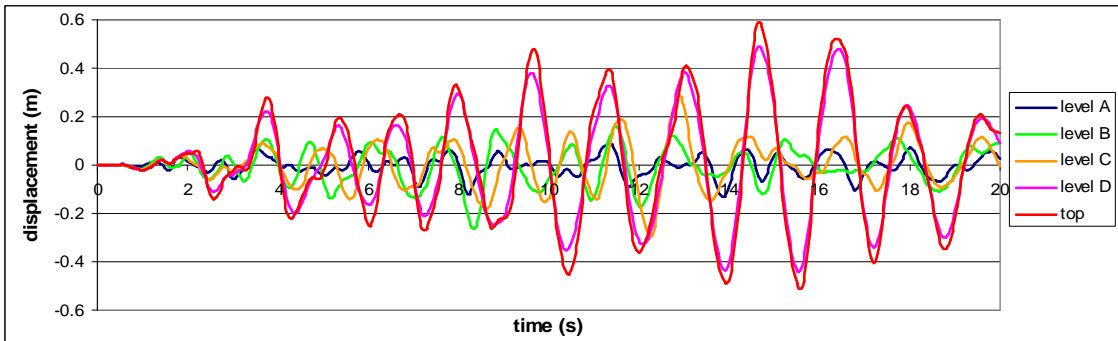


Figure 8-47 Mast C – EC8-4 stay level deflection, X-direction (time history)

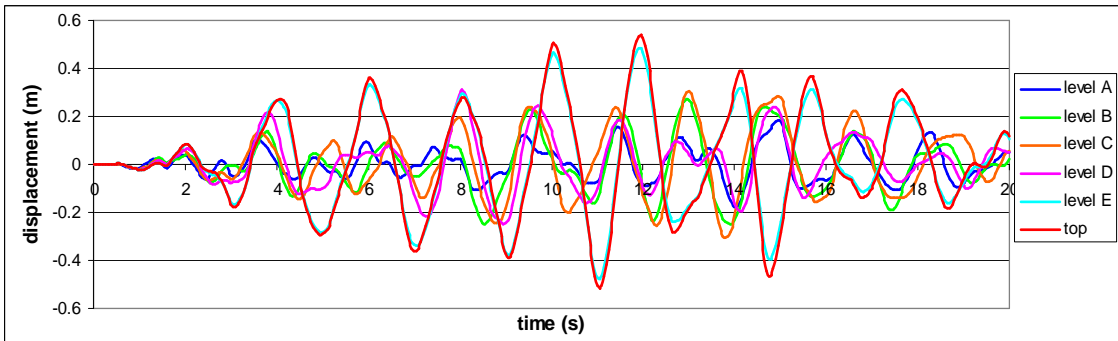


Figure 8-48 Mast D – EC8-4 stay level deflection, X-direction (time history)

As expected the response of the shorter mast A is significantly different to the other three masts with a much higher frequency of oscillation. Mast A also shows more deflection in the positive X direction (loosening of the cable in plane with the vibration) as the stiffness in this direction is lower. The period of vibration at the top sections of masts B, C and D is more or less regular implying a dominant mode of vibration, however at lower levels, particularly in masts C and D, a more irregular vibration is present implying that some higher modes were active in the response of the lower sections of the masts. Although the lower natural frequencies will dominate a displacement response, particularly in regions of the mast where displacements are highest, the relatively smooth pattern of oscillation does imply that mast oscillation is governed by a particular mode. The lower stiffness of the level C cables in mast B is clearly shown by substantially higher amplitudes of oscillation than the surrounding levels. This caused the bulge in the peak displacement profile in this region.

Figures 8-49 to 8-52 show a comparison of the time history deflection response of the masts at two stay levels for the EC8 and El Centro analyses at 4m/s^2 scaling.

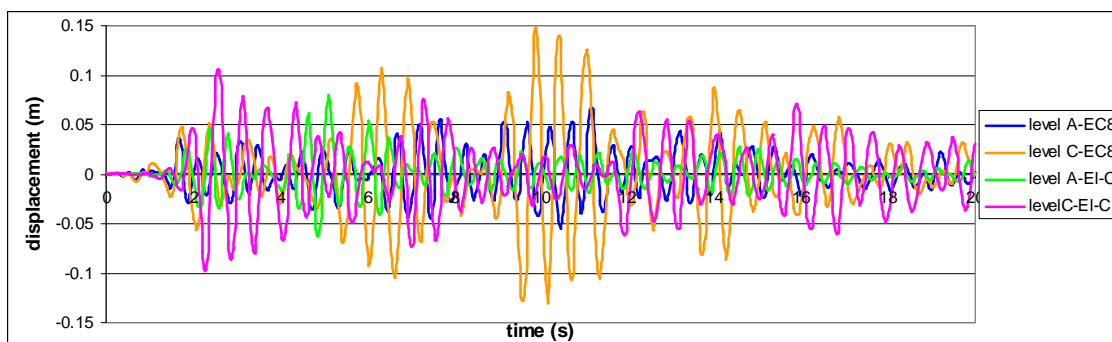


Figure 8-49 Mast A – EC8 and El Centro time history deflection comparison (levels A and C)

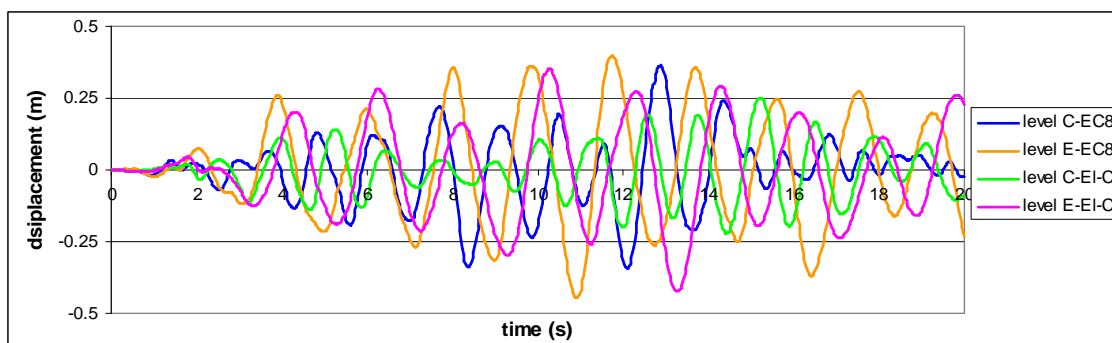


Figure 8-50 Mast A – EC8 and El Centro time history deflection comparison (levels C and E)

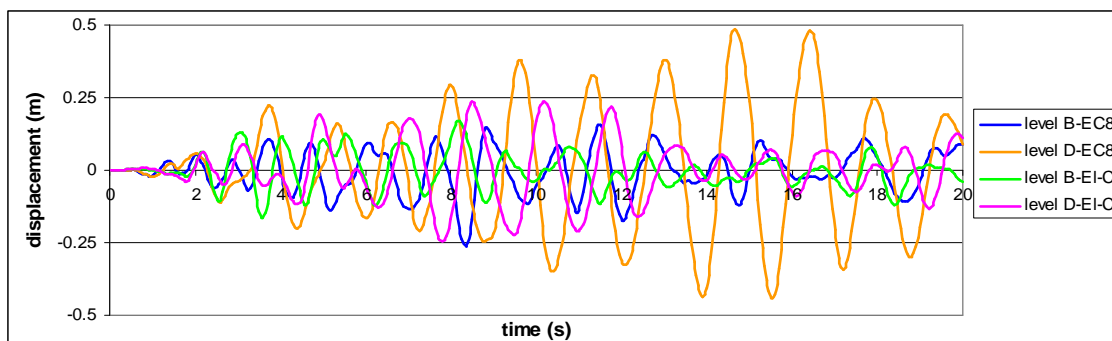


Figure 8-51 Mast C – EC8 and El Centro time history deflection comparison (levels B and D)

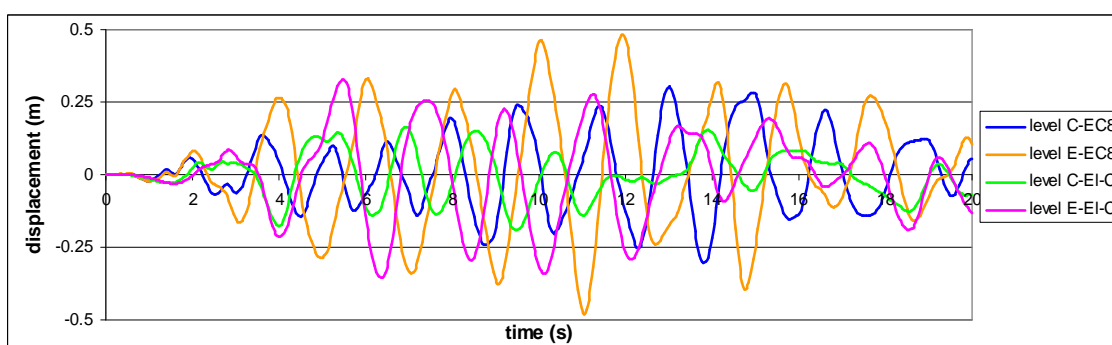


Figure 8-52 Mast D – EC8 and El Centro time history deflection comparison (levels C and E)

Interesting similarities are shown between the behaviour of the masts to the EC8 and El Centro ground motion. Although the amplitude of oscillation varies, the period of each oscillation is similar with each peak in the EC8 response, usually having a corresponding peak in the El Centro response. Mast A is the only mast that is significantly excited by the first 5 seconds of El Centro high amplitude ground motion as the higher natural periods of masts B, C and D require more repetitive oscillations to generate any considerable motion. It is for this reason that the response of these masts was significantly lower to the Parkfield ground motion. The shorter natural periods of mast A allow it to respond more significantly to variations in each accelerogram, whereas masts B, C and D all show a relatively consistent response throughout the EC8 analyses and higher amplitude oscillations between 6s and 12s during El Centro analyses.

8.4 Mast Axial Forces

The following Figures 8-53 to 8-56 show the peak axial response of the four masts to the three accelerograms. Axial forces in the mast are primarily produced by the self weight of the mast and cables and the pretension in the cables. The distribution is characterized by a steady increase in magnitude with decreasing height, and sharp increases at stay connection points where stay weight and pretension are added to the mast. The compression introduced at each stay level generally increases with increasing height.

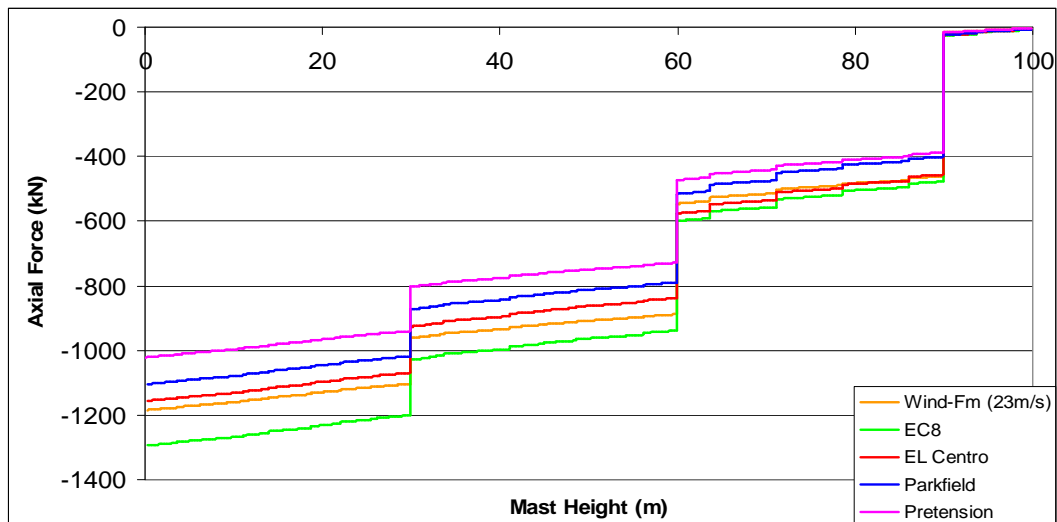


Figure 8-53 Mast A – peak axial force for 4m/s^2 scaling

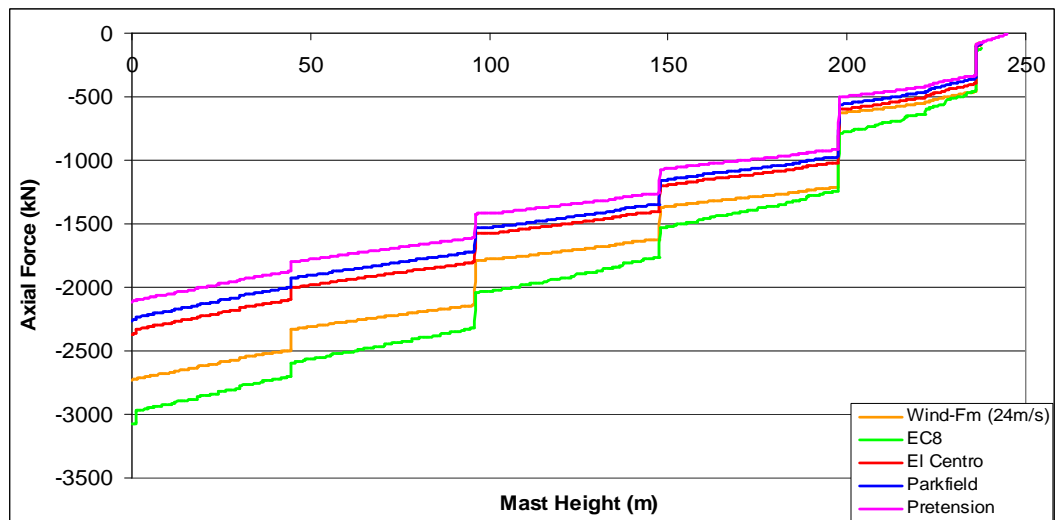


Figure 8-54 Mast B – peak axial force for 4m/s^2 scaling

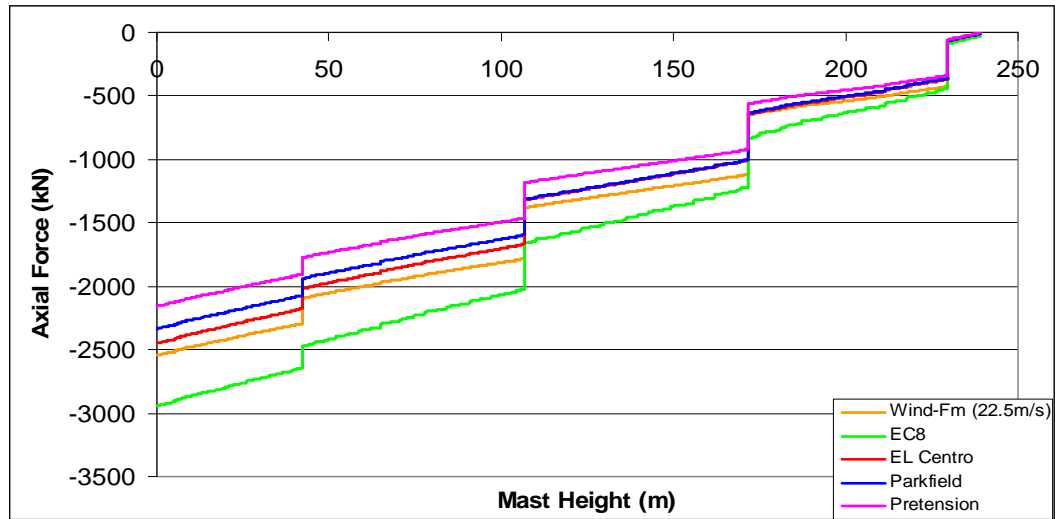


Figure 8-55 Mast C – peak axial force for $4m/s^2$ scaling

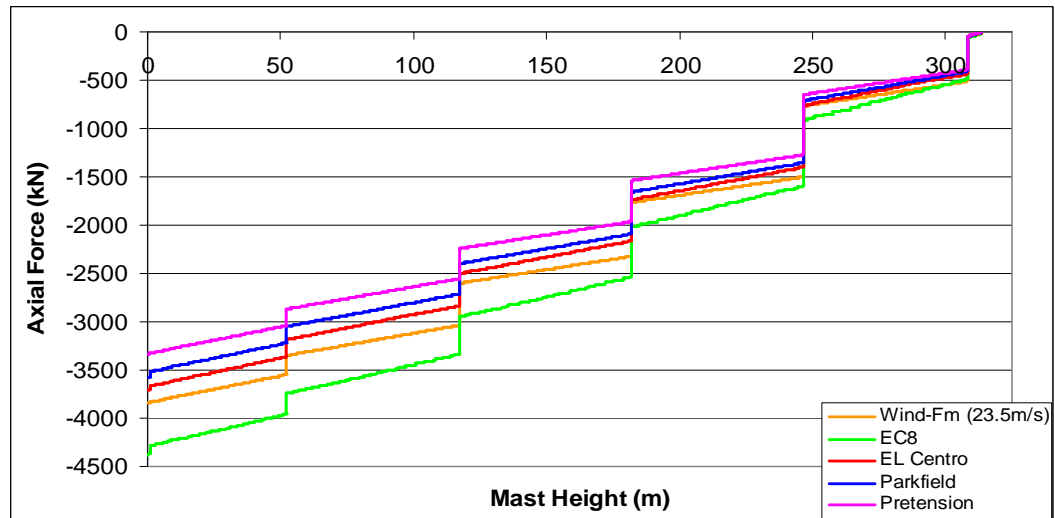


Figure 8-56 Mast D – peak axial force for $4m/s^2$ scaling

A regular distribution of peak axial forces is shown in all four masts subjected to analysis with an increase in compression exerted by the stays at all levels. The increase in compression forces between stay levels is larger at higher levels (particularly subject to the EC8 accelerogram) which may indicate that higher mast sections are more susceptible to vertical vibration. The response of all of the masts to the EC8 time history is significantly

higher than their response to the El Centro and Parkfield accelerograms and axial forces from this analysis are higher (for $4m/s^2$ scaling) than those from the design wind analysis.

Figures 8-57 to 8-60 show the peak axial force at the base of the masts for the various accelerograms against PGA scale factor.

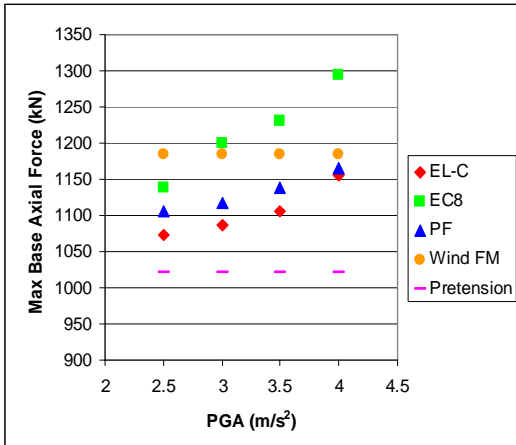


Figure 8-57 Mast A – peak base axial forces

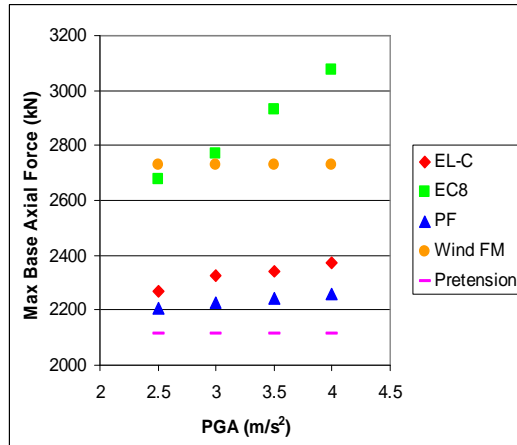


Figure 8-58 Mast B – peak base axial forces

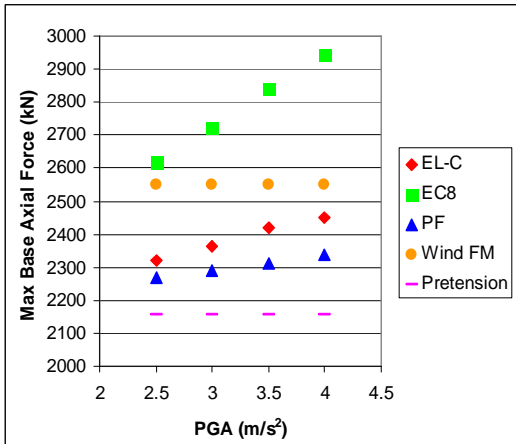


Figure 8-59 Mast C – peak base axial forces

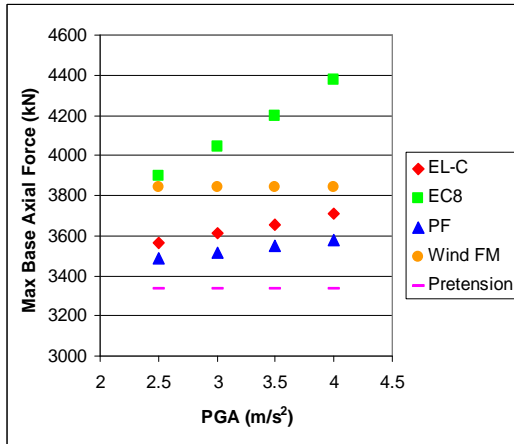


Figure 8-60 Mast D – peak base axial forces

Most of the peak results increase in a linear manner with increase in scale factor. The increase in peak axial force with increase in PGA scale factor is far more significant for the EC8 analyses than the other two (approximately of 5% of total force increase between scale factors). Eleven of the twelve EC8 analyses conducted across the masts yielded higher base

axial forces than the wind design force, whereas none of the El Centro or Parkfield analyses were above this level.

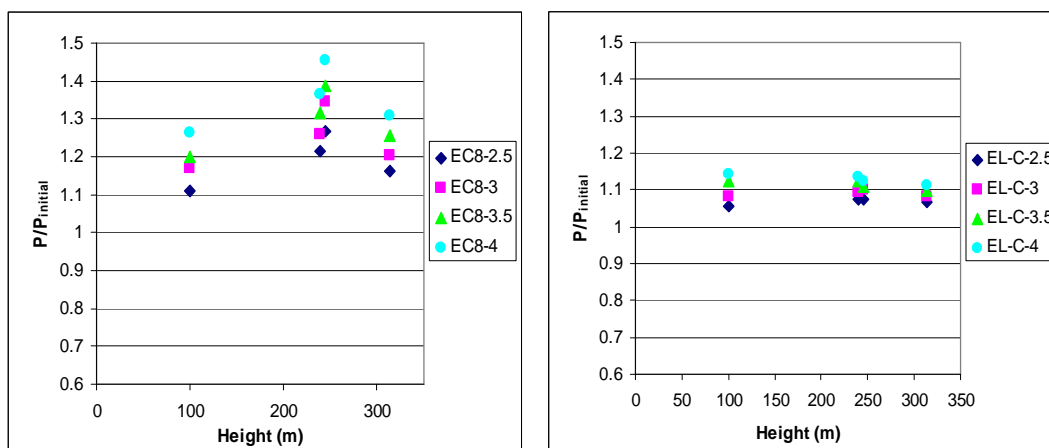


Figure 8-61 Increase in base axial Force for EC8 and El Centro Analyses

Figure 8-61 shows that all of the masts responded considerably more to the EC8 than the El Centro loading. The El Centro analysis showed that the ratio $P/P_{initial}$ was reasonably constant for a particular scale factor across the four masts with a maximum range of 3% and average ratio of 1.13 for the highest scaled analysis. This range was closer to 20% for the EC8 analyses with an average ratio of 1.35 for the highest scaled analysis. The highest axial force increases were shown by mast B (approximately 45%). It seems likely that the EC8 analysis might over estimate axial force response and if further analyses based on existing earthquake records could show that the more consistent El Centro response was more likely, this would be a very useful observation for the development of a static method of analysis. However more investigation is needed to substantiate this.

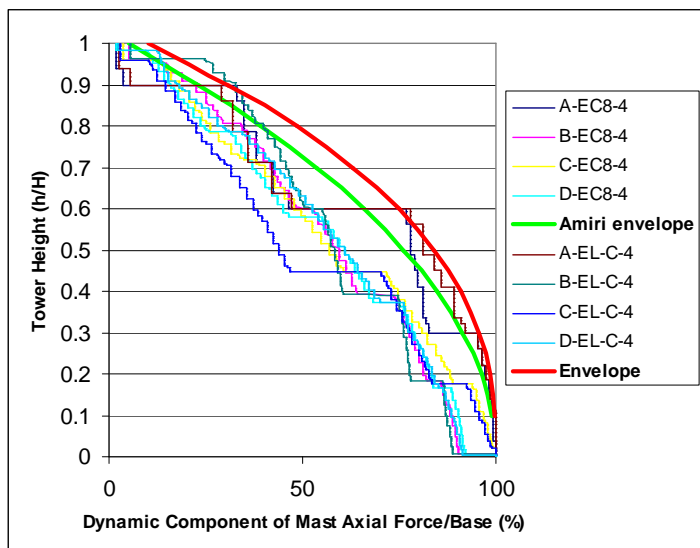


Figure 8-62 Dynamic axial force distribution for EC8 and El Centro analyses (4m/s² scaling)

Figure 8-62 shows the distribution of the peak dynamic axial force throughout the mast across the four masts as a percentage of dynamic base axial force against relative tower height. The envelope curve developed by Amiri (equation 1.3) has been added for comparison. Although interrupted by dynamic force applied at the stay supports, the gradients of the curves are relatively similar and are shallower towards the top of the masts. Again this suggests that the top regions of the masts interact more in the vertical plane than lower regions. Amiri's curve has been altered slightly to produce a conservative envelope that encompasses the results from these analyses; this is shown in Figure 8-62. The governing equation of this envelope is:

$$P_{dyn} / Base_{dyn} = 100 - 90(h / H)^{2.5} \quad (8.6)$$

where H is the total height of the mast and h is the specific height concerned.

8.5 Cable Tensions and Cable Behaviour

8.5.1 Peak Tensions

Assessing the variation in cable tensions is important in understanding the response of a guyed mast during a dynamic seismic analysis. Figures 8-63 to 8-79 show the peak cable tension reached in each cable (cables on side 1 only), subject to the three time histories at four different scale factors. The EC8 limit (twice initial tension) and wind design tension are also shown for comparison, as well as a 95% stiffness utilization tension i.e. the tension needed for the cable to behave in a ‘close to’ linear range when loading (similar to that of the equivalent rod).

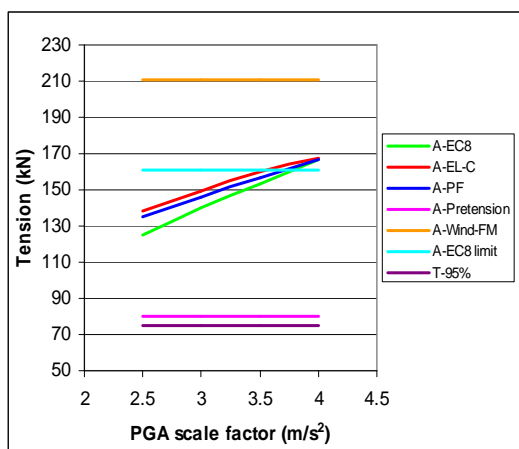


Figure 8-63 Mast A – level A1 cable tensions

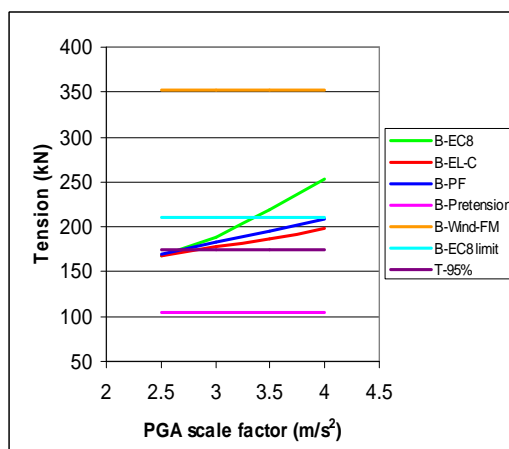


Figure 8-64 Mast A – level B1 cable tensions

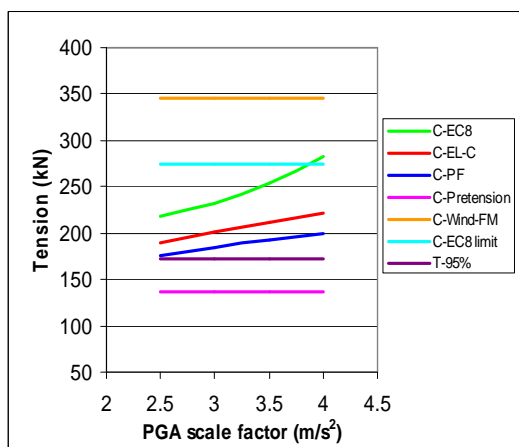


Figure 8-65 Mast A – level C1 cable tensions

Mast A cable pretensions show high stiffness utilization which suggests that much of the masts peak response to increases in PGA should be linear. Figures 8-63 to 8-65 show this to be the case although a slight nonlinear response is shown by the EC8 time history, particularly between a scaling of 3m/s^2 to 3.5m/s^2 . The response of the cables is not consistent with regard to each time history. Level A cables show higher tensions in the El-Centro and Parkfield analyses, whereas levels B and C show considerably higher tensions developing in the EC8 analysis, particularly at higher scale factors. The longer duration of EC8 motion is likely to cause excitation of the whole mast producing higher tensions in upper regions, whereas the pulse and shorter duration of motion of the Parkfield and El-Centro acceleragrams is primarily resisted at the base and 1st stay level.

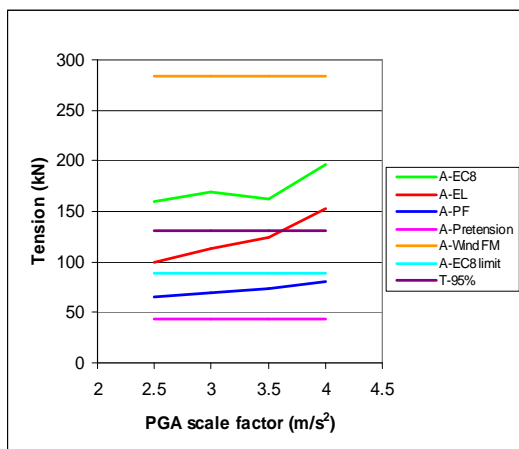


Figure 8-66 Mast B – level A1 cable tensions

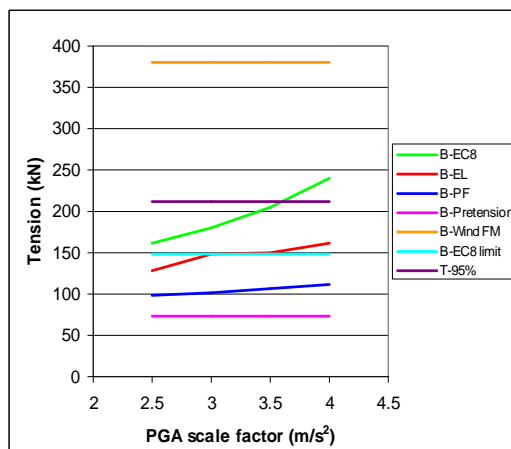


Figure 8-67 Mast B – level B1 cable tensions

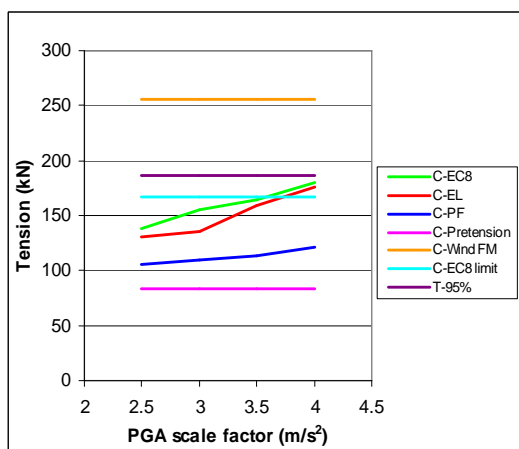


Figure 8-68 Mast B – level C1 cable tensions

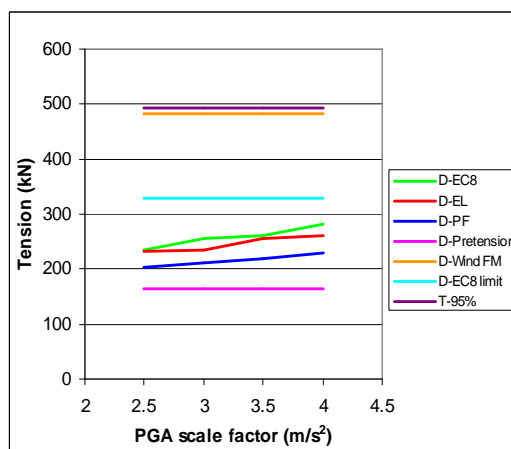


Figure 8-69 Mast B – level D1 cable tensions

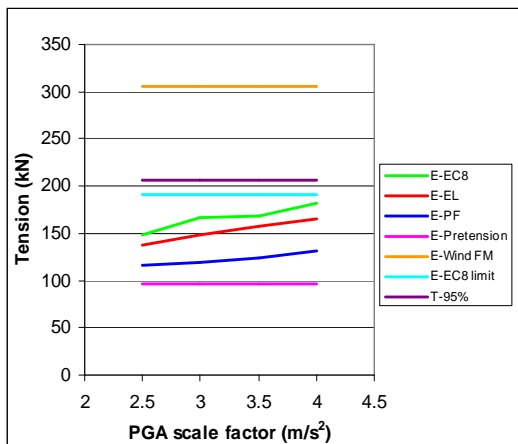


Figure 8-70 Mast B – level E1 cable tensions

The peak cable response of mast B with respect to time history scaling is far more nonlinear than the response of mast A. With initial cable tensions in the 40% to 60% stiffness utilization range any movement of the stay supports (either loading or unloading) is in the nonlinear range. The percentage increase in cable tension is higher at the bottom two levels where most tensions exceed the EC8 limit.

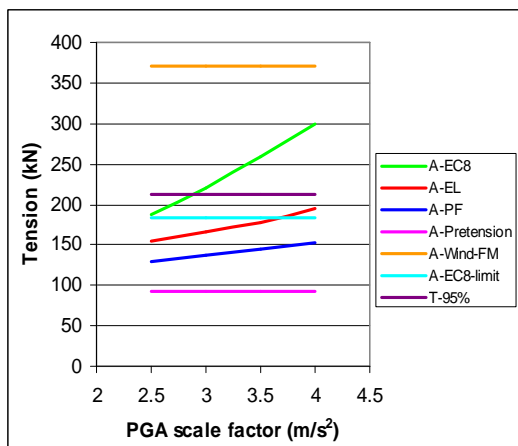


Figure 8-71 Mast C – level A1 cable tensions

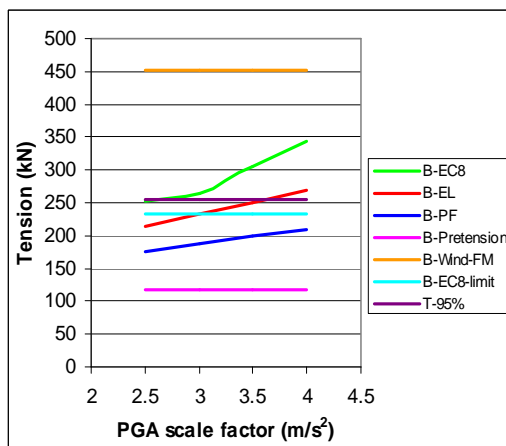


Figure 8-72 Mast C – level B1 cable tensions

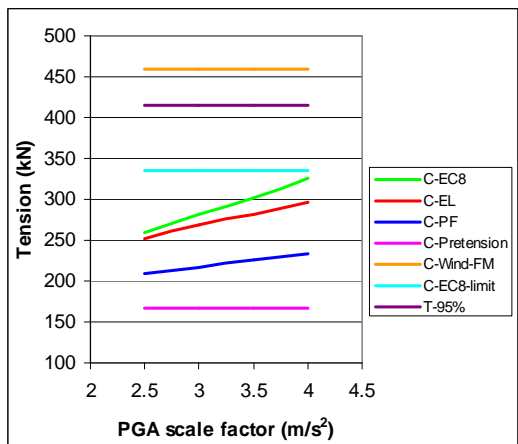


Figure 8-73 Mast C – level C1 cable tensions

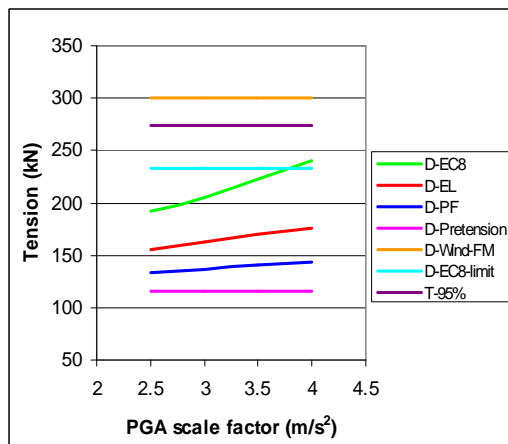


Figure 8-74 Mast C – level D1 cable tensions

The peak cable response of mast C is approximately linear with respect to PGA apart from an initial nonlinear response at level B to the EC8 earthquake. The initial stiffness utilization of the cables in mast C is approximately 10% to 20% higher than in mast B which may explain the more linear peak cable response (as they are closer to a linear range). As with mast B, the percentage increase in peak cable tension is higher for the bottom two levels A and B. The EC8 limit is exceeded at both these levels for all the EC8 analyses and the EL Centro analyses with higher scale factors.

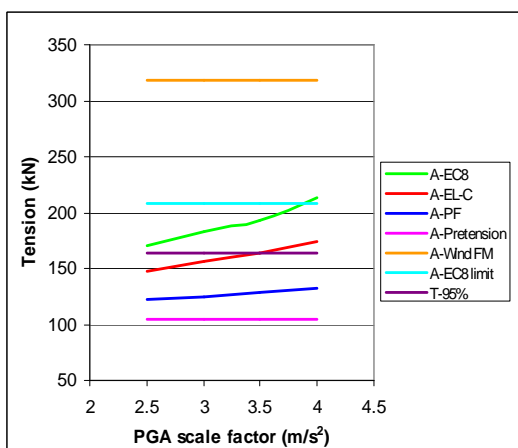


Figure 8-75 Mast D – level A1 cable tensions

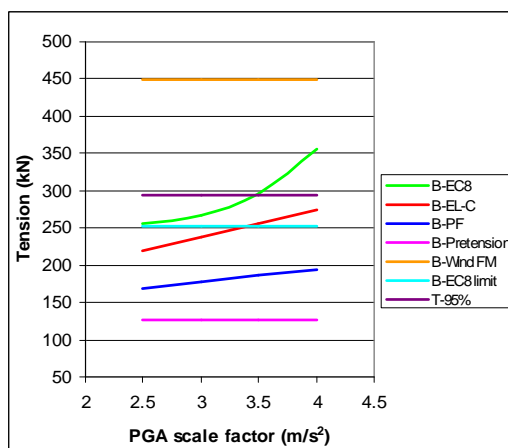


Figure 8-76 Mast D – level B1 cable tensions

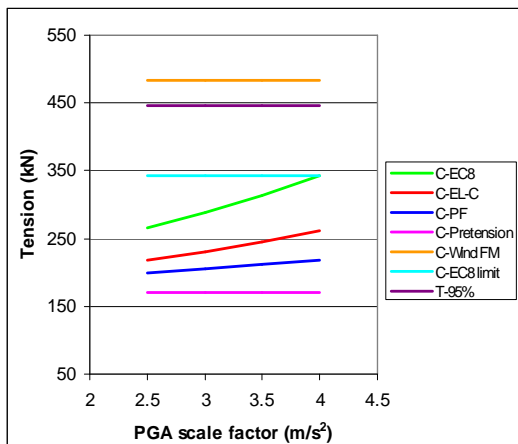


Figure 8-77 Mast D – level C1 cable tensions

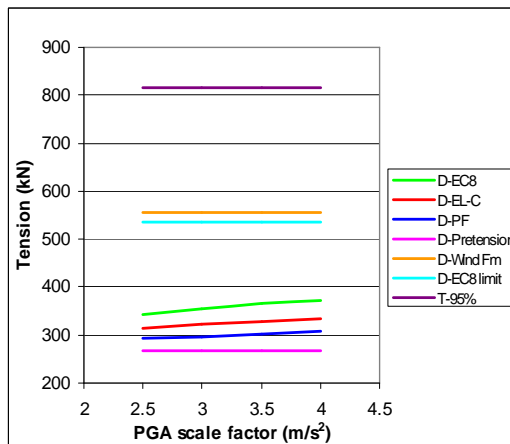


Figure 8-78 Mast D – level D1 cable tensions

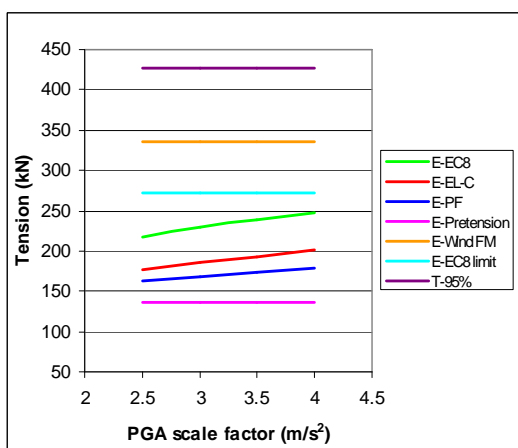


Figure 8-79 Mast D – level E1 cable tensions

Apart from level A and B, all other cables in mast D operate well below the 95% stiffness utilization range. Despite this, the peak response of the majority of the cables is roughly linear compared to PGA scale factor. As with the other masts, the percentage increase in cable tension is higher at lower levels, with cables at levels A, B and C showing tensions close to, if not exceeding, the EC8 limit.

Apart from isolated responses, the peak cable behaviour across all masts showed a roughly linear relationship with respect to PGA, despite many of the cables operating well below any linear range. For reasons described in section 8-2 concerning the opposing oscillation of adjacent spans during a dynamic seismic analysis, the design wind tension significantly exceeds peak seismic tension. The EC8 limit, however, was exceeded by many of the cables

particularly at lower levels. This is consistent with the findings of both Amiri [1] and Hensely [8] where increases above this limit were common.

8.5.2 Other Cable Behaviour

Appendix 2 shows all of the extreme cable tensions produced during the analyses. It can be seen that a wide range of cable forces have been produced and that a number of the lower cables of masts A, B and C have dipped into compression at some stage during the analysis. A compression limit in the cables was omitted from the models to avoid convergence problems as the cables would buckle if any compression occurred. In comparison to the forces exerted on the masts by the cables on the opposing side, the compression exerted by the few cables is insignificant and thus unlikely to have had any appreciable effect on the mast response. The worst compression produced in any cable occurred in mast B level A (19.7kN). Close investigation of this cable showed that during a static analysis with deflections far exceeding those that occurred during the seismic analysis, the cable would not go into compression, however the time history response shown in Figure 8-80 shows that whilst vibrating a small number of oscillations generated short intervals with minimal compression.

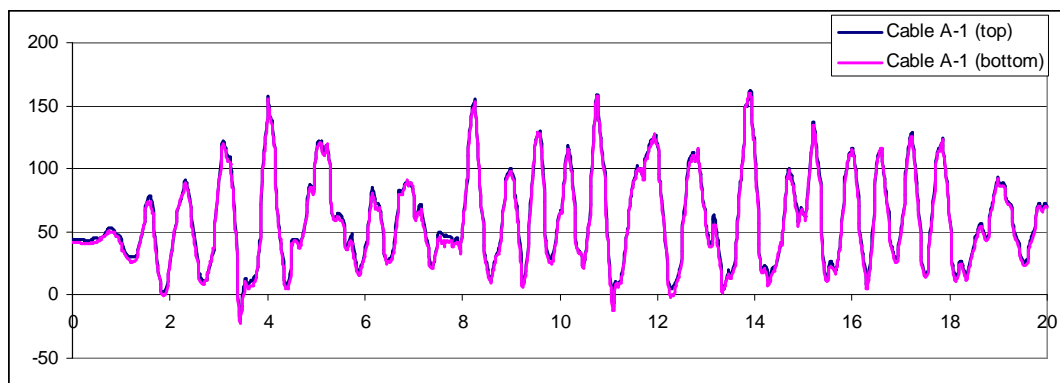


Figure 8-80 Mast B – level A1 cable tension response (EC8, 3m/s² scaling)

Cable compression only occurred at isolated extreme peaks in cable oscillation and as this represents the most significant occurrence of cable compression in all analyses, it can be

concluded that the development of compression had minimal effect on the behaviour of masts in these analyses.

The wide range of forces that developed in the cables suggests that the use of any linear method based on the assumption of a) small deflections and b) flat parabolic profile, is unlikely to accurately model cables for this type of analysis, however further analyses would be needed to substantiate this.

8.6 Acceleration Profiles

The following Figures 8-81 to 8-84 show the peak acceleration of the masts during the EC8 analyses against mast height. The acceleration is in the X direction and shown relative to the ground motion.

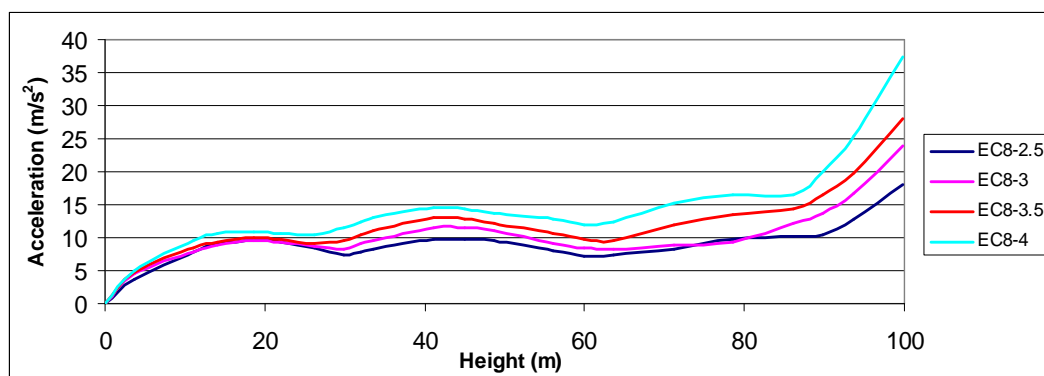


Figure 8-81 Mast A – EC8 acceleration profiles in X direction

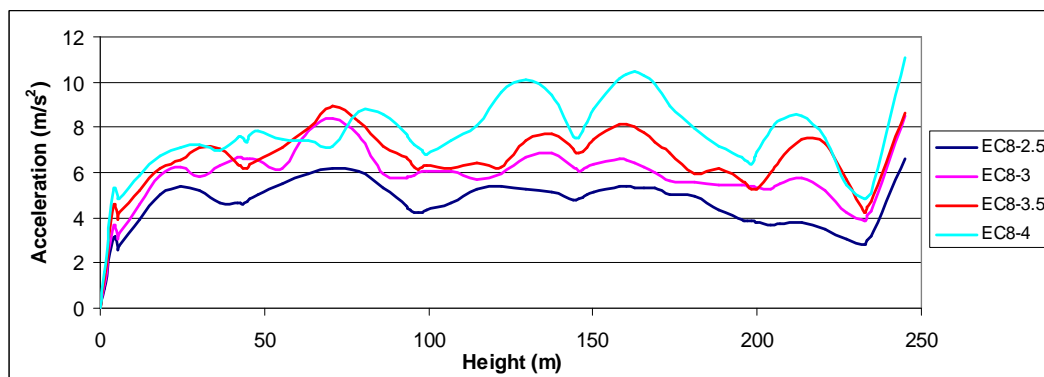


Figure 8-82 Mast B – EC8 acceleration profiles in X direction

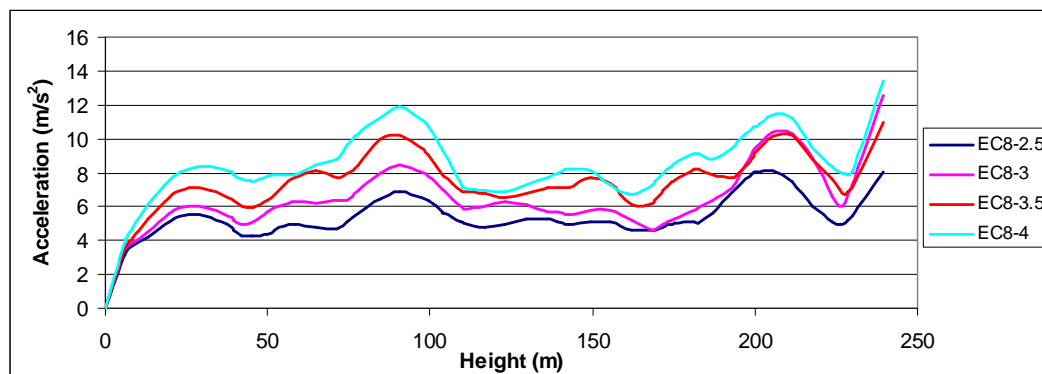


Figure 8-83 Mast C – EC8 acceleration profiles in X direction

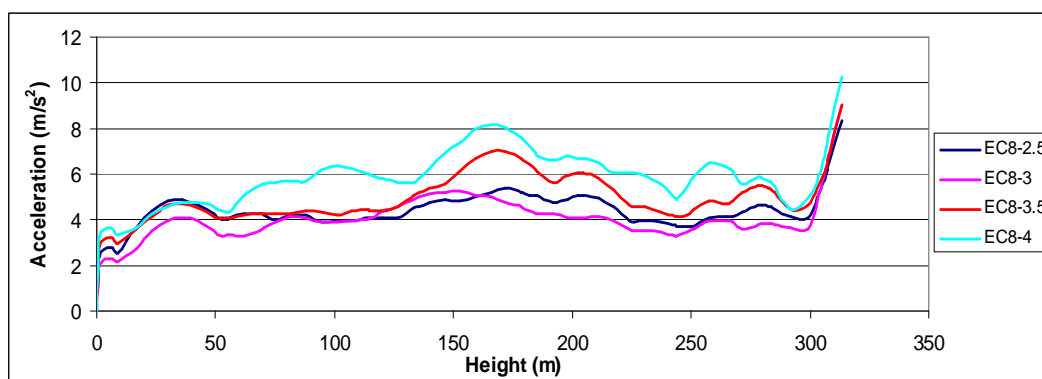


Figure 8-84 Mast D – EC8 acceleration profiles in X direction

The profiles generally show that there is increased acceleration in the spans and in the cantilevers, although the mass distribution throughout the mast seems to have an effect in distorting this trend, producing somewhat irregular profiles. Increases in PGA generally produce increases in mast acceleration, although the profiles are not always consistent (particularly in masts B and D). The more nonlinear nature of mast B is again shown by highly inconsistent acceleration profiles in the lower two spans. Of particular interest is that the average acceleration generally decreases with increases in total mast height. The higher frequency response of mast A generated accelerations of the order of 25% to 50% higher than the other three masts, whilst mast D generated the lowest accelerations in the region of 25% lower than masts B and C. Peak acceleration is a measure of ‘effective earthquake force’ on a structure and therefore it is consistent that this acceleration trend relating to mast

height is similar to the trends observed for the shear and bending response, i.e. increases in normalized force response with reduction in height.

Amiri [1] used the acceleration profile as a model to describe the fundamental mode shape of the mast. Due to the uneven nature of these profiles (apart from mast A), these results cannot be used in this way.

9 Stage 2: Travelling Wave Effect – Results and Discussion

In order to assess the significance of the travelling wave effect, this section presents aspects of mast response from the travelling wave analyses in comparison to those from analyses with uniform ground motion.

9.1 Mast Forces

The following tables and figures show the variation in peak base forces and bending moment distribution across the four masts for the same EC8 and El Centro accelerograms (scaled at 3m/s^2) with three different shear wave speeds (270m/s, 580m/s and 800m/s).

Case	Mast Base Shear	% change	Total Base Shear	% change	Mast Base Axial	% change
EC8-3	22.3	N/A	182.5	N/A	1200.2	N/A
EC8-Wv270	21.3	-4.4	189.5	3.8	1266.0	5.5
EC8-Wv580	23.7	6.3	221.8	21.5	1187.7	-1.0
EC8-Wv800	21.3	-4.2	207.8	13.9	1186.6	-1.1
EL-C-3	22.2	0.0	189.3	0.0	1109.2	0.0
EL-C-Wv270	12.0	-46.1	111.8	-40.9	1222.4	10.2
EL-C-Wv580	19.2	-13.4	181.4	-4.1	1157.3	4.3
EL-C-Wv800	20.1	-9.5	190.9	0.9	1138.7	2.7

Table 9-1 Mast A – stage 2 key response forces (kN)

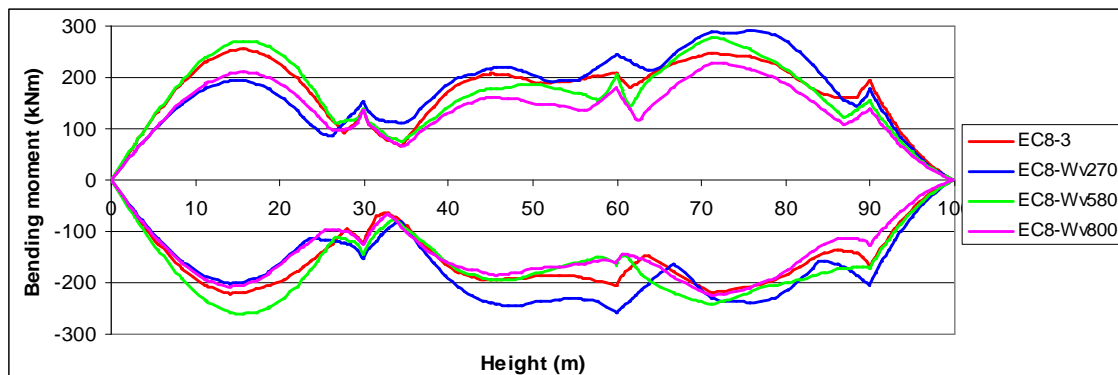


Figure 9-1 Mast A – stage 2 bending moment envelopes (about Y axis)

The response of mast A shows increases in total base shear for all three wave speeds in the EC8 analysis (maximum of 21.5%), whilst the mast base shear is usually reduced. This implies greater excitation of the higher regions of the mast for all three wave speeds. The

distribution of moments also shows more significant increases/variations in the upper spans. The changes shown in the EC8 analyses are not consistent with trends from the El Centro analyses. The total base shear and mast base shear are reduced for all three El Centro wave speeds. This is greatest for the 270m/s analysis where reductions of up to 46% were shown. This suggests a large change in the vibration pattern from the uniform ground motion analyses and implies that loads from the cables caused by the asynchronous ground motion may have been applied ‘out of phase’ with the oscillation of the mast i.e. in the same direction as the mast oscillation thereby having less of an effect.

Case	Mast Base Shear	% change	Total Base Shear	% change	Mast Base Axial	% change
EC8-3	51.0	0.0	291.8	0.0	2840.7	0.0
EC8-Wv270	42.4	-16.9	350.1	20.0	2808.2	-1.1
EC8-Wv580	40.5	-20.6	370.4	26.9	2808.2	-1.1
EC8-Wv800	45.9	-9.9	359.6	23.2	2695.3	-5.1
EL-C-3	40.6	0.0	236.9	0.0	-2325.3	0.0
EL-C-Wv270	39.8	-1.8	175.4	-25.9	-2444.9	5.1
EL-C-Wv580	39.4	-2.9	200.6	-15.3	-2335.6	0.4
EL-C-Wv800	37.9	-6.7	220.0	-7.1	-2317.3	-0.3

Table 9-2 Mast B – stage 2 key response forces (kN)

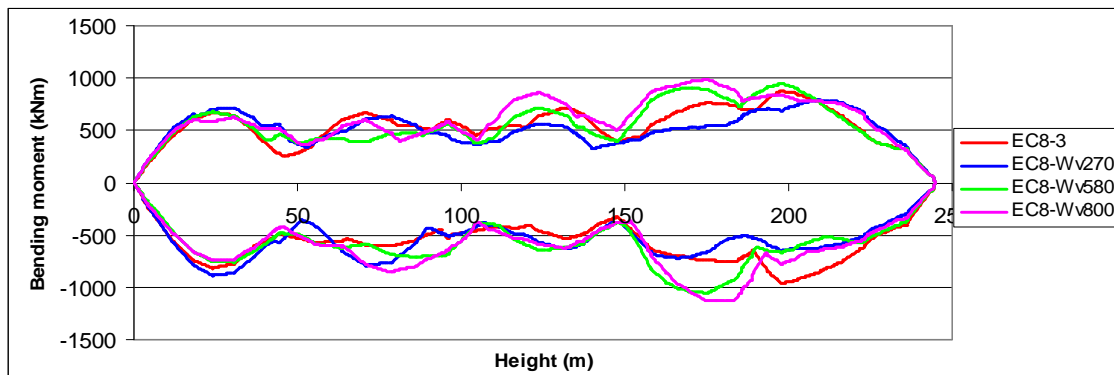


Figure 9-2 Mast B – stage 2 bending moment envelopes (about Y axis)

The response of mast B also shows considerable variation in results, although some similar observations can be made. Increases of up to 26% in total base shear are shown for the EC8 analyses, while reductions in mast base shear of up to 20% are shown in the same analyses.

This apparent increase in excitation at higher levels during the wave analyses is supported to some degree by higher moments in the upper spans for the 580m/s and 800m/s wave analyses.

As with mast A, the mast base shear response to the El Centro wave analyses is substantially lower than that of the uniform base motion analysis with total base shear reductions of up to 25% in the 270m/s analysis.

Case	Mast Base Shear	% change	Total Base Shear	% change	Base Axial	% change
EC8-3	68.8	0.0	392.0	0.0	2720.8	0.0
EC8-Wv270	44.2	-35.7	353.1	-9.9	2769.2	1.8
EC8-Wv580	56.4	-17.9	390.7	-0.3	2710.0	-0.4
EC8-Wv800	64.3	-6.6	383.0	-2.3	2581.7	-5.1
EL-C-3	66.5	0.0	277.2	0.0	2363.1	0.0
EL-C-Wv270	34.9	-47.5	187.2	-32.5	2480.6	5.0
EL-C-Wv580	48.9	-26.5	263.9	-4.8	2694.1	14.0
EL-C-Wv800	68.4	2.8	252.5	-8.9	2376.0	0.5

Table 9-3 Mast C – stage 2 key response forces (kN)

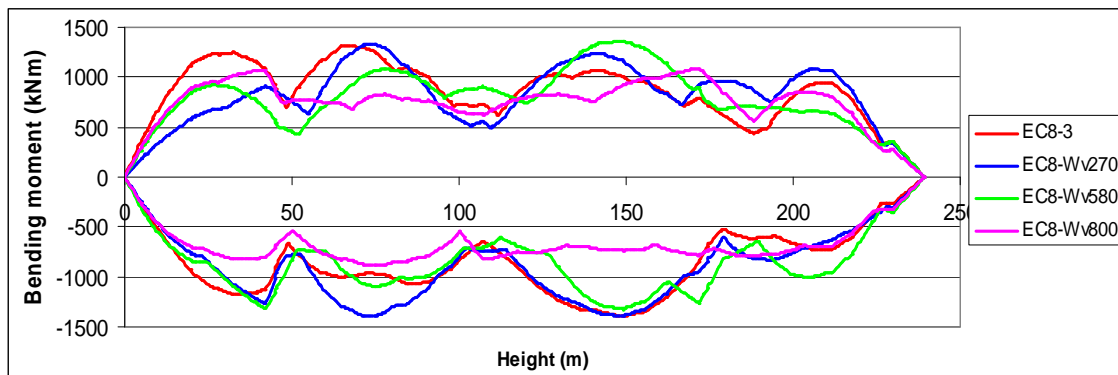


Figure 9-3 Mast C – stage 2 bending moment envelopes (about Y axis)

The forces produced in mast C are again irregular, however the majority of analyses showed a reduction in both mast and total base shear when compared to the uniform ground motion model. The reduction is greatest for the 270m/s analyses, where both the EC8 and El Centro analyses show reductions of over 35% mast base shear, and reductions of 10% and 32%

respectively are shown for total base shear. An irregular redistribution of the synchronous motion bending moment is shown across the EC8 analyses.

Case	Mast Base Shear	% change	Total Base Shear	% change	Base Axial	% change
EC8-3	45.3	0.0	353.6	0.0	4014.2	0.0
EC8-Wv270	52.1	14.9	411.9	16.5	4106.0	2.3
EC8-Wv580	40.2	-11.3	476.8	34.8	4104.2	2.2
EC8-Wv800	43.5	-4.1	436.0	23.3	3980.4	-0.8
EL-C-3	42.7	0.0	290.5	0.0	3609.2	0.0
EL-C-Wv270	27.9	-34.5	173.3	-40.3	3631.2	0.6
EL-C-Wv580	35.1	-17.8	216.4	-25.5	3576.3	-0.9
EL-C-Wv800	39.3	-7.8	235.1	-19.1	3565.8	-1.2

Table 9-4 Mast D – stage 2 key response forces (kN)

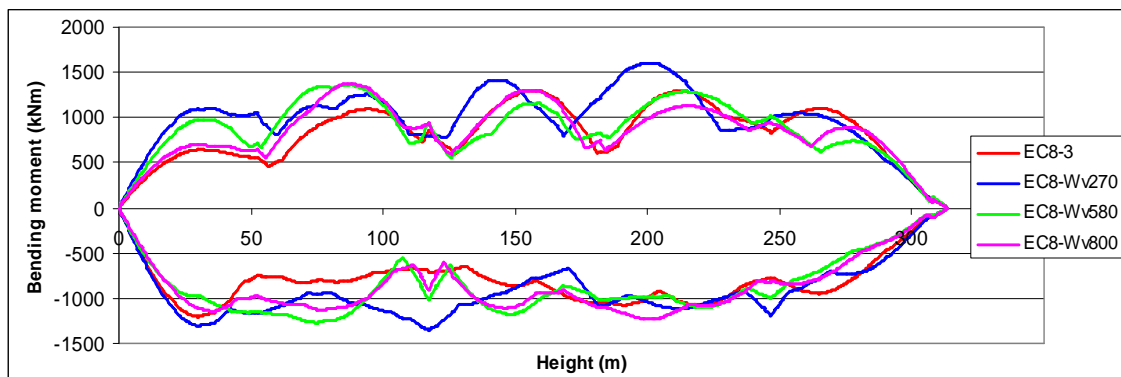


Figure 9-4 Mast D – stage 2 bending moment envelopes (about Y axis)

Mast D results show similarities to those of masts A and B, with decreases in the mast base shear and increases in total base shear for most of the EC8 analyses indicating more interaction of the upper mast with the vibration. Reductions in both these parameters are evident from the El Centro analyses; in particular the 270m/s analysis where reductions of 34% and 40% are seen for mast base shear and total base shear respectively.

9.2 Cable Tensions

During differential ground motion analyses, much of the loading on the masts is applied through the cables. Investigation into the peak cable tensions during analysis is therefore a key indicator in understanding the behaviour of a mast with this effect.

The following tables show the peak cable tensions produced during the travelling wave analyses for the EC8 and El Centro accelerograms.

Case	Cable A1	% change	Cable B1	% change	Cable C1	% change
EC8-3	139.6	N/A	190.5	N/A	234.1	N/A
EC8-Wv270	150.2	7.6	219.0	15.0	260.8	11.4
EC8-Wv580	136.3	-2.4	202.2	6.1	215.5	-7.9
EC8-Wv800	136.1	-2.6	195.0	2.4	209.0	-10.7
EL-C-3	151.3	N/A	177.7	N/A	200.7	N/A
EL-C-Wv270	128.4	-15.1	162.7	-8.4	210.4	4.9
EL-C-Wv580	146.0	-3.5	180.6	1.7	209.3	4.3
EL-C-Wv800	150.5	-0.5	181.6	2.2	205.6	2.4

Table 9-5 Mast A – stage 2 peak cable tensions (kN)

Case	Cable A1	% change	Cable B1	% change	Cable C1	% change	Cable D1	% change	Cable E1	% change
EC8-3	168.7	0.0	179.7	0.0	155.7	0.0	255.0	0.0	166.3	0.0
EC8-Wv270	147.2	-12.8	224.9	25.2	149.3	-4.1	286.3	12.3	160.7	-3.3
EC8-Wv580	139.5	-17.3	203.7	13.4	171.4	10.1	292.4	14.7	170.5	2.5
EC8-Wv800	149.5	-11.4	206.4	14.8	164.4	5.6	281.5	10.4	168.4	1.3
EL-C-3	113.1	0.0	148.7	0.0	136.1	0.0	233.7	0.0	148.0	0.0
EL-C-Wv270	124.6	10.2	138.3	-7.0	117.4	-13.7	242.6	3.8	132.9	-10.3
EL-C-Wv580	124.8	10.3	141.3	-5.0	143.5	5.5	229.6	-1.7	139.2	-6.0
EL-C-Wv800	113.9	-8.7	155.4	10.0	144.9	0.9	230.4	0.3	143.0	2.8

Table 9-6 Mast B – stage 2 peak cable tensions (kN)

Case	Cable A1	% change	Cable B1	% change	Cable C1	% change	Cable D1	% change
EC8-3	219.4	0.0	264.1	0.0	281.6	0.0	204.8	0.0
EC8-Wv270	273.0	24.4	251.9	-4.6	289.3	2.7	204.2	-0.3
EC8-Wv580	275.0	25.3	261.9	-0.8	313.5	11.3	250.0	22.1
EC8-Wv800	221.8	1.1	246.1	-6.8	317.3	12.7	240.6	17.5
EL-C-3	166.6	0.0	232.3	0.0	267.8	0.0	162.6	0.0
EL-C-Wv270	176.2	5.8	184.9	-20.4	228.4	-14.7	142.6	-12.3
EL-C-Wv580	192.5	15.6	262.6	13.1	275.3	2.8	171.2	5.3
EL-C-Wv800	191.4	14.9	224.1	-3.5	261.3	-2.4	155.3	-4.5

Table 9-7 Mast C – stage 2 peak cable tensions (kN)

Case	Cable A1	% change	Cable B1	% change	Cable C1	% change	Cable D1	% change	Cable E1	% change
EC8-3	182.8	0.0	266.7	0.0	288.4	0.0	355.9	0.0	228.9	0.0
EC8-Wv270	226.9	24.1	344.4	29.1	338.1	17.3	386.2	8.5	227.2	-0.8
EC8-Wv580	234.6	28.3	307.7	15.4	376.3	30.5	413.0	16.0	224.3	-2.0
EC8-Wv800	209.6	14.6	296.3	11.1	364.9	26.6	396.9	11.5	219.2	-4.2
EL-C-3	155.8	0.0	238.2	0.0	229.8	0.0	322.2	0.0	185.6	0.0
EL-C-Wv270	152.7	-2.0	206.9	-13.2	241.6	5.2	324.1	0.6	184.0	-0.9
EL-C-Wv580	153.6	-1.4	239.6	0.6	241.5	5.1	306.2	-5.0	161.2	-13.1
EL-C-Wv800	155.9	1.5	243.1	1.4	242.9	0.6	316.6	3.4	169.3	5.0

Table 9-8 Mast D – stage 2 peak cable tensions (kN)

The random nature of the masts’ response to a travelling wave is again shown by the wide spread of cable tension results. Table 9-9 shows the average and maximum percentage change in cable tension for the various masts subjected to the different travelling wave speeds.

	Mast A Average % change	Max % change	Mast B Average % change	Max % change	Mast C Average % change	Max % change	Mast D Average % change	Max % change
EC8	2.1	15.0	4.1	25.2	8.7	25.3	15.1	30.5
El Centro	-1.3	4.9	-0.6	10.3	0.0	15.6	-0.8	5.2

Table 9-9 Breakdown of stage 2 cable tension results

The effect of the travelling wave is clearly worse for the EC8 analyses and, for these analyses, tends to be worse for the taller masts. This is expected as the effect is magnified for larger cable support spacing. The change in cable response for a particular analysis is not always consistent across the cable levels. This may be explained by different spans being affected at different times due to the delay of loading, and the loads applied through the cables may be either ‘in phase’ or ‘out of phase’ with the oscillation of the mast.

10 Stage 3: Uniform Ground Motion without Vertical Motion – Results and Discussion

In order to assess the significance of vertical motion on guyed mast response, this chapter presents the results of analyses conducted without the inclusion of vertical motion, in comparison to those conducted with vertical motion.

10.1 Mast Forces

The following tables and graphs show the variation in peak base forces and force distribution across the four masts for the same EC8 and El Centro accelerograms (scaled at 3m/s^2) with and without (as with prefix XY) the inclusion of vertical motion.

Mast	Force	EC8	EC8-(XY)	% change	EL-C	EL-C-(XY)	% change
A	Mast Base Shear	22.3	23.5	5.3	22.2	22.2	0.1
	Total Base Shear	182.5	186.9	2.4	189.3	189.4	0.1
	Base Axial Force	1200.2	1153.0	-3.9	1109.2	1092.0	-1.5
B	Mast Base Shear	51.0	55.6	9.2	40.6	39.8	-1.9
	Total Base Shear	291.8	317.4	8.8	236.9	261.3	10.3
	Base Axial Force	2840.7	2328.3	-18.0	2325.3	2258.9	-2.9
C	Mast Base Shear	68.8	70.8	2.9	66.5	66.5	0.0
	Total Base Shear	392.0	403.3	2.9	277.2	277.2	0.0
	Base Axial Force	2720.8	2388.4	-12.2	2363.1	2317.3	-1.9
D	Mast Base Shear	45.3	42.1	-7.2	42.7	42.8	0.4
	Total Base Shear	353.6	366.3	3.6	290.5	291.0	0.2
	Base Axial Force	4014.2	3538.1	-11.9	3609.2	3495.1	-3.2

Table 10-1 Peak base force summary for stage 3 analyses (kN)

	EC8	EC8-(XY)	% change	EL-C	EL-C-(XY)	% change
A	178.8	131.6	-26.4	87.7	70.6	-19.6
B	728.5	216.2	-70.3	213.1	146.7	-31.2
C	563.4	230.9	-59.0	205.7	159.9	-22.3
D	677.6	201.5	-70.3	272.6	158.5	-41.8

Table 10-2 Dynamic base axial force variation for stage 3 analyses (kN)

Table 10-1 indicates a largely consistent response across the four masts to the absence of vertical motion. Reductions in base axial force were shown for all masts, with a maximum reduction of 18% shown in mast B during the EC8 analysis. This is not particularly

significant when initial axial forces are considered. However, Table 10-2 shows reductions in dynamic base axial force up to a maximum of 70%. This reduction is far higher in the EC8 analyses. The shear force response of the masts is of particular interest. In most cases, both the mast base shear and the total base shear show an increase when vertical motion is omitted. Mast B shows increases in the region of 10% of both mast and total base shear.

Figures 10-1 to 10-6 show typical variations in peak response for masts A and D that are representative of the response of all of the masts.

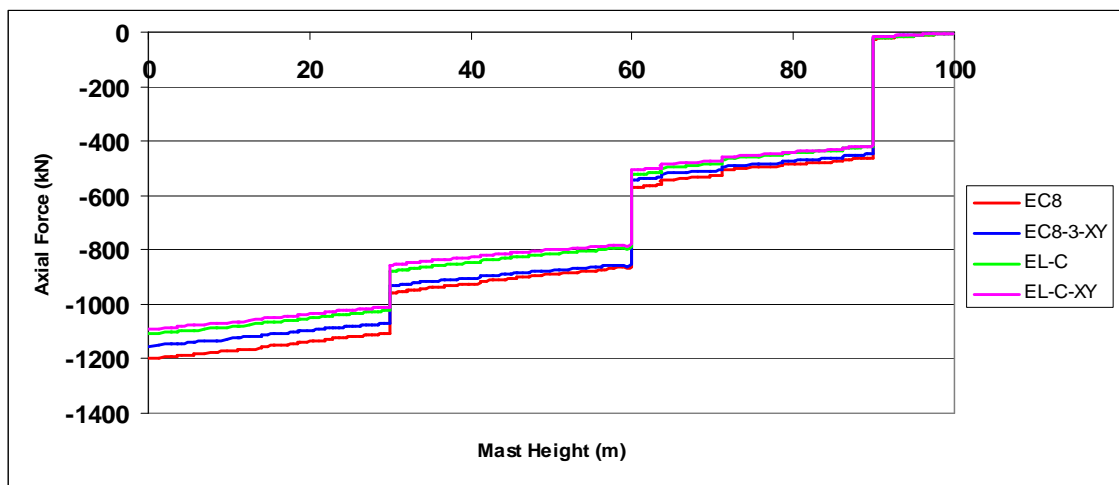


Figure 10-1 Mast A – stage 3 axial force distribution

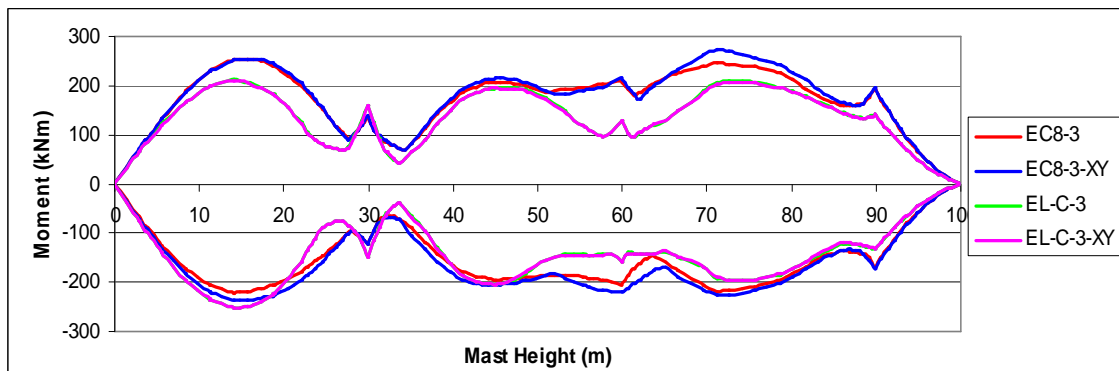


Figure 10-2 Mast A – stage 3 bending moment distribution (about Y axis)

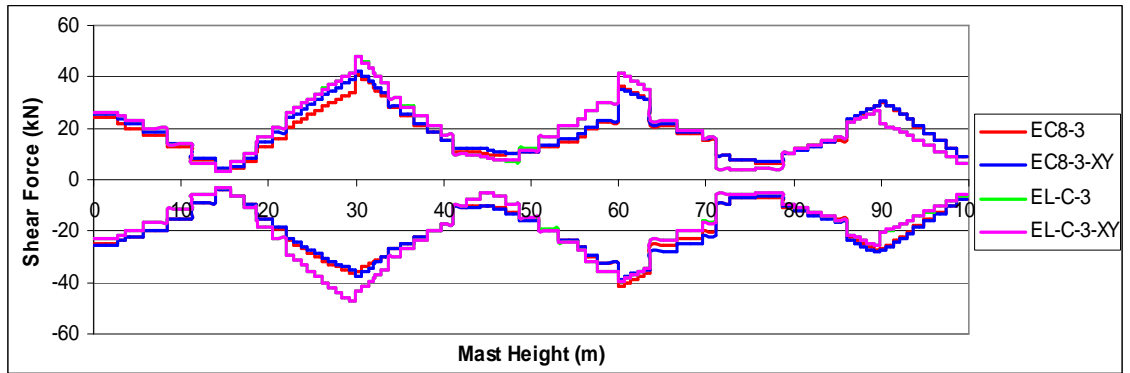


Figure 10-3 Mast A – stage 3 shear force distribution (X direction)

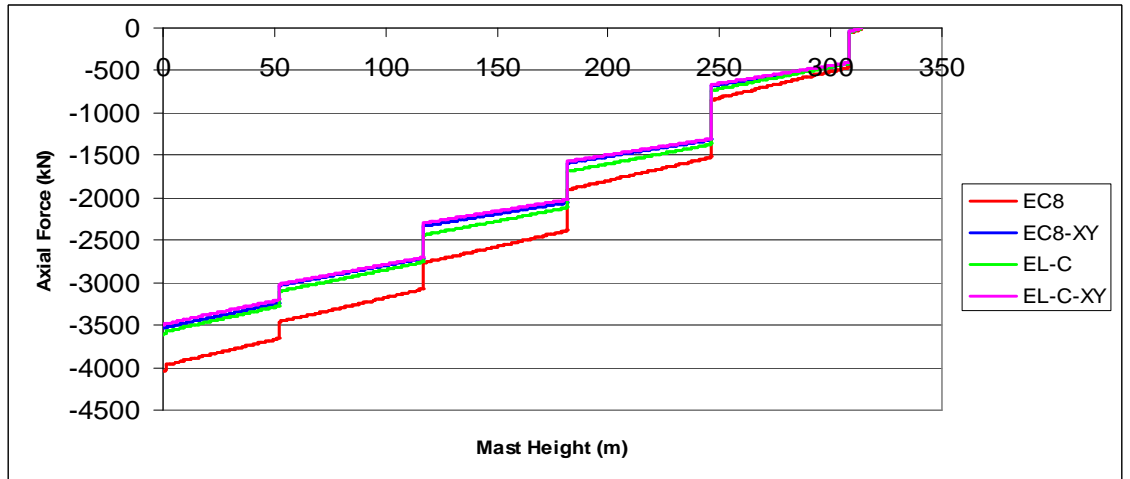


Figure 10-4 Mast D – stage 3 axial force distribution

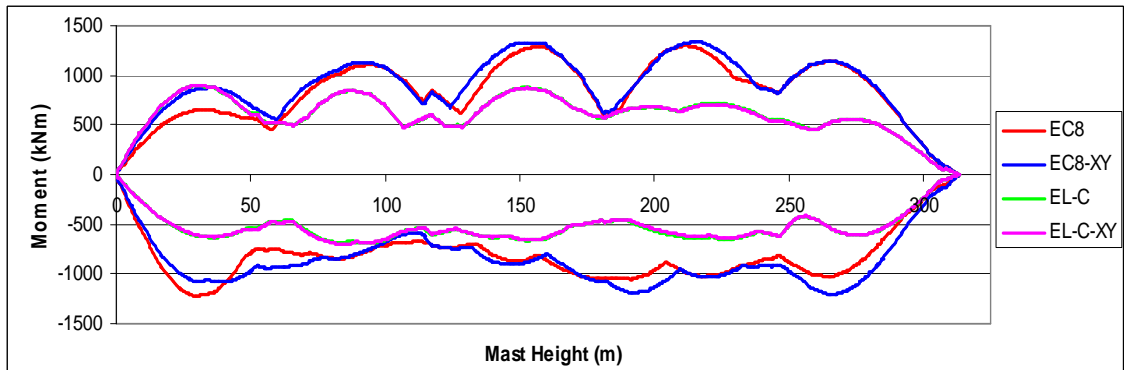


Figure 10-5 Mast D – stage 3 bending moment distribution (about Y axis)

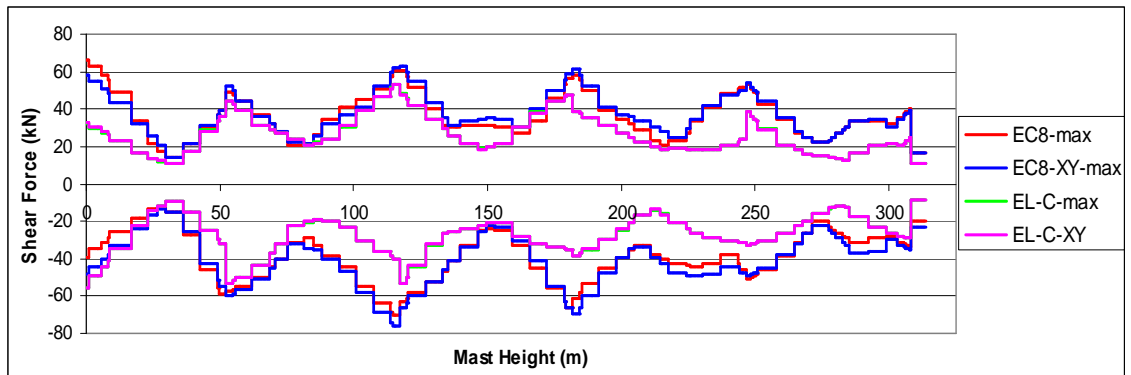


Figure 10-6 Mast D – stage 3 shear force distribution (X direction)

The variation in axial force distribution is consistent with the base axial force response with considerable reductions shown throughout mast D without vertical motion in response to the EC8 motion. This reduction is evident to a lesser extent in mast A. Minimal variations are shown in response to the El Centro motion.

The lateral response to the El Centro accelerograms is almost identical with and without vertical motion, whilst slight variations in both moment and shear distribution are shown in response to the EC8 accelerograms. Variations in lateral response are caused by variations in axial force in the mast that lead to changes in the $P-\Delta$ force distribution when the mast is deflected. This causes changes in local moment distribution and thus variations in shear distribution. Although these effects are difficult to analyse by looking at force envelopes, these slight variations show that SAP2000 is modelling the $P-\Delta$ forces in the mast and that they are having a noticeable effect, although the overall effect may be insignificant.

10.2 Cable Tensions

Mast	Cable	EC8	EC8-(XY)	% change	EL-C	EL-C-(XY)	% change
A	A1	139.7	144.4	3.3	149.5	150.8	0.9
	B1	187.9	183.3	-2.4	178.4	177.5	-0.5
	C1	232.5	238.6	2.6	200.7	201.8	0.6
B	A1	168.7	177.9	5.5	113.1	117.1	3.5
	B1	179.7	188.3	4.8	148.7	146.6	-1.4
	C1	155.7	151.0	-3.0	136.1	135.2	-0.7
	D1	255.0	249.1	-2.3	233.7	233.1	-0.2
	E1	166.3	165.3	-0.6	148.0	147.7	-0.2
C	A1	219.4	218.1	-0.6	166.6	167.9	0.8
	B1	264.1	258.2	-2.2	232.3	233.2	0.4
	C1	281.6	280.0	-0.6	267.8	268.1	0.1
	D1	204.8	201.7	-1.5	162.6	163.1	0.3
D	A1	182.8	181.2	-0.9	155.8	156.4	0.4
	B1	266.7	276.9	3.8	238.2	239.9	0.7
	C1	288.4	286.6	-0.6	229.8	233.2	1.5
	D1	355.9	357.1	0.3	322.2	325.0	0.9
	E1	228.9	215.8	-5.7	185.6	184.1	-0.8

Table 10-3 Maximum cable tensions for stage 3 analysis (kN)

The peak cable tension response shown in Table 10-3 is very irregular when subject to time history motion with and without the inclusion of vertical motion. Exactly 50% of cables showed a slight increase in peak tension when vertical motion was included, whilst the remainder showed a slight decrease. The maximum variation was shown by mast D with a 5.7% reduction of tension in cable E1 with the exclusion of vertical motion.

Although irregular, the variation in peak cable behaviour with and without vertical motion is less than 6% and therefore of little cause for concern. The results show that the addition of vertical motion does not generate sufficient axial strains in the masts, or generate sufficient variations in lateral behaviour to generate significant variations in cable tensions. The possible excitation of vertical cable modes also has minimal effect.

11 Response Spectrum Analysis

11.1 Introduction

A response spectrum analysis is suggested or implied by numerous guidelines (including Eurocode 8: part 6 although it is somewhat open to interpretation) as a suitable option for the seismic analysis of guyed masts. Its suitability is questionable as it relies on the structure exhibiting a linear response to seismic loads with little or no variation in natural frequencies or mode shapes during loading. As the lateral response of guyed masts is very nonlinear and the natural frequencies in the deformed position are likely to be appreciably different from those in the undeformed position, the accuracy of this method of analysis used with guyed masts is likely to be far worse than when used with linear structures.

This section assesses how suitable the use of this method of analysis is, by comparing the design forces produced in the four masts from a response spectrum analysis using SAP2000 with those already produced during a time history analysis using the corresponding accelerograms.

11.2 Details of Analyses

11.2.1 Response Spectra

Response spectra were generated from the El Centro time histories at 3m/s^2 PGA scaling in the three directions using the Seismosignal software package. Type 1 EC8 elastic response spectra for soil type C with 3m/s^2 design acceleration were also generated, with a factor of $5/6$ and $3/4$ applied to the Y and Z directions respectively. All response spectra were generated for 2% damping, the same damping ratio used in the time history analyses. The El Centro and EC8 spectra are shown in Figures 11-1 and 11-2.

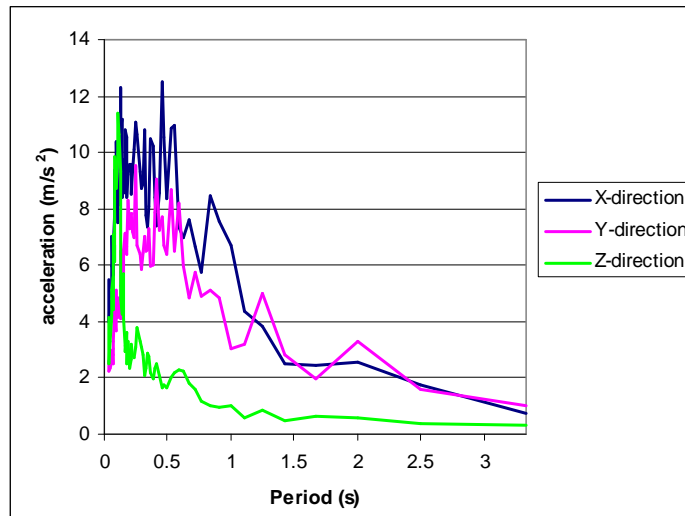


Figure 11-1 El Centro response spectra used (3m/s^2 scaling)

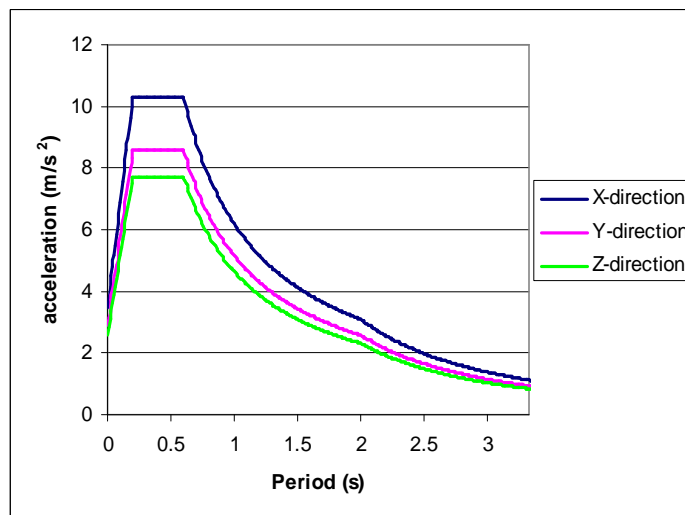


Figure 11-2 EC8 response spectra used (3m/s^2 scaling)

11.2.2 Directional and Modal Combination Rules

The square root sum of squares combination method was used to compute the overall response of the mast subject to response spectrum loading in all three directions. The SRSS method and the CQC method (described in section 2.4.2) were both used to combine modal responses and compute the overall response of the mast. A comparison of results using both methods is presented.

11.3 Results and Discussion

11.3.1 Mast Forces

The following tables and graphs show the magnitude and distribution of forces in the four masts during a response spectrum analysis using the El Centro and EC8 elastic response spectra. Forces produced during the equivalent time history analysis are included for comparison and the percentage difference between response spectrum, using CQC method (as this was shown to be closer in all response areas), and the time history analyses is given in the tables. The overall response from the response spectrum analyses is calculated using the SRSS rule from the individual directional component response. Two representations of the time history response are shown in the graphs. One curve was calculated using the SRSS rule to combine the peak directional component response, the second is an indicative curve generated using the peak vector sum of these components in the time domain giving a more accurate representation of maximum force.

Mast	Force	EC8	EC8-RS (SRSS)	EC8-RS (CQC)	% change (CQC)	EL-C	EL-C-RS (SRSS)	EL-C-RS (CQC)	% change (CQC)
A	Mast Base Shear	22.3	16.1	19.8	-11.3	22.2	14.4	17.6	-20.8
	Total Base Shear	182.5	183.7	198.3	8.7	189.3	181.8	194.3	2.6
	Base Axial Force	1200.2	1093.3	1107.3	-7.7	1109.2	1087.9	1100.7	-0.8
B	Mast Base Shear	51.0	32.6	39.5	-22.4	40.6	25.9	31.1	-23.3
	Total Base Shear	291.8	339.7	359.6	23.2	236.9	297.6	315.0	33.0
	Base Axial Force	2840.7	2431.8	2590.3	-8.8	2325.3	2252.7	2321.9	-0.1
C	Mast Base Shear	68.8	65.4	68.7	-0.1	66.5	65.1	67.8	2.0
	Total Base Shear	392.0	328.7	345.4	-11.9	277.2	284.5	299.0	7.9
	Base Axial Force	2720.8	2487.7	2687.2	-1.2	2363.1	2274.9	2346.9	-0.7
D	Mast Base Shear	45.3	34.5	43.0	-5.1	42.7	28.3	35.8	-16.2
	Total Base Shear	353.6	301.9	358.5	1.4	290.5	249.2	293.5	1.0
	Base Axial Force	4014.2	3921.2	3986.6	-0.7	3609.2	3791.5	3845.9	6.6

Table 11-1 Key forces from response spectrum analysis (kN)

The key force response shows considerable variations in peak forces when compared to the nonlinear time history response. Mast base shear is almost always lower, up to a maximum

of 23% in mast B. Total base shear, although not a particularly useful indicator as the cable behaviour is so different, generally shows a substantial increase in comparison with the time history analyses. Base axial forces are almost always lower up to a maximum of 8.8% in mast B.

The use of the CQC method is shown to be superior to the SRSS method for modal combination as all the results (apart from total base shear which is usually overestimated) show forces closer to those from the nonlinear time history analysis.

Figures 11-3 to 11-10 show a selection of force envelopes that represent the response across the four masts.

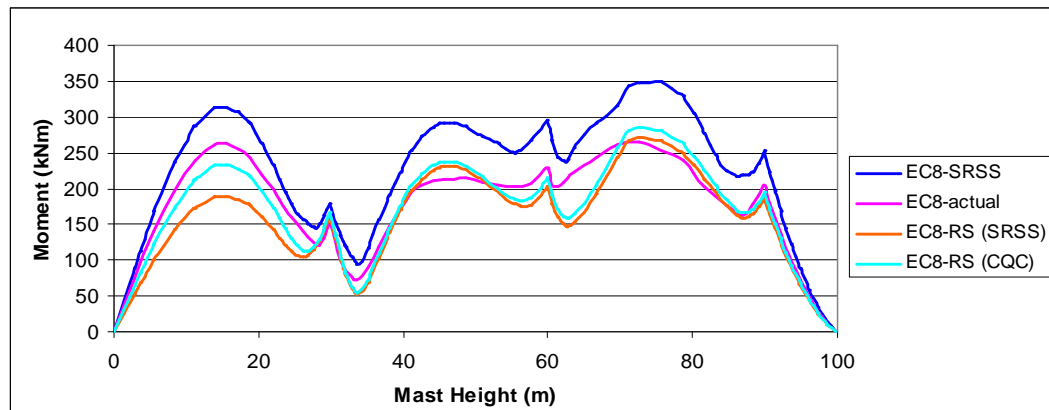


Figure 11-3 Mast A – EC8 response spectrum bending moment envelopes

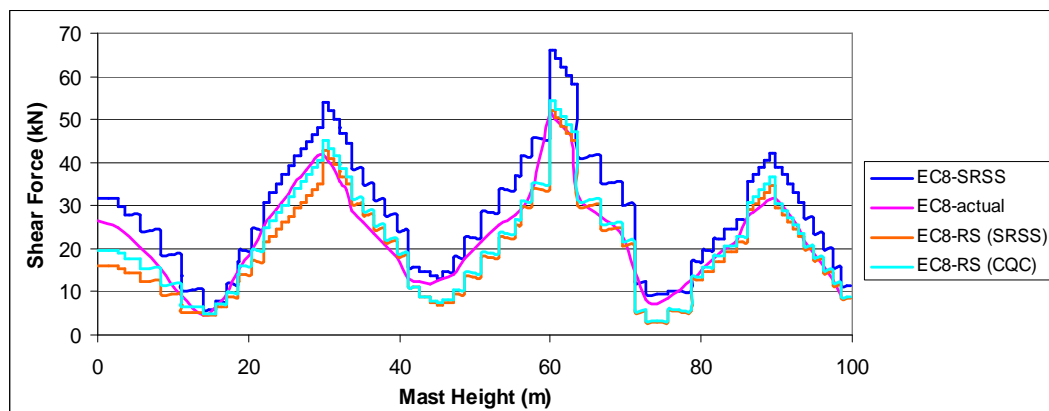


Figure 11-4 Mast A – EC8 response spectrum shear force envelopes

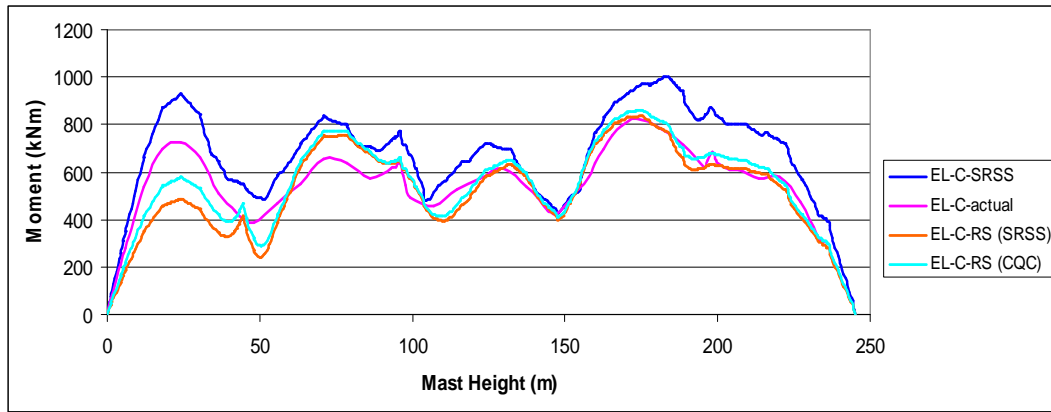


Figure 11-5 Mast B – El Centro response spectrum bending moment envelopes

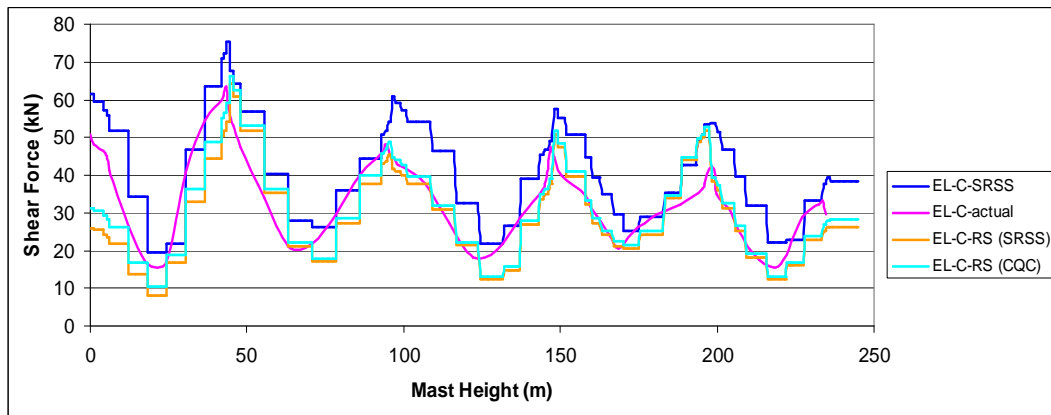


Figure 11-6 Mast B – El Centro response spectrum shear force envelopes

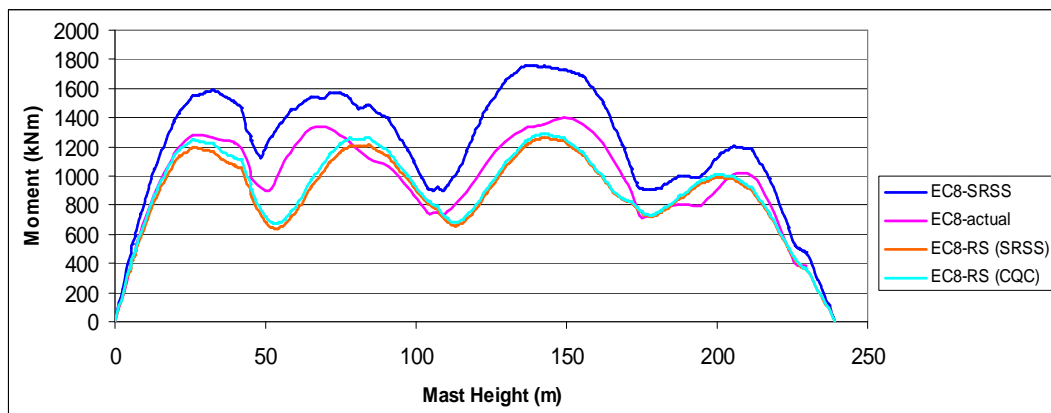


Figure 11-7 Mast C – EC8 response spectrum bending moment envelopes

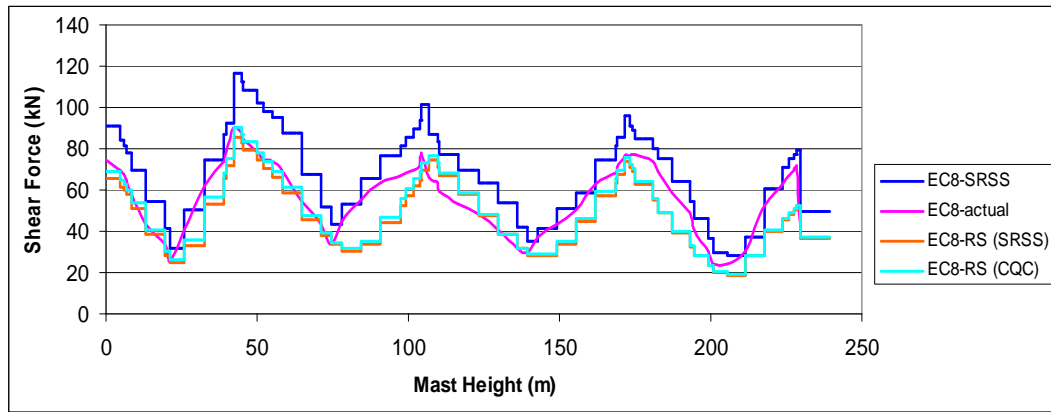


Figure 11-8 Mast C – EC8 response spectrum shear force envelopes

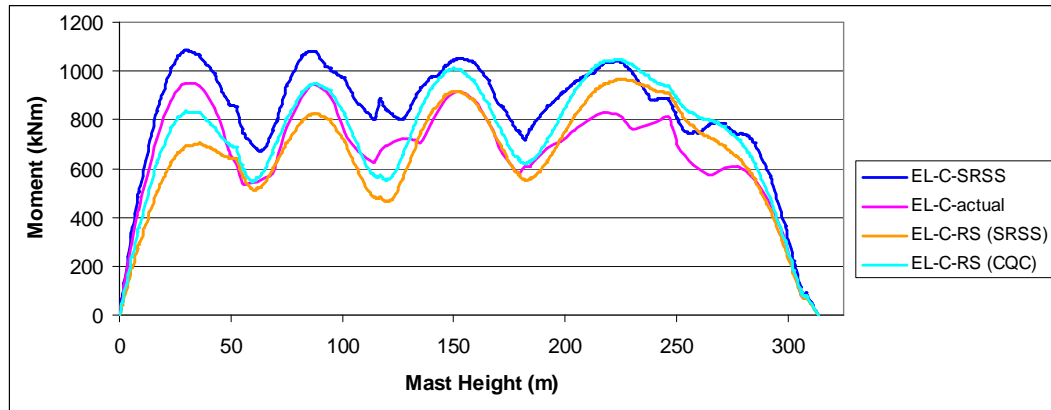


Figure 11-9 Mast D – El Centro response spectrum bending moment envelopes

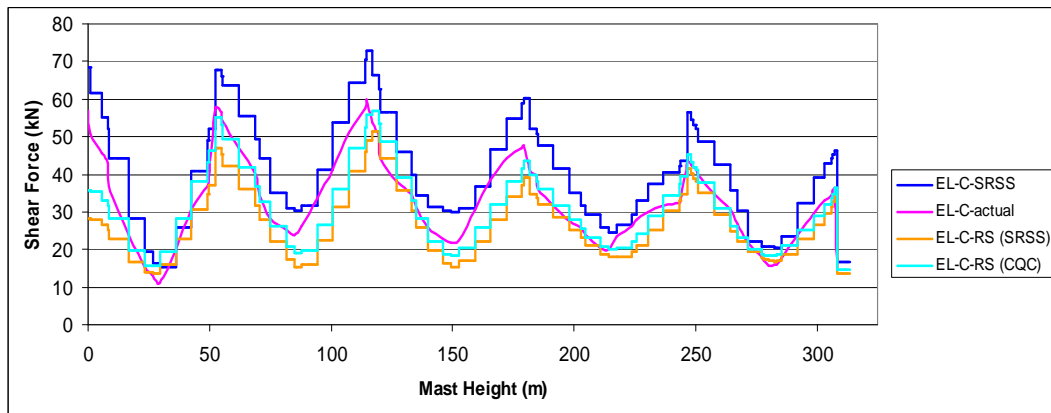


Figure 11-10 Mast D – El Centro response spectrum shear force envelopes

Figures 11-3 to 11-10 all show that the peak component response (combined using the SRSS rule) of all four masts in a response spectrum analysis is always significantly lower than that of the time history analyses. However, the distribution of bending and shear forces is surprisingly similar to those from the nonlinear time history analyses. Unlike other simple static analyses attempted by the author that lead to force envelopes with shapes similar to a wind loading assessment, the method is able to determine whether significant hogging will occur at stay connection points (as in mast A) or whether this region of bending is of less importance.

Although the individual components of peak force response are significantly different in magnitude, a more useful comparison for design purposes is the actual magnitude calculated from combining the component response in the time domain. As the timing of component input motion is not directly coupled, the component response is unlikely to be coupled and combining the peak component response overestimates the overall response. The magnitudes of response spectrum design forces, although usually slightly lower, are much closer to the actual forces produced from the time history analysis, and for most regions may be considered adequate. Response areas where appreciable differences in these magnitudes appear more likely are bending in the first span and base shear.

Again the use of the CQC method is shown to be superior to the SRSS method of modal combination, as forces produced are always closer to those from the nonlinear time history analyses.

11.3.2 Cable Tensions

The cable behaviour during a response spectrum analysis is totally different to their behaviour in a nonlinear time history analysis. Although natural frequencies and mode shapes are based on the stiffness from the pretension load case, the response spectrum analysis allows for no cable pretension, no nonlinear change in stiffness, and allows equivalent linear behavior in tension and compression. Thus each stay cluster behaves more like a 'tripod' than a guyed cable cluster. In order to calculate cable tensions that can be

compared to a time history analysis, or used for design purposes, the magnitude of the cable forces produced have been added to the initial pretensile load and are shown in Table 11-2.

Mast	Cable	EC8	EC8-RS (SRSS)	EC8-RS (CQC)	% change (CQC)	EL-C	EL-C-RS (SRSS)	EL-C-RS (CQC)	% change (CQC)
A	A1	139.7	126.6	134.8	-3.6	149.5	128.3	140.7	-5.9
	B1	187.9	178.8	187.5	-0.2	178.4	180.8	195.7	9.7
	C1	232.5	211.0	219.1	-5.7	200.7	200.5	203.9	1.6
B	A1	168.7	132.2	139.0	-17.6	113.1	116.1	122.9	8.7
	B1	179.7	141.4	152.0	-15.4	148.7	128.8	143.1	-3.7
	C1	155.7	152.3	154.6	-0.7	136.1	136.0	136.8	0.6
	D1	255.0	256.1	259.8	1.9	233.7	235.1	237.4	1.6
	E1	166.3	139.5	146.7	-11.7	148.0	133.2	135.8	-8.3
C	A1	219.4	173.6	183.1	-16.6	166.6	164.1	180.9	8.6
	B1	264.1	215.3	225.2	-14.7	232.3	200.0	216.6	-6.7
	C1	281.6	255.5	260.4	-7.5	267.8	235.4	239.6	-10.5
	D1	204.8	189.9	193.0	-5.7	162.6	165.4	167.3	2.9
D	A1	182.8	157.4	171.3	-6.3	155.8	149.8	156.5	0.5
	B1	266.7	217.9	235.4	-11.7	238.2	204.2	205.6	-13.7
	C1	288.4	241.7	257.6	-10.7	229.8	221.0	228.4	-0.6
	D1	355.9	325.9	335.9	-5.6	322.2	323.8	326.4	1.3
	E1	228.9	193.3	197.6	-13.7	185.6	186.1	185.3	-0.1

Table 11-2 Cable tensions from response spectrum analysis (kN)

Seventy percent of cables (95% in the EC8 analyses) showed lower peak tensions in a response spectrum analysis than in the equivalent time history analysis. However, all tensions were within 18% of the time history results. The largest variation was cable A1 in mast B which showed a variation in tension of 17.6% (lower).

12 Summary and Conclusions

This research modelled the full nonlinear time history response of four existing UK guyed masts to a range of seismic loadings as well as to an indicative BS8100-4 wind loading assessment, and a linear seismic response spectrum analysis. The results were used to assess similarities in behaviour between the masts, and identify any factors that could be used to characterize their response. Comparisons have also been drawn between their nonlinear seismic response and that from both a BS8100-4 wind loading analysis and a linear response spectrum analysis. Although existing earthquake records were used in this study, the majority of trends were developed from the response to a synthesized accelerogram with a response spectrum matching that of EC8 soil type C. The response to motions in other ground types is therefore beyond the scope of this research.

12.1 Response to Simultaneous Ground Motion

As one might expect from the frequency content and the various durations of high amplitude ground motion of the three accelerograms, the masts generally responded significantly more to the synthesized EC8 input than to the recorded El Centro and Parkfield input. Mast A, with a natural frequency range of 1.75 to 2.55 Hz, generated considerable forces in response to all three ground motions, whilst the remaining masts with significantly lower natural frequency ranges responded more to the EC8 input and less to the Parkfield input. The natural frequencies of masts B, C and D are typically less than 1 Hz, thus their response is affected significantly more by the duration of high amplitude ground motion. The short ‘spike’ in the Parkfield accelerogram and the three to four second ‘bursts’ in the El Centro accelerogram cannot compare to the 15 second continuous high amplitude vibration of the synthesized EC8 ground motion. For this reason the response to the EC8 ground motion may overestimate the extreme mast response to actual earthquakes. Conversely the response may be underestimated by the El Centro and Parkfield ground motion as their range of spectral peaks may miss the natural frequency range of the mast. Further analyses using more earthquake records are needed to substantiate this.

As the response to the Parkfield accelerogram was usually variable and significantly lower than to the El Centro and EC8 accelerograms, trends and discussions are developed primarily in response to the latter two, although the response to the Parkfield ground motion is also reported. For this reason analyses assessing the travelling wave effect and the effect of vertical motion were only conducted using the El Centro and EC8 motion.

12.1.1 Bending Moments

All the masts generated substantial bending moments during analysis. The comparatively high stiffness and stiffness utilization of the cables in mast A caused a different distribution of moments for this mast with high moments produced both at the stay connection points (hogging) and at midspan. The remaining masts generated significant moments at midspan only, with only isolated local peaks at some stay connection levels. The peak bending response to increases in the peak ground acceleration of the earthquake is largely linear across all of the masts (particularly in response to the El Centro earthquake), with some areas of nonlinearity shown at the higher scale factors, particularly in mast B.

A simple method for normalizing the peak bending across the four masts using equation 8.1 showed that, when plotting this ratio against average span a trend based on a power function is observed. The Normalized Moment Ratio can be estimated using equation 8.2, however analysis over a wider range of earthquake records and masts is needed to confirm this result.

12.1.2 Shear Forces

The shear force distribution largely resembles that of a continuous beam with regions of high shear at stay connection points and regions of low shear near midspan. As with the bending response, the peak shear response throughout the mast shows a largely linear increase with increases in peak ground acceleration, however significant nonlinear increases are shown by mast B when PGA is increased from 3.5m/s^2 to 4m/s^2 . The peak mast base shear and total base shear also showed this largely linear increase, however isolated analyses showed irregular increases or even slight decreases. Most of the nonlinear response was shown in response to the EC8 accelerograms.

Plotting the total base shear (normalized by the total mast weight) versus mast height, shows a trend (using a power function) similar to that shown by Amiri 2001 [1]. The differences between the trend shown by this research and that of Amiri's, can be explained by the fact that ancillary loading was not taken into account in Amiri's models. The peak total base shear shown by this research can be estimated using equation 8.5.

Using the simple normalization method for shear in the mast described by equation 8.3, a strong trend based on a power function is observed when this ratio is plotted against total mast height. The Normalized Shear Ratio can be estimated using equation 8.4, however its use would need to be verified by a wider range of masts and earthquake records. This suggests that shear forces in the mast (not only base shear) are also dependent on the total height of the mast in addition to span length, mass and PGA.

12.1.3 Axial Forces

All of the masts showed appreciable increases in axial force during analysis, with maximum increases at the base in the order of 25% to 45%. Increases in axial force between stay levels appear more significant in the top sections of the mast, particularly for masts B, C and D. Most of the increase in force shown in mast A was applied at the stay levels. As with most of the other forces, the peak axial response to changes in PGA was relatively linear with more significant increases shown in response to the EC8 accelerograms. The $P_{\max}/P_{\text{initial}}$ ratio at the base of the masts for a particular PGA scale was relatively constant in response to the El Centro ground motion with a maximum range of 3% for a particular PGA across the masts (average ratio 1.13 for PGA of 4m/s^2). This range was closer to 20% in response to the EC8 ground motion (average ratio of 1.35 for PGA of 4m/s^2).

The distribution of dynamic axial forces in the masts as a function of the peak base dynamic axial force can be conservatively described by equation 8.6. This is a slight modification on the curve fit shown by Amiri and again suggests that higher regions of the masts interact more in the vertical plane.

12.1.4 Cable Tensions

The peak cable tension response of the masts is difficult to characterize. A largely linear increase in peak cable tension with PGA (apart from isolated results) was shown by masts A, C and D with irregular results shown for mast B. Maximum percentage increases are shown for mast B level A, with an increase of 343% of initial tension in response to the EC8 accelerogram (PGA of 4m/s^2). The range of extreme cable tensions shown in Appendix 2 shows that the full range of cable behaviour (described in section 2.2.1) is experienced during analysis. This suggests that the use of any linearized model of cable behaviour based on a) small deflections and b) flat parabolic profile, is likely to be inaccurate for this type of analysis, although further research is needed to substantiate this. In many instances the tension limit set by Eurocode 8: part 6 (twice the initial pretension) is close to, or exceeded by, the peak cable tensions and as all of the peak tensions were less than 23% of breaking tension, the validity of this limit is questionable.

12.2 Comparison of Seismic Response to Design Wind Response

Forces generated during the seismic analyses were generally within the envelope produced during an indicative BS8100-4 wind assessment (with actual design wind speeds), particularly in response to the El Centro and Parkfield ground motion. However, bending moments in some midspan regions of all four masts did exceed the wind design envelope for the EC8 analyses with the higher scale factors. This vulnerability usually appears to be a result of an imbalance of bending forces produced by the design wind loading. Areas of low midspan bending moments in the wind analysis are flanked by areas with high hogging moments at the stay supports. The patch load method therefore has less of an effect in amplifying the design moment in these midspan regions and consequently the seismic forces are higher. If little variation in bending capacity was designed for (as is likely to be the case) between support and midspan and the peak hogging moments were used, then these apparent areas of vulnerability would be taken care of, however if the design were highly efficient and strictly followed the design moment, the area may be susceptible to seismic loading.

Generally the shear force response was well within the wind design shear force for all of the analyses, apart from a few insignificant midspan regions. The base shear in mast C is the only other region that produced similar shear forces to the wind design shear during seismic loading. Again this appears to be the result of an unbalanced design for wind, as the arrangement of spans and loading produced a low base shear during the mean wind load assessment and thus a relatively low design shear force.

All of the axial forces generated in the masts during the El Centro and Parkfield analyses were lower than the corresponding wind design forces; however 80% of EC8 analyses produced higher axial forces than the corresponding wind forces. It seems likely that the vertical accelerogram used for this analysis generated a response that overestimated an actual seismic response, however this would need to be verified by further analyses using existing earthquake data.

Peak seismic cable tensions were all substantially lower than those from the design wind analysis. Mast A level C cable showed a peak tension of 82% of the wind design tension, while the majority of peak tensions were of the order of 50% or less of the wind design tension.

During a static wind analysis the entire load is applied in one direction and consequently this entire load needs to be resisted. During a dynamic analysis it is unlikely that adjacent spans will oscillate in the same direction simultaneously; thus part of the overall acceleration load from each span will be applied in opposing directions causing a lower reaction force in the cables. The opposing bending in adjacent spans reduces the hogging moment at the supports and increases the sagging moment in each respective span. The shear force response in the mast is not affected to the same extent and consequently the seismic bending response is comparable to the design wind analyses, whereas the shear and cable response is not.

This study has shown that the majority of forces produced during a seismic analysis with peak design accelerations in the region of 3m/s^2 to 4m/s^2 , are within the mast design forces from a wind analysis using the Patch Load method to BS8100-4 (mean hourly design wind speeds ranging from 22.5m/s to 24m/s across the masts). If a conservative approach was

taken to the design of the masts to resist bending forces, a fair degree of confidence can be had that the designs will resist seismic forces generated by earthquakes similar to those used in this study.

Indicative wind analyses conducted with mean hourly winds of 20m/s and 28m/s (10 minute average of 21.4m/s and 30m/s respectively) showed that mast forces can be doubled with this increase in design wind speed of 8m/s. This is because both the mean and patch loading are proportional to V^2 . For areas with mean hourly wind loading close to 20m/s, it is likely that the design wind bending response will be exceeded by a seismic response caused by seismic events similar to those used in this study. However other response forces are unlikely to be exceeded. Figure 12-1 shows a wind map of Europe which shows that the design wind speeds used for masts in this study are relatively low in comparison to many areas in Europe. This provides a relative degree of confidence in the design of masts in a number of European countries in seismic regions, particularly Italy, Greece and Turkey where design wind speeds are relatively high.

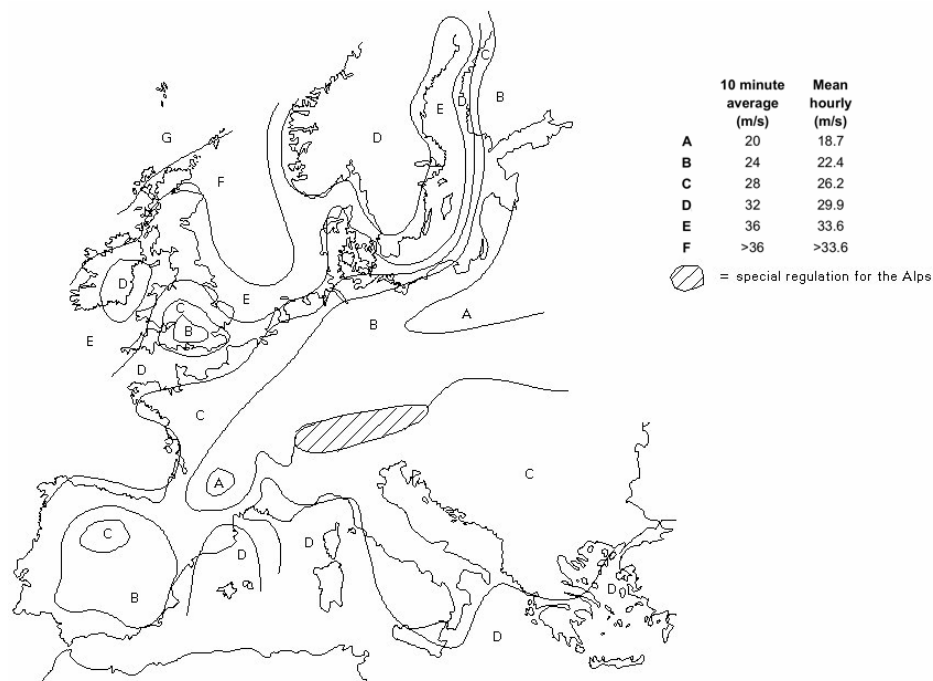


Figure 12-1 European wind map [35]

12.3 Response to Travelling Wave Effect

Forces generated during analyses with asynchronous support motion that modelled the travelling wave effect showed a large variation in mast response. Bending and shear force variations of up to 45% of the equivalent force generated during synchronous motion analyses were shown. Although these variations were often reductions, particularly in response to the El Centro motion, increases of up to 25% were common and usually produced at higher levels on the mast. Variations in axial forces were shown up to a maximum increase of 14%. Although this represents a significant increase in the effective dynamic force, the overall effect is of less concern.

Peak cable tension variation (summarized in Table 9-9) gives perhaps the most comprehensive breakdown of mast behaviour in this analysis. A far more significant effect is shown in response to the EC8 time histories. Most variations in response to El Centro motion were within 10% of the synchronous motion results, with a maximum increase in peak cable tension of 15%. Most of the EC8 analyses however showed substantial increases in cable tension across the set of analyses, up to maximum increase of 31%. As expected the increase shown in taller masts is more significant due to the larger variation in motion at supports.

The irregular nature of mast response to the travelling wave effect may be a cause for concern if masts are designed close to the force envelope produced from a synchronous motion analysis. This significance appears exaggerated when using an EC8 synthesized accelerogram as increases in response are far lower to the more realistic El Centro ground motion. However this would need to be substantiated by further analyses using a wider range of masts and earthquake records.

12.4 Effect of Vertical Motion

The variation in mast response caused by the absence of vertical motion is primarily shown by significant reductions in axial force. Maximum reductions of 70% of the dynamic base axial force were shown, however these reductions only represented between 10% and 18% of the total axial force for the EC8 analyses and less than 4% for the El Centro analyses. It is interesting to note that the lateral shear and bending response were often increased with the absence of vertical motion; however variations shown were less than 10% and virtually non-existent for the El Centro analyses. These variations in mast lateral forces show that vertical ground motion can introduce variations in P- Δ forces in the mast that cause minor variations in mast behavior. However these differences are unlikely to affect mast design and in many cases may aid the mast lateral design. The effect of vertical motion on axial mast design should certainly be taken into account.

12.5 Response Spectrum Analysis

Despite the fundamental differences in analysis method, the response spectrum analysis showed surprising consistencies in force distribution when compared to the nonlinear time history analyses. The magnitude of the component response in each direction was significantly lower than that of the time history analyses, however when comparing design forces for the response spectrum (SRSS rule for directional combination) and the peak response force calculated from X and Y component time histories, the magnitudes were for the most part within 10% of each other. Regions where appreciable differences in force magnitude appear more likely are base shear and bending in the first span. A peak cable tension comparison also showed that, although lower, all cable tensions from the response spectrum analysis were within 18% of the time history analyses. Due to the close frequency spacing of modes the use of the CQC method of modal was shown to be superior to the SRSS method producing force magnitudes much closer to those from the time history values.

Although the use of this method in this study has shown encouraging results, it should be noted that it is by no means a simple analysis technique and cannot be attempted without

advanced analysis software. It is feasible that a small number of elements with linear stiffness could be used in such an analysis to model the cables, thereby significantly reducing the number of modes that need to be generated. However this would alter the cable modes, the significance of which is beyond the scope of this research.

This research has shown that, although not conclusive in accurately determining the seismic response of guyed masts, the use of the modal response spectrum method is a useful starting point and if used conservatively can be appropriate for design.

12.6 Summary and Need for Further Research

This research has shown how complicated and unpredictable the response of guyed masts can be to seismic loading and how even highly sophisticated software can have difficulties with their analysis. Large numbers of elements, stability problems and time consuming analyses (as long as 18 hours) make this type of analysis an unfavourable option in a design office and emphasize the need for a simpler approach. It has also shown that although their response and behaviour is largely nonlinear, much of their peak response exhibits linear trends when compared to peak ground accelerations. Trends relating the peak response of the four masts in terms of height, mass and span length are also evident and could be developed further.

Although the majority of seismic forces are likely to be within the force envelope produced from a design wind assessment, certain parts of the structure may be susceptible to seismic loading, particularly where forces from a wind loading assessment are unevenly distributed or when the mean hourly design wind speed is close to the 20m/s to 22m/s range. In areas of high seismic activity a seismic assessment is therefore recommended.

The interpretation of Eurocode 8 with regard to the analysis of guyed masts leaves much open to the designer. Whether a linear response spectrum analysis is suitable as a design option for nonlinear masts is not addressed and few modeling guidelines are given for nonlinear analysis. It is the opinion of the author that enough common seismic behaviour

exists between guyed masts to suggest that the development of an equivalent static method of seismic analysis is feasible. Future expansion of the current study using an increased number of masts (with varying properties) subjected to a larger variety of existing and synthesized earthquake data could build on the trends identified in this study. Earthquake records should take into account all possible ground types stipulated by EC8. A static method based on loadings derived from these trends could then be calibrated to yield similar force envelopes to those of the dynamic analyses. This may result in a ‘patch loading’ type method or a method utilizing a seismic excitation factor applied to the various response forces of the masts following initial loading. Given the complexities of accurate nonlinear dynamic analysis, this would be a very useful tool for designers.

13 References

Journal Articles and Papers

- [1] Amiri, G., Seismic Sensitivity Indicators for Tall Guyed Telecommunication Towers, *Computers and Structures*, 80, p.349-364, 2002
- [2] Davenport, A.G., Dynamic Behaviour of Massive Guy Cables, *Journal of the Structural Division*, ASCE, p.43-70, April 1965
- [3] Davenport, A.G., Sparling, B.F., Dynamic Gust Response Factors for Guyed Towers, *Journal of Wind Engineering and Industrial Aerodynamics*, 44, p.2237-2248, 1992
- [4] Dean, D.L., Static and Dynamic Analysis of Guy Cables, *Transactions*, ASCE, Part 2 of Vol. 127, p.382-419, 1962
- [5] Gerstoft, P., Simplified Methods for Dynamic Analysis of a Mast, MSc Thesis, University of Western Ontario, 1984
- [6] Goldberg, J.E., Gaunt, J.T., Stability of Guyed Towers. *Journal of the Structural Division*, ASCE, p.741-756, April 1973
- [7] Harichandran, R.S., Spatial Variation of Earthquake Ground Motion, A report produced for Dept of Civil Engineering, Michigan State University, 1999
- [8] Hensely, G., Finite Element Analysis of the Seismic Behaviour of Guyed Masts, MSc Thesis, Virginia Polytechnic Institute and State University, 2005
- [9] IASS. Recommendations for Guyed Masts, International Association for Shell and Spatial Structures, Madrid, Spain, 1981
- [10] Irvine, H.N., Caughey, T.K., The Linear Theory of Free Vibration of a Suspended Cable, *Proceedings of the Royal Society*, London, Series A, 341 p 299-315, 1974
- [11] Irvine, H.M., Free Vibrations of Inclined Cables, *Journal of the Structural Division*, ASCE, 104(ST2), p.343-347, 1978
- [12] Kahla, N. B., Equivalent Beam-Column Analysis of Guyed Towers, *Computers and Structures*, Vol. 55 (4), p.631-645, 1995
- [13] Mulherin, N.D., Atmospheric Icing and Tower Collapse in the US, *Proceedings of the Seventh International Workshop on Atmospheric Icing of Structures*, University of Quebec, Canada, 1996

-
- [14] Madugula, M.K.S., Wahba, Y.M.F., Monforton, G.R., Dynamic Response of Guyed Masts, *Engineering Structures*, Vol.20 No.12, p.1097-1101, 1998
- [15] Newmark, N.M., A Method of Computation for Structural Dynamics, *Journal of the Engineering Mechanics Division*, ASCE, Vol. 85 No. EM3, 1959
- [16] Raof, M., Davies, T. J., Determination of the Bending Stiffness for Spiral Strand Cables, *Journal of Strain Analysis*, Vol. 39(1), p.1-13, 2004
- [17] Schiff, A.J., Case Study of Earthquake Performance of Communication Towers, Prepared for the Electric Power and Communications Committee, USA
- [18] Sparling, B.F., Smith, B.W., Davenport, A.G., Simplified Dynamic Analysis Methods for Guyed Masts in Turbulent Winds, *Journal of the International Association for Shell and Spatial Structures*, 37(2), p. 89-106, 1996
- [19] Sparling, B.F., Davenport, A.G., Nonlinear Behaviour of Guy Cables in Turbulent Winds, *Canadian Journal of Civil Engineering*, 28, p.98-110, 2001
- [20] Vellozzi, J.W., Tall Guyed Tower Response to Wind Loading, *Proceedings of the 4th International Conference on Wind Effects on Buildings and Structures*, London, 1975
- [21] Wahba, J., Brinker, D., Malouf, P., Erichsen, J., New Standards for Broadcast Structures ANSI/EIA/TIA-222-G, *National Association of Broadcasters Paper*, 2003
- [22] Wahba, Y.M.F., Madugula, M.K.S., Monforton G.R., Evaluation of Nonlinear Analysis of Guyed Antenna Towers. *Computers and Structures*, 68, p.207-212, 1998
- [23] Wilson, E., Technical Paper, Dynamic Analysis using the Response Spectrum Method, www.csiberkeley.com
- [24] Wilson, E., Technical Paper, Dynamic Analysis by Numerical Integration, www.csiberkeley.com
- [25] Wilson, E., Dynamic Response by Step-By-Step Matrix Analysis, *Proceedings of the Symposium on the use of Computers in Civil Engineering*, Lisbon, 1962
- Books**
- [26] Buchholdt, H.A., *Introduction to Cable Roof Structures*, Cambridge University Press, 1985

-
- [27] CSI Analysis Reference Manual, For SAP2000[®], ETABS[®] and SAFE[®], Computers and Structures, Inc. Berkeley, California, USA, September 2004
- [28] Irvine, H.M., *Cable Structures*, The MIT Press, Cambridge, Massachusetts and London, England, 1981
- [29] Madugula, M. (Editor), *Dynamic Response of Lattice Towers and Guyed Masts*, ASCE, Virginia, 2002

Codes

- [30] British Standard, BS8100-4: 1995, Lattice Towers and Masts
- [31] European Standard, Eurocode 8: Design of Structures for Earthquake Resistance, Part 1: General rules, Seismic Actions and Rules for Buildings, BS EN 1998-1:2004
- [32] European Standard, Eurocode 8: Design of Structures for Earthquake Resistance, Part 6: Towers, Masts and Chimneys, BS EN 1998-6:2005

Websites

- [33] <http://peer.berkeley.edu/smcat/>
- [34] <http://nsmp.wr.usgs.gov/>
- [35] <http://www.kuleuven.ac.be/bwk/materials/Teaching/master/wg01b/10300.htm>
(Lecture 1B.3 Background to Loadings)
- [36] <http://www.seismosoft.com/>

Software Used

SAP2000 Advanced 9.1.1, Structural Analysis Program, Computers and Structures,

Berkeley

SEISMOSIGNAL, version 3.1.0, Seismosoft (www.seismosoft.com)

SIMQKE-1 Developer: E.H. Vanmarcke, C.A. Cornell, D.A. Gasparini, and S.N. Hou,
Department of Civil Engineering, Massachusetts Institute of Technology,
Cambridge, Massachusetts 1976, Modified: T.F. Blake, Newbury Park,
California [PC DOS version] 1990

Microsoft Excel 2002

Microsoft Word 2002

14 Appendices

Appendix 1: Accelerograms used in Seismic Analyses

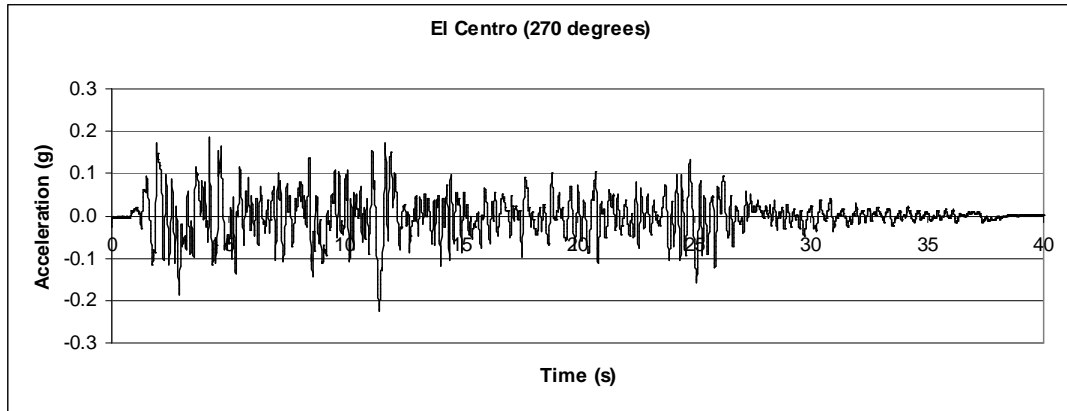


Figure 14-1 El Centro accelerogram in Y direction for $3m/s^2$ scaling

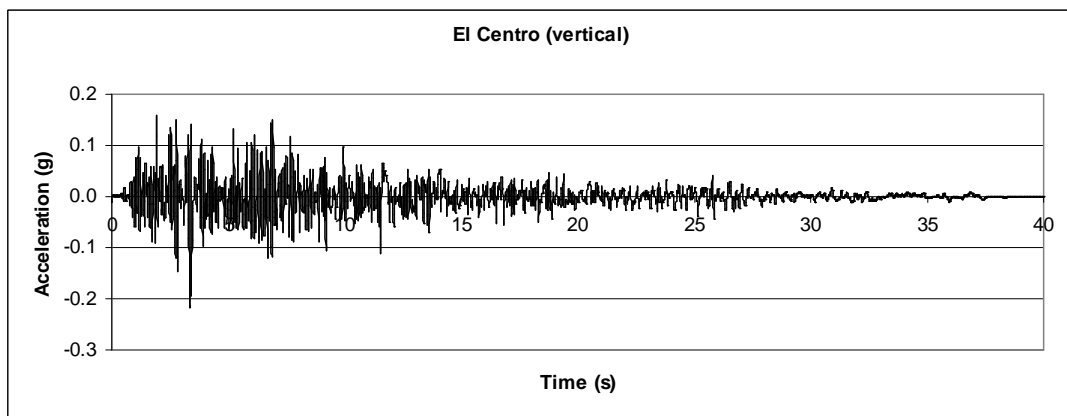


Figure 14-2 El Centro accelerogram in vertical direction for $3m/s^2$ scaling

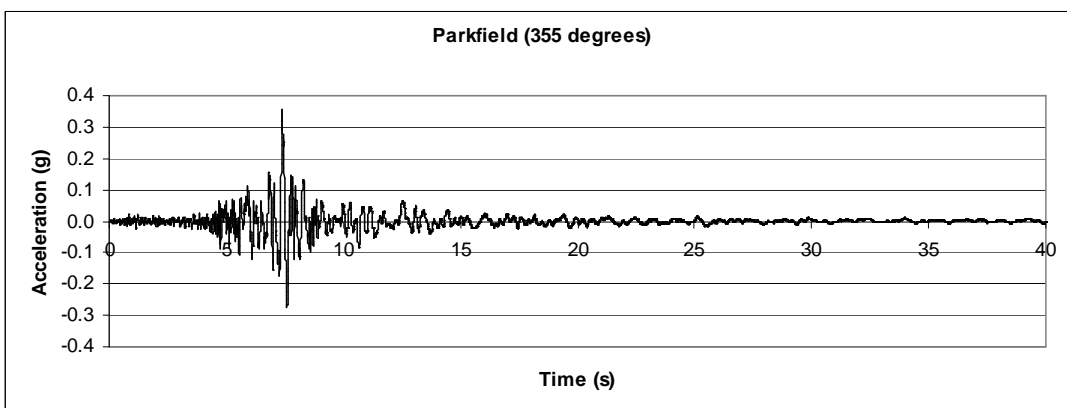


Figure 14-3 Parkfield accelerogram in Y direction for $3m/s^2$ scaling

Appendix 1 (cont.): Accelerograms used in Seismic Analyses

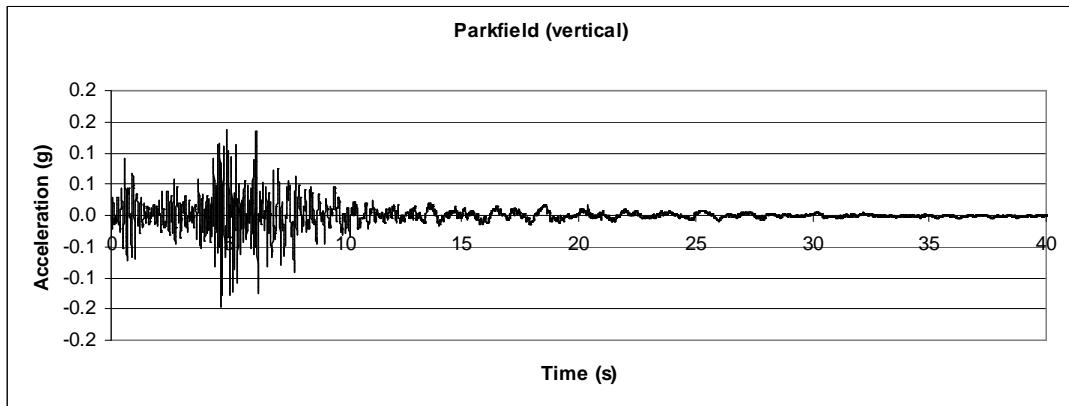


Figure 14-4 Parkfield accelerogram in vertical direction for $3m/s^2$ scaling

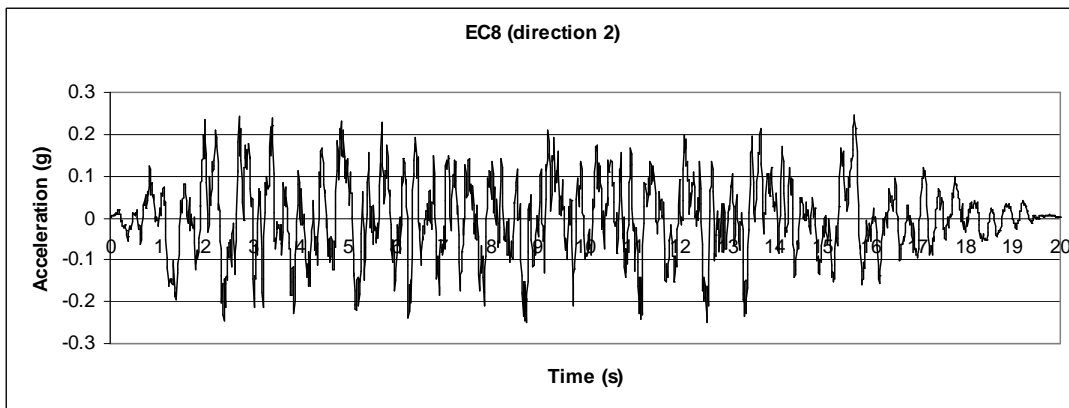


Figure 14-5 EC8 accelerogram in Y direction for $3m/s^2$ scaling

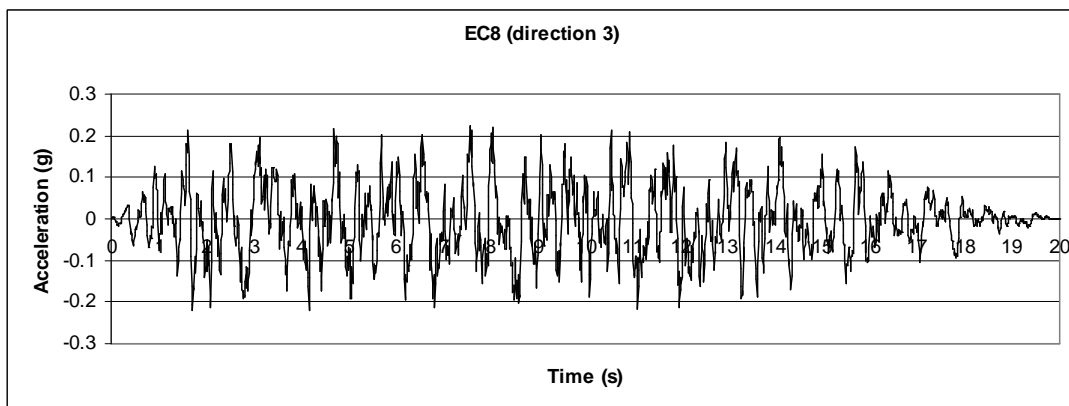


Figure 14-6 El Centro accelerogram in vertical direction for $3m/s^2$ scaling

Appendix 2: Extreme Cable Forces produced in Seismic Analyses

Cable	Pretension	EC8-2.5		EC8-3		EC8-3.5		EC8-4	
		max	min	max	min	max	min	max	min
A1	80.3	125.0	29.8	139.7	24.5	153.1	19.6	166.6	10.9
B1	104.9	168.3	37.5	187.9	36.6	219.5	32.1	252.7	21.5
C1	137.0	218.0	60.9	232.5	52.3	254.0	54.4	283.3	49.0
		EI Centro-2.5		EI Centro-3		EI Centro-3.5		EI Centro-4	
		max	min	max	min	max	min	max	min
A1	80.3	138.3	13.7	149.5	3.1	159.7	-2.2	167.7	-2.8
B1	104.9	168.0	29.3	178.4	15.3	186.4	4.1	198.0	-1.3
C1	137.0	190.2	82.1	200.7	71.8	211.2	61.7	222.2	51.3
		Parkfield-2.5		Parkfield-3		Parkfield-3.5		Parkfield-4	
		max	min	max	min	max	min	max	min
A1	80.3	135.1	24.7	145.9	14.1	156.5	4.0	166.6	-5.3
B1	104.9	170.3	63.6	184.0	59.6	195.7	54.9	209.0	46.5
C1	137.0	176.3	100.6	184.2	93.4	192.0	86.3	199.7	79.2

Table 14-1 Mast A cable tensions (kN)

Cable	Pretension	EC8-2.5		EC8-3		EC8-3.5		EC8-4	
		max	min	max	min	max	min	max	min
A1	44.1	159.8	-14.1	168.7	-18.4	161.9	-19.7	195.8	-15.1
B1	73.8	160.9	-11.1	179.7	-2.3	204.3	-3.3	239.3	3.6
C1	83.4	137.8	24.7	155.7	20.6	164.5	15.3	180.5	-7.8
D1	164.7	235.8	103.0	255.0	96.6	261.2	88.8	282.3	74.9
E1	95.7	147.9	47.6	166.3	32.2	167.9	32.6	182.2	30.1
		EI Centro-2.5		EI Centro-3		EI Centro-3.5		EI Centro-4	
		max	min	max	min	max	min	max	min
A1	44.1	99.1	-5.9	113.1	4.7	123.8	-1.2	153.2	-5.1
B1	73.8	129.0	23.1	148.7	9.5	149.4	10.4	162.4	7.4
C1	83.4	130.4	40.4	136.1	33.6	158.8	18.4	175.9	17.9
D1	164.7	231.9	102.7	233.7	93.7	256.1	83.6	259.9	67.1
E1	95.7	137.1	58.0	148.0	49.5	157.2	41.7	164.7	33.3
		Parkfield-2.5		Parkfield-3		Parkfield-3.5		Parkfield-4	
		max	min	max	min	max	min	max	min
A1	44.1	66.1	18.4	70.2	13.8	74.0	9.3	79.9	4.8
B1	73.8	98.0	54.2	102.4	50.3	106.6	46.3	111.9	42.1
C1	83.4	105.4	61.8	109.7	57.8	114.0	54.0	121.7	45.9
D1	164.7	203.1	126.5	210.6	119.5	218.4	112.7	230.7	101.6
E1	95.7	115.8	78.1	119.8	74.5	123.9	70.9	131.2	63.8

Table 14-2 Mast B cable tensions (kN)

Appendix 2 (cont.): Extreme Cable Forces produced in Seismic Analyses

Cable	Pretension	EC8-2.5		EC8-3		EC8-3.5		EC8-4	
		max	min	max	min	max	min	max	min
A1	92.0	187.3	-1.4	219.4	-4.4	258.8	5.4	298.8	-0.4
B1	116.7	252.3	25.1	264.1	21.6	304.2	26.1	344.4	12.5
C1	167.6	259.1	65.9	281.6	48.7	301.2	34.8	326.2	20.6
D1	116.3	191.5	52.9	204.8	40.8	223.1	37.5	240.1	35.5
		El Centro-2.5		El Centro-3		El Centro-3.5		El Centro-4	
		max	min	max	min	max	min	max	min
A1	92.0	154.3	36.0	166.6	25.6	178.6	15.8	194.8	6.5
B1	116.7	213.4	49.4	232.3	36.7	250.7	24.5	269.0	13.0
C1	167.6	251.9	101.9	267.8	90.9	282.4	81.4	296.0	70.9
D1	116.3	155.5	78.3	162.6	71.4	169.9	64.9	176.3	58.4
		Parkfield-2.5		Parkfield-3		Parkfield-3.5		Parkfield-4	
		max	min	max	min	max	min	max	min
A1	92.0	130.2	50.5	137.8	42.2	145.3	33.9	152.7	25.6
B1	116.7	174.6	57.2	186.6	46.4	198.5	36.3	210.2	27.0
C1	167.6	208.7	125.3	217.0	117.9	225.3	111.3	233.6	106.0
D1	116.3	133.6	94.5	136.9	90.1	140.2	85.7	143.4	81.3

Table 14-3 Mast C cable tensions (kN)

Cable	Pretension	EC8-2.5		EC8-3		EC8-3.5		EC8-4	
		max	min	max	min	max	min	max	min
A1	104.0	170.8	34.6	182.8	32.1	193.3	40.3	213.2	32.0
B1	126.1	255.3	16.2	266.7	17.1	295.7	13.7	356.7	6.5
C1	170.9	265.9	50.3	288.4	40.8	314.2	46.9	342.1	55.3
D1	267.6	343.9	186.4	355.9	173.0	365.5	161.2	372.7	151.5
E1	136.2	216.8	72.2	228.9	65.8	238.7	62.4	247.0	63.4
		El Centro-2.5		El Centro-3		El Centro-3.5		El Centro-4	
		max	min	max	min	max	min	max	min
A1	104.0	147.2	63.8	155.8	51.6	164.4	38.6	173.4	27.5
B1	126.1	220.1	42.0	238.2	31.4	255.7	25.0	273.6	23.4
C1	170.9	218.7	120.2	229.8	110.8	245.2	102.2	262.4	94.1
D1	267.6	314.8	214.7	322.2	206.1	328.6	198.5	334.1	191.5
E1	136.2	177.7	97.1	185.6	92.2	193.2	88.4	201.0	83.0
		Parkfield-2.5		Parkfield-3		Parkfield-3.5		Parkfield-4	
		max	min	max	min	max	min	max	min
A1	104.0	121.7	85.4	125.3	81.8	128.9	78.2	132.5	74.6
B1	126.1	168.9	86.6	177.4	78.8	185.9	71.1	194.2	63.6
C1	170.9	200.0	146.1	205.8	141.2	211.6	136.4	217.4	131.6
D1	267.6	292.8	243.5	297.6	238.9	302.3	234.3	306.8	229.8
E1	136.2	163.0	111.7	168.3	106.8	173.4	102.0	178.6	97.3

Table 14-4 Mast D cable tensions (kN)